A MODEL FOR TRANSFORMATION OF FULLY DISPERSIVE NONLINEAR WAVES

A Dissertation

by

SAMIRA ARDANI

Submitted to the Office of Graduate and Professional Studies of
Texas A&M University
in partial fulfillment of the requirements for the degree of

DOCTOR OF PHILOSOPHY

Chair of Committee,	James M. Kaihatu
Committee Members,	Robert D. Hetland
	Scott A. Socolofsky
	Jun Zhang
Head of Department,	Robin Autenrieth

August 2016

Major Subject: Civil Engineering

ABSTRACT

In this dissertation, we evaluate the performance of nonlinear models, and the effects of bound waves in nearshore wave models are studied mathematically and numerically. The first part of this study concerns the evaluation of different nearshore models and their capability in the estimation of wave spectra and higher order wave statistics. Four different nearshore wave models (three fully dispersive models and a consistent shoaling model) are compared to field and experimental data sets. Comparison of these nearshore models reveals that the nearshore models' performance in predicting higher frequency energy evolution is not as skillful as at lower frequencies. Therefore, a new wave transformation model is derived. The model includes nonlinear wave interaction effects up to third order in wave steepness and is based on the fully dispersive second order model. Transforming the problem into the frequency domain and using multiple scale analysis in space and perturbation theory, the model is expanded up to third order in wave steepness. The result is a set of evolution equations which explicitly contains quadratic near-resonant interactions, non-resonant bound waves, and cubic resonant interactions. The results of the numerical modeling for the aforementioned nearshore model show that the model is verified reasonably well in terms of the harmonics tests and the spectral analysis for experimental and field data sets. However, the calculation of higher order statistical parameters is quite sensitive to how the free parameters in the model are chosen.

In addition, the dissipation characteristics of the breaking waves has been investigated using the high-resolution laboratory datasets. The free parameter in a probabilistic breaking model and the threshold parameter in the instantaneous dissipation model is parameterized at each gauge location separately, and the dependency of the calculated damping coefficient in the formulation to frequency components is

extensively discussed. Moreover, the relationship between the third moments of free surface elevation and the parameterized threshold parameter in the instantaneous dissipation model is represented.

DEDICATION

I dedicate this work to my beloved husband Hamid Shafiezadeh for all his support, to my mother, Robabeh Ardani and the memory of my father, Nasser Ardani for their encouragement and spiritual support during my entire educational path.

ACKNOWLEDGEMENTS

This project was funded by ONR grant No. N00014-10-1-0389. I would like to express my appreciation to Dr. Kaihatu for his valuable and constructive suggestions during this research work. His willingness to give his time so generously is very much appreciated. He provided me with valuable knowledge.

Beside my advisor, I would like to thank my other committee members Dr. Scott Socolofsky, Dr. Jun Zhang and Dr. Robert Hetland for their valuable comments.

My great and special thanks to my husband, Hamid Shafiezadeh for his moral support during the time of PhD. He always enlightened me with his brilliant ideas and encouraged me not only in academic path but also in the whole life.

Thanks to my friends, Ying-Po Liao, the IT girl, who helped me alot to run my simulations on coastal cluster and other fellow friends in our research group, Wonhyun Lee, John Goertz, Wongsuk Pae and Chi Liu for the fun moments during the past four years. I would like to thank my great officemates and friends, Inok Jun, Maryam Rezvani, Anusha Dissanayake, Binbin Wang, Samin and Vadoud Dehkharghanian and Azadeh Motlagh for all happy times we had in campus.

Last but not the least, I would like to show my gratitude to my mom and the rest of the family, my sister, Nasrin and my brothers Mansour and Massoud for their support. Remembering the memory of my Father and his kindness was also a great spiritual support for me.

TABLE OF CONTENTS

Page

ABSTRACT ii

DEDICATION iv

ACKNOWLEDGEMENTS v

TABLE OF CONTENTS vi

LIST OF FIGURES viii

LIST OF TABLES xii

1. INTRODUCTION 1

2. NEARSHORE WAVE MODELS AND COMPARISONS TO DATA 9

2.1 Consistent model of Freilich and Guza (1984) 9
2.2 Mase and Kirby (1992) 10
2.3 Kaihatu and Kirby (1995) 12
2.4 Eldeberky and Madsen (1999) 12
2.5 Comparison of the models with field data set 15
2.6 Summary 18

3. FULLY DISPERSIVE NONLINEAR WAVE MODEL 27

3.1 Model assumptions 27
3.2 Mathematical derivation of the model in freqency domain 28
3.2.1 Second order equation 34
3.2.2 Third order equation 37
3.2.3 Dissipation mechanism due to the wave breaking 38
3.2.4 Comparison of the mathematical model with Kaihatu and Kirby (1995) 39
3.2.5 Comparison of the mathematical model with Janssen et al. (2006) 39
3.3 Numerical analysis and verification of the model 40
3.3.1 Harmonic test of Chapalain et al. (1992) 41

3.3.2 Comparison of the model with laboratory datasets for random waves . . . 47
3.3.3 Comparison of the model with field data sets in terms of spectra 52
3.3.4 Comprehensive comparison of the model with field data 61
3.3.5 Evolution of the model with an arbitrary TMA spectrum . . . 66
3.3.6 Comparison of the model with experimental datasets in terms of higher order statistical parameters . . . 69
3.4 Summary . . . 73

4. CHARACTERIZING THE DISSIPATION IN BREAKING WAVES 76

4.1 Introduction . . . 76
4.2 Classification of wave breaking models . . . 80
4.2.1 Thornton and Guza (1983) . . . 80
4.2.2 Zelt (1991) . . . 81
4.2.3 Frequency dependency formulation of wave breaking . . . 82
4.3 Parameterization . . . 84
4.3.1 Parameterization of γ and Zelt parameter . . . 84
4.4 Analysis and comparisons . . . 88
4.4.1 The frequency dependency of breaking waves . . . 88
4.4.2 Skewness and asymmetry . . . 91
4.5 Summary . . . 92

5. CONCLUSION AND FUTURE WORKS . . . 93

REFERENCES . . . 96

LIST OF FIGURES

FIGURE Page

2.1 Verification of the hybrid model of Mase and Kirby (1992) with Case 2 of their experimental data set. (The blue line is the measured data and the magenta dash-dot is the model results. Depths are calculated from wavemaker) 11

2.2 Verification of the model of Eldeberky and Madsen (1999) with Mase and Kirby (1992) data set. (The blue line is the measured data and the magenta dash-dot is the model results. Depths are calculated from wavemaker) 14

2.3 Schematic view of Duck 94 experiment, U.S. Army Field Research Facility at Duck, North Carolina, USA (Birkemeier and Thornton, 1994), Left: Plan view; Right: Section view 18

2.4 Comparison of spectra for model of Kaihatu and Kirby (1995) and Duck 94 field data set with (top four) and without using tail (bottom four) for offshore spectra (line: measured field data and dash-line: model result.) 21

2.5 Comparison of Kaihatu and Kirby (1995) and Freilich and Guza (1984) with measured data for Hrms. (from top to bottom, gauge no.2, 6 and 10 sorted from offshore to nearshore. Left: model of Freilich and Guza (1984) ; Right: model of Kaihatu and Kirby (1995). The green and the blue lines are the 45 degree line and the best fit line respectively.) 22

2.6 Comparison of Kaihatu and Kirby (1995) and Freilich and Guza (1984) with measured data for variance. (from top to bottom, gauge no.2, 6 and 10 sorted from offshore to nearshore. Left: model of Freilich and Guza (1984) ; Right: model of Kaihatu and Kirby (1995). The green and the blue lines are the 45 degree line and the best fit line respectively.) 23

2.7 Comparison of Kaihatu and Kirby (1995) and Freilich and Guza (1984) with measured data for skewness. (from top to bottom, gauge no.2, 6 and 10 sorted from offshore to nearshore. Left: model of Freilich and Guza (1984) ; Right: model of Kaihatu and Kirby (1995). The green and the blue lines are the 45 degree line and the best fit line respectively.) 24

2.8 Comparison of Kaihatu and Kirby (1995) and Freilich and Guza (1984) with measured data for asymmetry. (from top to bottom, gauge no.2, 6 and 10 sorted from offshore to nearshore. Left: model of Freilich and Guza (1984) ; Right: model of Kaihatu and Kirby (1995). The green and the blue lines are the 45 degree line and the best fit line respectively.) 25

2.9 Comparison of model of Kaihatu and Kirby (1995) and Freilich and Guza (1984) with Duck94 field data set. (gauge no.2, 6 and 10 sorted from offshore to nearshore) 26

3.1 Comparison of Chapalain et al. (1992) experiment with real amplitude model, Kaihatu and Kirby (1995) mild slope model and the consistent model of Freilich and Guza (1984), $h = 0.4m$ and $T = 2.5S$ 43

3.2 Comparison of Chapalain et al. (1992) experiment with real amplitude model, Kaihatu and Kirby (1995) mild slope model and the consistent model of Freilich and Guza (1984), $h = 0.4m$ and $T = 3.5S$ 44

3.3 Comparison of Chapalain et al. (1992) experiment with real amplitude model, Kaihatu and Kirby (1995) mild slope model and the consistent model of Freilich and Guza (1984), $h = 0.3m$ and $T = 2.5S$ 45

3.4 Comparison of Chapalain et al. (1992) experiment with real amplitude model, Kaihatu and Kirby (1995) mild slope model and the consistent model of Freilich and Guza (1984), $h = 0.4m$ and $T = 3S$ 46

3.5 Mase and Kirby (1992) experimental setup 48

3.6 Comparison of Mase and Kirby (1992) experiments with real amplitude model and the mild slope model of Kaihatu and Kirby (1995) . . 49

3.7 Comparison of Mase and Kirby (1992) experiments with real amplitude model and the mild slope model of Kaihatu and Kirby (1995) . . 50

3.8 Bowen and Kirby (1994) experimental setup 51

3.9 Comparison of Bowen and Kirby (1994) experiments with real amplitude model, Kaihatu and Kirby (1995) mild slope model and the consistent model of Freilich and Guza (1984) 52

3.10 Comparison of Duck94-0903100 field dataset with real amplitude model, Kaihatu and Kirby (1995) mild slope model and the consistent model of Freilich and Guza (1984)-256 frequency components 54

3.11 Comparison of Duck94-09011000 field dataset with real amplitude model, Kaihatu and Kirby (1995) mild slope model and the consistent model of Freilich and Guza (1984)-256 frequency components . . 55

3.12 Comparison of Duck94-09011600 field dataset with real amplitude model, Kaihatu and Kirby (1995) mild slope model and the consistent model of Freilich and Guza (1984)-256 frequency components . . 56

3.13 Comparison of Duck94-09051600 field dataset with real amplitude model, Kaihatu and Kirby (1995) mild slope model and the consistent model of Freilich and Guza (1984)-256 frequency components . . 57

3.14 Comparison of Duck94-09030100 field dataset with real amplitude model, Kaihatu and Kirby (1995) mild slope model and the consistent model of Freilich and Guza (1984)-400 frequency components . . 58

3.15 Comparison of Duck94-09011000 field dataset with real amplitude model, Kaihatu and Kirby (1995) mild slope model and the consistent model of Freilich and Guza (1984)-400 frequency components . . 59

3.16 Comparison of Duck94-09011600 field dataset with real amplitude model, Kaihatu and Kirby (1995) mild slope model and the consistent model of Freilich and Guza (1984)-400 frequency components . . 60

3.17 Comparison of Duck94-09051600 field dataset with real amplitude model, Kaihatu and Kirby (1995) mild slope model and the consistent model of Freilich and Guza (1984)- 400 frequency components . . 61

3.18 Comparison of real amplitude model with the model of Kaihatu and Kirby (1995), 256 frequency components, band:1. Left to right: real amplitude model; model of Kaihatu and Kirby (1995) and model of Freilich and Guza (1984); Top to bottom: gauges 2, 6 and 10 from offshore to nearshore. 63

3.19 Comparison of real amplitude model with the model of Kaihatu and Kirby (1995), 256 frequency components, band:2. Left to right: real amplitude model; model of Kaihatu and Kirby (1995) and model of Freilich and Guza (1984); Top to bottom: gauges 2, 6 and 10 from offshore to nearshore. 64

3.20 Comparison of real amplitude model with the model of Kaihatu and Kirby (1995), 256 frequency components, band:3. Left to right: real amplitude model; model of Kaihatu and Kirby (1995) and model of Freilich and Guza (1984); Top to bottom: gauges 2, 6 and 10 from offshore to nearshore. 65

3.21 Evolution of TMA spectrum. (The blue line: the original TMA spectrum; the red dash-line: the TMA spectrum after evolution) 68

3.22 Changes in Waveform during the transformation to nearshore (Ole Secher Madsen, 2010) 71

3.23 Third order comparison with Mase and Kirby (1992) dataset. The value of the ϵ is 0.01. (The blue line: the observed data; the dash-dot magenta: the model results) 72

3.24 Third order comparison with Mase and Kirby (1992) dataset after changing the ϵ. The value of ϵ is 0.001. (The blue line: the observed data; the dash-dot magenta: the model results) 73

4.1 Parameterization of γ for BK94 dataset. Black circle: Case A, Green asterisk: Case B; Red square: Case C 86

4.2 Calibrated Zelt parameter at each gauge for three cases of Bowen and Kirby (1994) 87

4.3 instantaneous dissipation after calibrating the threshold Zelt parameter 88

4.4 Comparing the slope of the spectra and $\alpha(n)$ 90

4.5 Relationship between wave shape parameters and Zelt parameter . . 91

LIST OF TABLES

TABLE Page

3.1 Parameters of Chapalain et al. (1992) experiments 42

3.2 Characteristics of field experiments cases 53

3.3 Summary of statistical skills for each model at band 1. The first row shows the standard deviation and the second row shows the correlation coefficient for each gauge. 66

3.4 Summary of statistical skills for each model at band 2. The first row shows the standard deviation and the second row shows the correlation coefficient for each gauge. 66

3.5 Summary of statistical skills for each model at band 3. The first row shows the standard deviation and the second row shows the correlation coefficient for each gauge. 67

4.1 Wave conditions for Bowen and Kirby (1994) experiments 85

1. INTRODUCTION

As waves transform from offshore to nearshore regions, their behavior changes due to the increasing influence of the bathymetry. One mechanism of this is a change in the nature of energy exchange among different frequencies comprising the wave field. Offshore waves do not differ significantly from sinusoidal waves in shape. By contrast, nearshore waves are more skewed (peak crest and wide troughs) and asymmetric (forward-leaning). More accurate predictions of wave shape may lead to better estimation of instantaneous sediment transport and sandbar migration, which directly affects surf zone morphology, as these process are dependent on local accelerations deriven by shape.

Battjes (1994) categorized water wave models into two major groups: phase averaged and phase resolving models. The former is suitable for modeling of waves in global or regional ($O(100km)$) domains and for waves with slow varying local properties. These models assume that the free surface elevations are statistically distributed with wave energy (or, in the case of wave-current interaction, wave action) being the dependent variable. Examples of these models include those based on the action balance equation such as WAVEWATCH (Tolman 1991) and SWAN (Booij et al. 1990). One advantage of these models is that they easily accomodate energy based dissipation and generation functions which are inherently statistical. However, as in shallow water, the random phase assumption inherent in phase-averaged models breaks down, as the individual phase correlate in order to lead to the higher skewed and asymmetric waveforms seen. In contrast, phase resolving models are applied at the scale of coastal domains and are appropriate for waves with rapid varying local properties on the scale of a wave length or less. These models, as the name

implies, resolve the free surface elevation and thus can represent the phase correlations inherent in shallow water waves (provided the associated nonlinear mechanism are included). This category of models includes deterministic models such as: mild slope equation models (e.g. Kaihatu and Kirby 1995); Stokes-type wave models with weak nonlinearity and mildly sloped bottom and Boussinesq models with weak nonlinearity and weak dispersion properties (e.g. Freilich and Guza 1984).

Phase resolving models can be formulated either in time domain or frequency domain. In time domain models, the dependent variables are functions of time and space, and all relevant motions are represented in the model. For frequency domain models, the free surface $\eta(x, y, t)$ is represented as:

$$\eta = \sum_{n=1}^{\infty} \frac{A_n}{2} e^{i\Psi_n} + c.c \tag{1.1}$$

$$\Psi_n = \int k_n dx - \omega_n t \tag{1.2}$$

$$\omega_n{}^2 = g k_n \; tanh \; k_n h \tag{1.3}$$

where A_n is a (real or complex) amplitude for the nth frequency, ω_n is the angular frequency and k_n is the wave number as defined by (1.3), the dispersion relation. In the frequency domain, the transient signal of the free surface elevation is decomposed into its fundamental frequency components. In nonlinear wave models expressed in frequency domain, the dependent variables are the amplitudes of each of the discrete frequencies defined for the computation. As a result of this transformation, the nonlinear terms in the model are defined explicitly as interactions between amplitudes of various frequencies in the random wave field. these are advantages and disadvantages to both approaches. Time-domain models can easily accomodate aperiodic, periodic, monochromatic, or random waves as initial conditions. The model's performance is

not affected by the type of initial condition. However, fine spacial resolution is often required, and the numerics of these models can be complex. In contrast, frequency domain models are numerically straightforward. However, their model run times are strongly dependent on the number of wave frequencies included in the calculation. It can be argued, however, that frequency domain models are useful transition models between phase averaged offshore models and time domain nearshore/surf models, so their study is warranted.

Nonlinearity in frequency domain models is represented via wave-wave interactions. Wave-wave interaction arises from the surface boundary condition, which are nonlinear and applied to a surface of unknown position. They consist of different combinations of free surface elevation, η and velocity potential ϕ. These boundary conditions are approximated (more details to come) and these approximate terms contains products such as $\eta^2, \eta\phi, \phi^2$ in second order and $\eta^3, \eta^2\phi, \eta\phi^2, \phi^3$ in third order. The solution contains terms proportional to $1, e^{\pm i\Psi}, e^{\pm 2i\Psi}$ and $e^{\pm 3i\Psi}$, where Ψ is the phase function (discussed extensively later). Based on the relationships between the various ϕ for the different waves in the wave field, two types of waves result from the interaction. The first, free waves, are individual waves that obey the dispersion relation (1.3). Each free wave has its own phase speed dictated by the linear dispersion relation. The nonlinear wave-wave interaction between free waves leads to exchange of energy among spectral components, which further allow changes in wave shape and spectral shape. The second type of waves discussed here are bound waves. Bound waves of a particular frequency do not obey the dispersion relation relevant to its frequency but has the same phase speed as its primary wave. While they do not exchange energy, bound waves do affect overall wave dynamics. In deep water, wave-wave interaction takes place among groups of four waves (quartet wave-wave interaction) with exact resonance condition.

$$\omega_l + \omega_m = \omega_p + \omega_n \tag{1.4}$$

$$\vec{k_l} + \vec{k_m} = \vec{k_p} + \vec{k_n} \tag{1.5}$$

This interaction takes place at third order and causes a weak transfer of energy between frequencies. However, at second order, in deep water, only bound waves are present. The amplitudes of these waves will always remain smaller by a fixed amount than their corresponding primary waves. In shallow water, however, the scenario is quite different. Here, the near-resonant condition (triad wave-wave interaction) causes significant energy transfers between frequencies.

$$\omega_l + \omega_m = \omega_n \tag{1.6}$$

$$k_l + k_m \approx k_n \tag{1.7}$$

The triad wave-wave interaction, at second order, can only be exactly satisfied at the shallow water limit. Despite the fact that it is only near-resonant, it causes significant energy transfers among wave frequencies (Benney 1963).

Early studies of nearshore waves originate from the modeling of Boussinesq equations (Boussinesq 1872). In these equations, both weak nonlinearity and weak dispersive effects of waves are taken into account for constant depth; dispersive and nonlinearity parameters are thus kept at first order. Later, Korteweg and de Vries (1895) developed a single equation for free surface elevation by combining two Boussinesq equations for a one dimensional propagation of waves in a constant depth. Mei and Le Mehaute (1966) and Peregrine (1967) developed Boussinesq type equations to investigate the effects of mildly varying depth. By transforming the varying-bottom Bousinesq equations in frequency domain, Freilich and Guza (1984) derived

two nearshore nonlinear models (a "consistent" model and a "dispersive" model) for the shoaling region where the water depth is approximately in the range of 3 to 10m. They also used the result of Benney (1962), who used multiple scale expansion to formulate a series of equations which account for significant energy exchange even in only near-resonant conditions. In an attempt to improve the dispersive characteristics of Boussinesq models, Witting (1984) presented a one dimensional extended Boussinesq model in time domain that used the polynomial approximation for dispertion relation. Although this model has fewer limitations for water depth, it is complicated to generate it in two horizontal dimension. Later, Madsen et al. (1991) developed a two dimensional model in time domain for constant depth by extending the velocity terms of Boussinesq equation using Taylor expansion about the bottom and added convective terms to improve the depth limitations of Boussinesq type equations. Similarly, Nwogu (1993) derived a new set of equations in time domain using the variable vertical velocity instead of a constant averaged velocity. Madsen and Sorensen (1992) extended the Boussinesq equations for mildly varying bottom slopes by developing linear dispesion characteristics of waves. Furthermore, Wei et al. (1995); and Wei and Kirby (1995) developed their higher order numerical method to simulate the Boussinesq equations of Nwogu (1993). In the frequency domain, Liu et al. (1985) applied the parabolic approximation method of Radder (1979) to modify both Boussinesq equations and KP (Kadomtsev and Petviashvili 1970) equation; the latter is a weak two-dimensional extension of the KdV equation. Chen and Liu (1995) established the frequency domain model for extended Boussinesq equations of Nwogu (1993) and developed their fourth order equation using parabolic approximation. Chen and Liu (1995) and Kaihatu and Kirby (1998) also extended the Boussinesq equations and found the optimized parameters for shoaling and dispersive terms. Madsen et al. (2003) introduced their extended Boussinesq model that

expanded the velocity potential with an arbitrary depth-dependence term. They argued that the model was less restrictive to the depth compared to the other extended Boussinesq models and is applicable for a wide range of wave numbers. Later, Bredmose et al. (2004) enhanced the efficiency of the time domain Boussinesq models by applying Fast Fourier Transforms for calculation of nonlinear interaction terms.

An alternative to the Boussinesq equation approach involves nonlinear extensions to linear, fully dispersive wave models. Bryant (1973) developed a model for long waves based on the boundary value problem and fully dispersive features of waves and compared the model with KdV (Korteweg and de Vries 1895) and Benjamin et al. (1972) equations. To establish the mathematical formulation of the model, he assumed that waves are periodic in space and nearly periodic in time and hence wave interactions are near resonant for lower frequencies. He demonstrated that fully dispersive wave models support the nonlinear triad wave-wave interaction. Moreover, Bryant (1974) demonstrated that the permanent form solution to his dispersive wave equation recovers the third order Stokes waves amplitudes (Kaihatu 2003). However, the assumption of spatial periodicity is not useful for waves propagating over varying water depth. Mei and Unluata (1972); Keller (1988); and Boczar-Karakiewicz et al. (1986) established a system of equations for interaction of two small amplitude waves for a varying bottom based on boundary value problem. As waves propagate from deep to shallow water region, the triad wave-wave interaction terms become more predominant compare to those of quartet interaction (Agnon et al. 1993). Starting from the boundary value problem, Agnon et al. (1993) derived a one dimensional fully dispersive model that includes triad wave-wave interactions. Kaihatu and Kirby (1995) presented a two dimensional fully dispersive model using the parabolic approximation method (Radder 1979). Following Berkhoff (1972), they assumed mild slope bathymetry variation to develop their model. The nonlinear part of their model

consists of the triad wave-wave interactions between frequency components. Wave breaking dissipation rate term was also calculated using the approach of Mase and Kirby (1992) and included in the aforementioned model. Developing this model into two dimensions, and assuming a periodic lateral domain, Agnon and Sheremet (1997) presented a stochastic model which used bispecta (e.g. Elgar and Guza 1985) to represent the nonlinear interaction between spectra at frequencies involved in triad interaction, and used bicoherence (e.g. Elgar and Guza 1985) to investigate the phase correlation involved. In addition, Kaihatu (2001); Eldeberky and Madsen (1999); and Eldeberky (2012) improved the fully dispersive parabolic model by extending the relationship between free surface elevation and velocity potential (used in developing the frequency domain model) up to second order. According to this improvement the higher order statistics of waves can be estimated more accurately leading to better evaluation of the model's ability to estimate wave shape. More recent studies for generating waves evolution equations in two dimension using the boundary value problem was carried out by Janssen et al. (2006). Following Chu and Mei (1970); Liu and Dingemans (1989); Suh et al. (1990), they expanded the free surface elevation and velocity potential and studied the effects of sub and super harmonic bound waves. According to their model, both triad and quartet wave wave interaction terms were taken into account in the model; however during wave transition process from deep to shallow water explicit shifting from one to another term is required (Tolman et al. 2013).

Briefly, the aim of this present work is to derive a transformation model for nearshore waves which extends the model of Kaihatu and Kirby (1995) to improve the performance of the model in higher frequencies. In Chapter 3, we introduce four nearshore wave models with different characteristics in nonlinearity and dispersion. This investigation allows us to understand the behavior of each model and their lim-

itations for different ranges of frequency components in the spectrum, which we then use to ascertain the necessary improvements required. In Chapter 4, the mathematical formulation of the proposed frequency domain model is derived. The derivation is based on the boundary value problem for velocity potential, Φ, the boundary condition equations are extended up to the third order of nonlinearity ($O(\epsilon^3)$) where $\epsilon = ka$, in which a is the amplitude. Assuming a mildly varying bottom and the periodicity of the waves. The effects of triad wave-wave interaction in second and third order, and bound waves in third order is discussed. The final form of the mathematical model is then verified numerically with suitable laboratory and field data. In Chapter 5, the dissipation characteristics of the nearshore models in surf zone are investigated and the free parameters of Thornton and Guza (1983) and the threshold parameter of Zelt (1991) for modeling breaking waves are characterized. We also discuss the relationship between the characteristics of wave breaking and the resultant effects on the free surface elevation spectrum. Finally, in Chapter 6, the conclusions and the future work for extending this study is presented.

2. NEARSHORE WAVE MODELS AND COMPARISONS TO DATA

When waves propagate to shallow water areas, they become increasingly affected by the presence of the sea bed. In this area, the relative water depth, kh, approaches shallow water limit ($kh << 1$) where k is the wave number and h is the water depth. In this regime, near-resonant conditions allow significant amount of energy to be transferred between different harmonics (Bryant 1973). In this study, first, different assumptions for modeling of nearshore waves for propagation of waves are discussed. Then, four different nearshore models are compared in terms of their ability to estimate spectra and the higher order statistical wave shape parameters.

2.1 Consistent model of Freilich and Guza (1984)

This model is the frequency domain extended version of Boussinesq-type equations for a mildy sloping sea bottom. Additionally, due to its weak dispersive characteristics, the model is only strictly valid for waves in shallow water. Freilich and Guza (1984) showed that their model agrees well with field data in shallow water.

Based on the Boussinesq model, the consistent model is formulated as

$$A_{nx} + \frac{h_x}{4h}A_n - \frac{in^3k^3h^2}{6}A_n + \alpha_n A_n + \frac{3ink}{8h}\left(\sum_{l=1}^{n-1} A_l A_{n-1} + 2\sum_{l=1}^{N-n} A_l^* A_{n+l}\right) = 0 \quad (2.1)$$

where A_n is the complex amplitude of free surface elevation for nth frequency, A^* is the conjugate form of A; and k and h are wave number and water depth respectively. Subscripts n, l, $n-l$ and $n+l$ denote deffierent frequency modes that the relationship between them is governed by triad resonant condition. The second term in the equation is the linear shoaling term and the third term is the dispersive term which

accounts for weak dispersion effects. The last terms also represent the nonlinear triad interaction of waves for transferring energy between frequencies in the spectrum. Dissipation in the model can be represented by $\alpha_n A_n$ where α_n is the damping coefficient.

2.2 Mase and Kirby (1992)

In this model the frequency domain KdV equation is modified so that the Green's Law used in the model of Freilich and Guza (1984) is replaced with the fully dispersive shoaling term. The dispersive characteristics of the model are also improved using the exact dispersion relationship instead of shallow water dispersion relation.

$$A_{nx}+\frac{c_{g_x}}{2c_g}A_n-ink_1(\sqrt{\frac{k_nh}{tanh\ k_nh}}-1)A_n+\frac{3ink_1}{8h}\left(\sum_{l=1}^{n-1}A_lA_{n-1}+2\sum_{l=1}^{N-n}A_l^*A_{n+l}\right)+\alpha_nA_n=0 \tag{2.2}$$

where c_g is the group velocity and α_n is the damping coefficient (will be extensively explained in next section). k_1 ($k_1 = \frac{\omega_1}{\sqrt{gh}}$) and k_n denote the non-dispersive wave number and fully dispersive wave number respectively. The second and third term in the equation denote the shoaling and dispersive terms respectively. The nonlinear interaction of waves is identical to the model of Freilich and Guza (1984). The model is also developed by including a dissipation term which is based on the probabilistic approach of Thornton and Guza (1983). The last term in the equation indicates the dissipation term discussed in detail in the next section. Figure 2.1 shows the comparison of the model of Mase and Kirby (1992) with case 2 of their experimental data set.

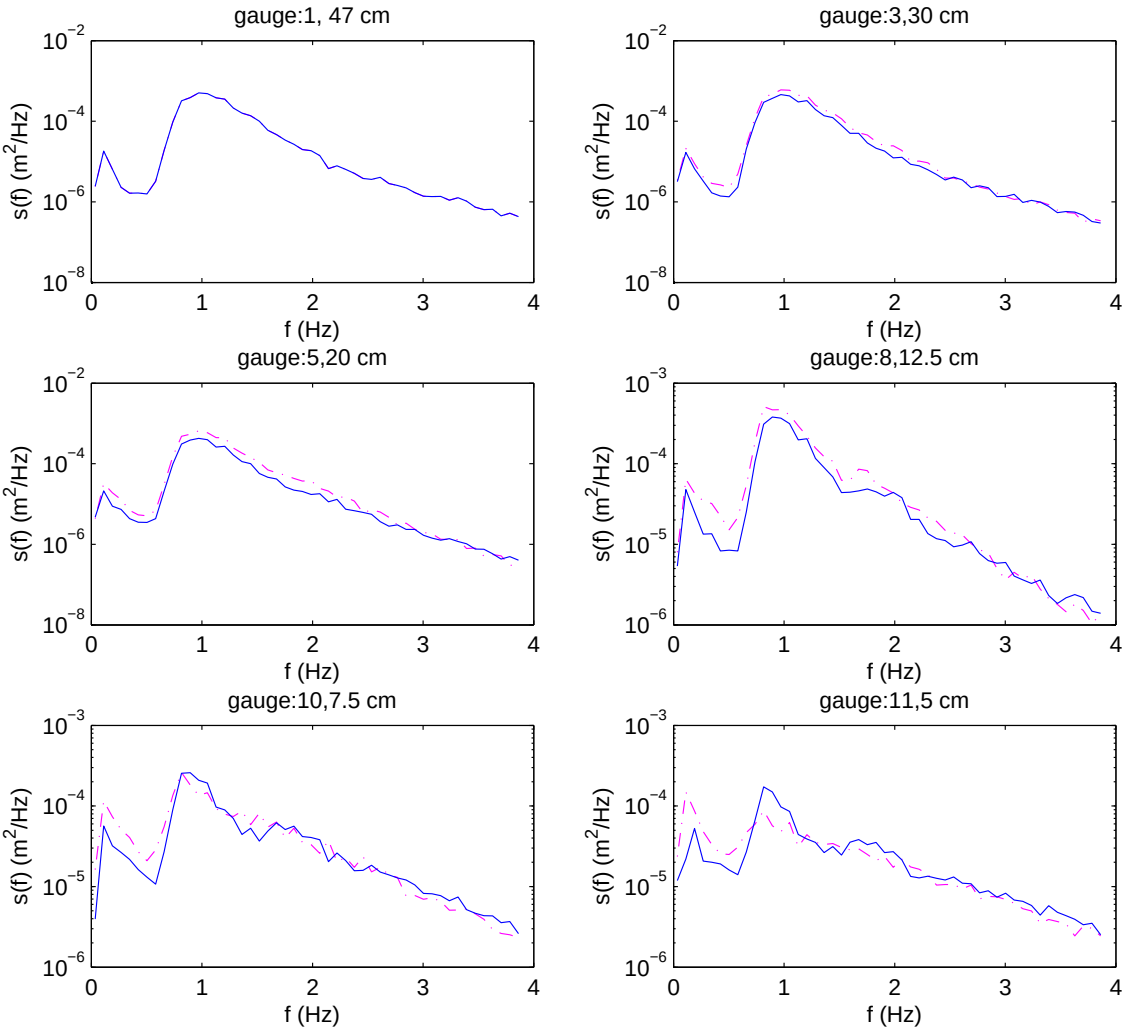

Figure 2.1: Verification of the hybrid model of Mase and Kirby (1992) with Case 2 of their experimental data set. (The blue line is the measured data and the magenta dash-dot is the model results. Depths are calculated from wavemaker)

2.3 Kaihatu and Kirby (1995)

In contrast to the two aforementioned Boussinesq-type models, this model uses the depth dependence from fully dispersive linear theory so as such is not limited to shallow water. The model not only includes the exact linear dispersion relation and shoaling terms, but also considers the phase mismatches between different frequencies. The model was derived as a parabolic two dimensional model. In this study, we analyze the one-dimensional version of the model which is formulated as

$$A_{nx} + \frac{c_{gx}}{2c_g}A_n + \alpha_n A_n = -\frac{i}{8kcc_g}\left(\sum_{l=1}^{n-1} RA_l A_{n-1} e^{i\int (k_l + k_{n-l} - k_n)dx} + 2\sum_{l=1}^{N-n} SA_l^* A_{n+l} e^{i\int (k_{n+l} - k_l - k_n)dx}\right) \quad (2.3)$$

where c is the wave celerity and R and S are nonlinear coefficients.

$$R = \frac{g}{\omega_l \omega_{n-l}}[\omega_n^2 k_l k_{n-l} + (k_l + k_{n-l})(\omega_{n-l}k_l + \omega_l k_{n-l})\omega_n] - \frac{\omega_n^2}{g}(\omega_l^2 + \omega_l\omega_{n-l} + \omega_{n-l}^2) \quad (2.4)$$

$$S = \frac{g}{\omega_l \omega_{n+l}}[\omega_n^2 k_l k_{n+l} + (k_{n+l} - k_l)(\omega_{n+l}k_l + \omega_l k_{n+l})\omega_n] - \frac{\omega_n^2}{g}(\omega_l^2 + \omega_l\omega_{n+l} + \omega_{n+l}^2) \quad (2.5)$$

The phase mismatches (the complex exponential terms in the nonlinear summations) dictate the degree to which the individual components are "locked"; a high degree of locking (small phase mismatch) indicates significant nonlinear energy exchange.

2.4 Eldeberky and Madsen (1999)

Based on the approach of Agnon et al. (1993) and Kaihatu and Kirby (1995), this model was formulated for transformation of waves from deep to shallow water.

Eldeberky and Madsen (1999) incorporated additional second order terms using the successive approximation method. The resulting model is:

$$A_{nx}+\frac{c_{gx}}{2c_g}A_n+\alpha_n A_n+i\left(\sum_{l=1}^{n-1}R'A_lA_{n-1}e^{i\int(k_n-k_l-k_{n-l})dx}-2\sum_{l=1}^{N-n}S'A_l^*A_{n+l}e^{i\int(k_n+k_l-k_{n+l})dx}\right)=0 \tag{2.6}$$

where

$$R' = \frac{\omega_n}{8g\ \omega_l\ \omega_{n-l}\ c_g}\left[g^2\omega_n^{-1}(\omega_{n-l}k_l^2+\omega_l k_{n-l}^2)+\left(2-\frac{2\ c_g\ (k_n-k_l-k_{n-l})}{\omega_n}\right)\right.$$
$$\left. g^2k_lk_{n-l}+\left(1-\frac{2\ c_g\ (k_n-k_l-k_{n-l})}{\omega_n}\right)(\omega_l^2\omega_{n-l}^2-\omega_n^2\omega_l\ \omega_{n-l})\right] \tag{2.7}$$

$$S' = \frac{\omega_n}{8g\ \omega_l\ \omega_{n+l}\ c_g}\left[g^2\omega_n^{-1}(\omega_{n+l}k_l^2+\omega_l k_{n+l}^2)-\left(2-\frac{2c_g(k_n+k_l-k_{n+l})}{\omega_n}\right)\right.$$
$$\left. g^2k_l.k_{n+l}+\left(1-\frac{2c_g(k_n+k_l-k_{n+l})}{\omega_n}\right)(\omega_l^2\omega_{n+l}^2-\omega_n^2\omega_l\omega_{n+l})\right] \tag{2.8}$$

Figure 2.2 shows the comparison of the model of Eldeberky and Madsen (1999) with the Mase and Kirby (1992) experimental data set.

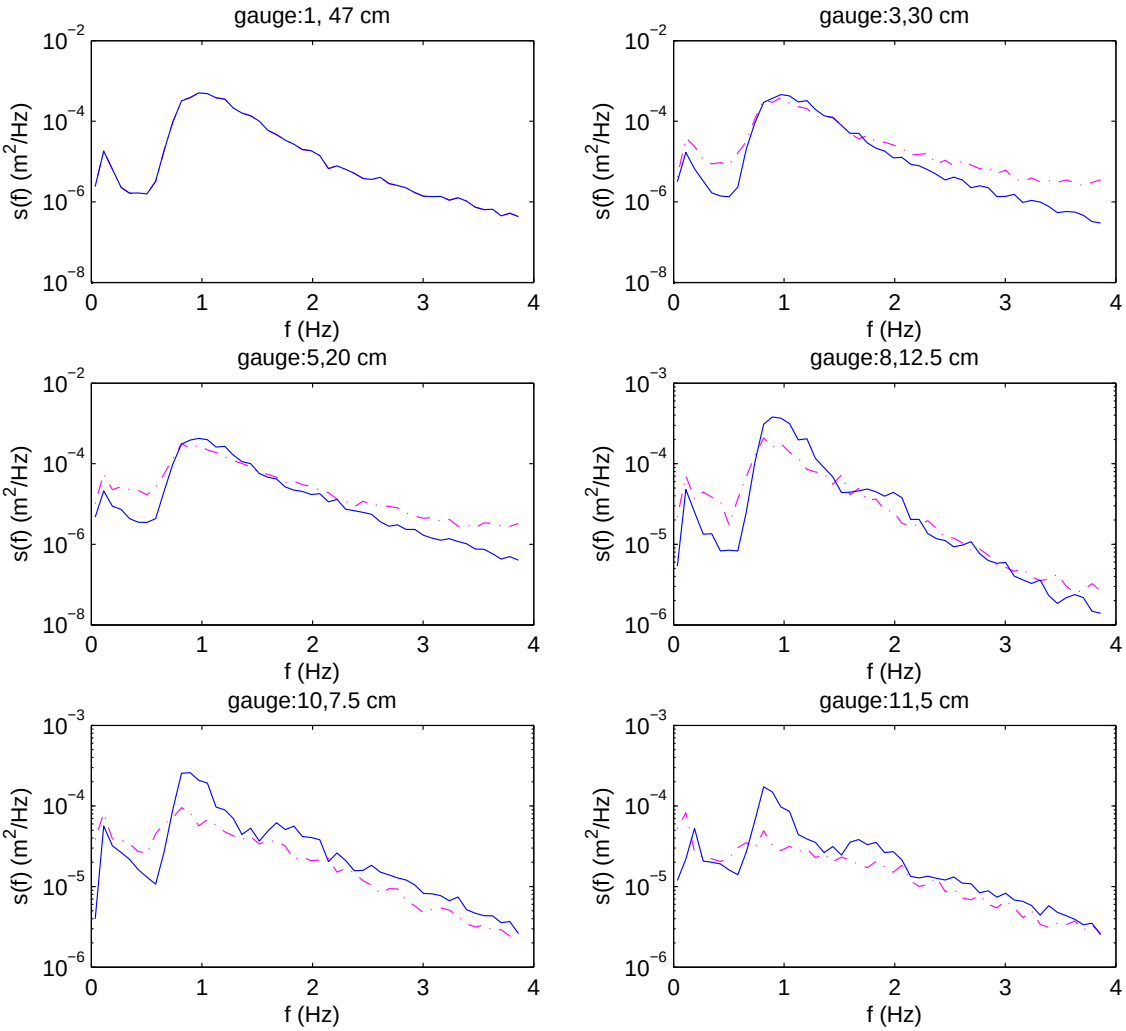

Figure 2.2: Verification of the model of Eldeberky and Madsen (1999) with Mase and Kirby (1992) data set. (The blue line is the measured data and the magenta dash-dot is the model results. Depths are calculated from wavemaker)

2.5 Comparison of the models with field data set

In this study, the Duck94 8-meter array field data set carried out in Fall 1994 during the two months of September and October is used to validate the behavior of nearshore models against data. Pressure gauges were used to record pressure at a sampling rate of 2 Hz which was then converted to free surface elevation. Each 3-hour free surface elevation time series is divided into 21 realizations of 512 seconds. These are several issues associated with the conversion between pressure and free surface elevation. The conversion becomes problematic at high frequencies, often overestimating the energy in this range. Additionally, the presence of bubbles in breaking waves may also affect the conversion. Figure 2.3 presents the schematic plan view and section view with the location of interested gauges of Duck94 area.

One problem with using measurments from pressure gauges is that high frequency motions are often unsampled because the wave motions are strongly attenuated. This can be a problem for nonlinear models, since their accuracy depends on the total variance retained in the simulation (Kaihatu and Kirby 1996). Additionally, the high frequency "cutoff" meant to address the attenuation will move to higher frequencies in shallower water; If a model had used deeper water conditions for initialization, these high frequencies would not be included in the simulation. One means to address this problem is by the addition of a high-frequency "tail" to the spectrum. Following Smith and Vincent (2003), Zakharov (1999) and Toba (1973); Kaihatu et al. (2007) defined the form of the high-frequency tail as

$$s(f) = \frac{2\pi}{cg}.s(k) \tag{2.9}$$

$$s(k) = \alpha_z k^{-4/3} \qquad kh < 1 \tag{2.10}$$

$$s(k) = \alpha_t k^{-5/2} \qquad kh > 1 \tag{2.11}$$

where $s(f)$ and $s(k)$ denote frequency spectra and wave number spectra respectively. α_z and α_t are obtained coefficients obtained from curve fitting. The wave number spectra is calculated using (2.10) and (2.11) and is transformed to frequency spectra via (2.9). The behavior of nearshore models to estimate the wave spectra against field data for two cases of "with" and "without" improvement of the higher frequency tail is compared. For this aim, the higher frequency tail of the input spectra was incorporated according to Kaihatu et al. (2007) and a series of simulations was carried out before and after enhancement of the input spectra. Figure 2.4 shows how the ability of the model to estimate the evolution of the spectra is improved by adding a tail to offshore spectra. Thus the first motivation for this study is to improve the functionality of the model at higher frequencies.

Although the performance of the models is improved after adding a high frequency tail to offshore spectra, there are still deviations between the model results and the measured field data, particularly in higher frequencies. Additionally, the high frequency tail offers no phase information, so random phases must be assumed. Hence, the second motivation of this study is to improve the behavior of the nearshore models in estimation of either spectral shape or higher order shape parameters at higher frequencies. For this aim, we focus on the model of Kaihatu and Kirby (1995), hereinafter KK95, as a reference and compare it with different types of nearshore models. The results of comparison between the reference model and the consistent model of Freilich and Guza (1984), hereinafter FG84, shows that despite the fact that the reference model has a better agreement with the measured data in terms of spectral analysis, it is not as good in estimation of wave shape parameters, particularly for skewness. Figure 2.5 to 2.8 show the comparison of each model to the estimates of

the statistical parameters of waves and Figure 2.9 shows the comparison of spectra form of these two models. The Duck94 data set for the two months of September and October 1994 is used for comparison with model results. These results compel us to review the physical aspects of each model. It is hypothesized that the reference model is not performing this transition from a partially unlocked state to a locked state correctly, and the incorporation of a third order bound wave component in the model (not presently incorporated) would improve this transition. It is anticipated that, with this improvement, the waves will accurately transition from unlocked, non-interacting waves to nearly resonant, locked waves as they transverse from deep to shallow water. We expect that the model can be improved by adding the third order bound waves since they generate coupling conditions among higher frequency components which are relevant for deep water. Therefore, the proposed model is a third order fully dispersive model with improvements in higher frequency part of the spectra and in estimation of higher order statistical parameters.

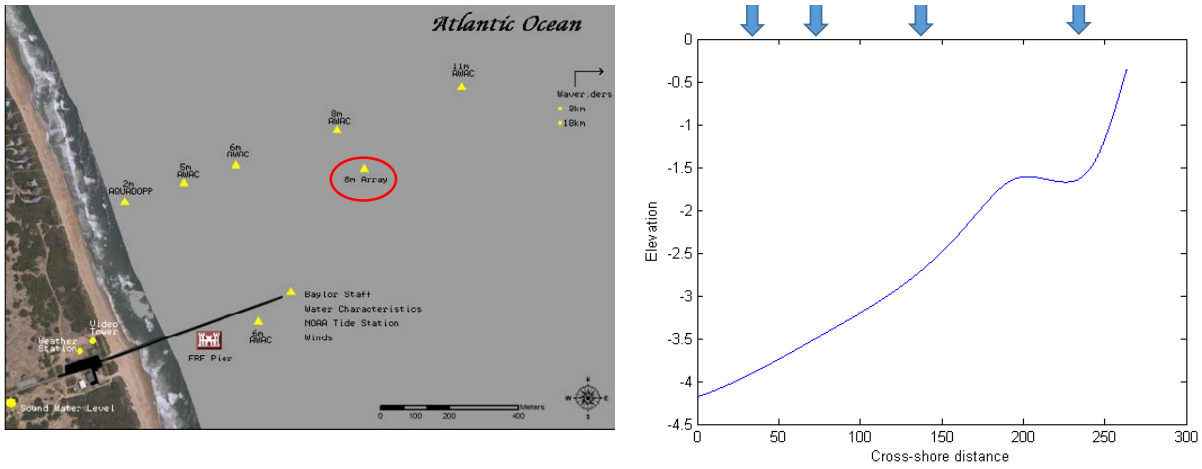

Figure 2.3: Schematic view of Duck 94 experiment, U.S. Army Field Research Facility at Duck, North Carolina, USA (Birkemeier and Thornton, 1994), Left: Plan view; Right: Section view

2.6 Summary

Our analysis so far consists of evaluation of different nearshore models and their skill in estimation of spectra and higher order wave velocity statistics. For this reason, four different nearshore wave models (the fully dispersive models of Kaihatu and Kirby 1995, Eldeberky and Madsen 1999, and Mase and Kirby 1992 ; and the consistent shoaling model of Freilich and Guza 1984) are compared to field and experimental data sets. The dissipation formulation of Thornton and Guza (1983) is applied to all four models to have equal conditions for comparisons. The free parameters in the breaking dissipation term for all models are calculated according to Apotsos et al. (2008) (dissipation mechanism due to the wave breaking is extensively explained in chapter 4).

In this chapter, four aforementioned nearshore wave models were reproduced and examined against the Mase and Kirby (1992) laboratory dataset. Comparisons show that the model of Eldeberky and Madsen (1999) does not add any improvements to the model of Kaihatu and Kirby (1995). The hybrid model of Mase and Kirby (1992) performs well, however this model is not mathematically consistent. Moreover, despite the fact that the higher frequncy part of the spectra in this model agrees well compare to other models, the performance of the model in lower frequencies is not as good as the model of Freilich and Guza (1984) and Kaihatu and Kirby (1995).

In addition, the nearshore wave models were also compared to Duck 94 field data. The modeling outputs were compared in terms of spectra at different gauge locations for different initial wave conditions in two different cases of with and without adding offshore spectra tail. The results of the analysis show that the offshore spectra tail improves the results of modeling in terms of spectral analysis especially for higher frequencies. It proves that part of the difference between model results and real field data is due to loss of higher frequency information in pressure gauges used for measuring the free surface elevation. Moreover, it identifies that nearshore models cannot estimate the higher order stochastic parameters (skewness and asymmetry) even after adding offshore spectra tail.

Generally, it is shown that in all of these models, the skill in estimation of the higher order statistics such as free surface elevation skewness and asymmetry is not as good as root mean square wave height and variance (Figure 2.5 to 2.8). In addition, it is shown that the problematic behavior of these models is generally evident at higher frequencies. From these preliminary comparison, it is concluded that we need a "consistent" model which is more accurate prediction of energy in higher frequencies prediction and higher order statistical parameters.

Comparisons between two models of Kaihatu and Kirby (1995) and Freilich and

Guza (1984) for statistical parameters of waves shows that although the model of Kaihatu and Kirby (1995) has a better agreement for $Hrms$ compare to the other model, it still needs more improvements for higher order statistical parameters: skewness and asymmetry.

In the next chapter, we investigate ways of ameliorating the behavior of the fully dispersive model of Kaihatu and Kirby (1995) and reformulations of this fully dispersive nonlinear wave model to account for the bound-wave portion of the high frequency waves. Thus, this study consists of developing a model that connects the deep water physics with those of shallow water. This model is expected to be mathematically consistent, which means that the transformation of energy from deep to shallow water and transitions between these asymptotes in intermediate water depth matches properly. This model should not only satisfies Stokes waves characteristics and quartet wave interactions for deep water but also takes into account the near resonant energy transformation of triad wave-wave interactions for nearshore regions. We would anticipate that the model would be better able to estimate spectral density at high frequencies with the inclusion of these third order terms. More accurate results of the spectra and wave shape lead to better estimation of longshore sediment transports, offshore and onshore sandbar motion and surf zone morphology. Additionally, breaking wave dissipation is also enhanced in the high frequency range; we will determine necessary alterations to our present dissipation scheme to improve high frequency wave prediction.

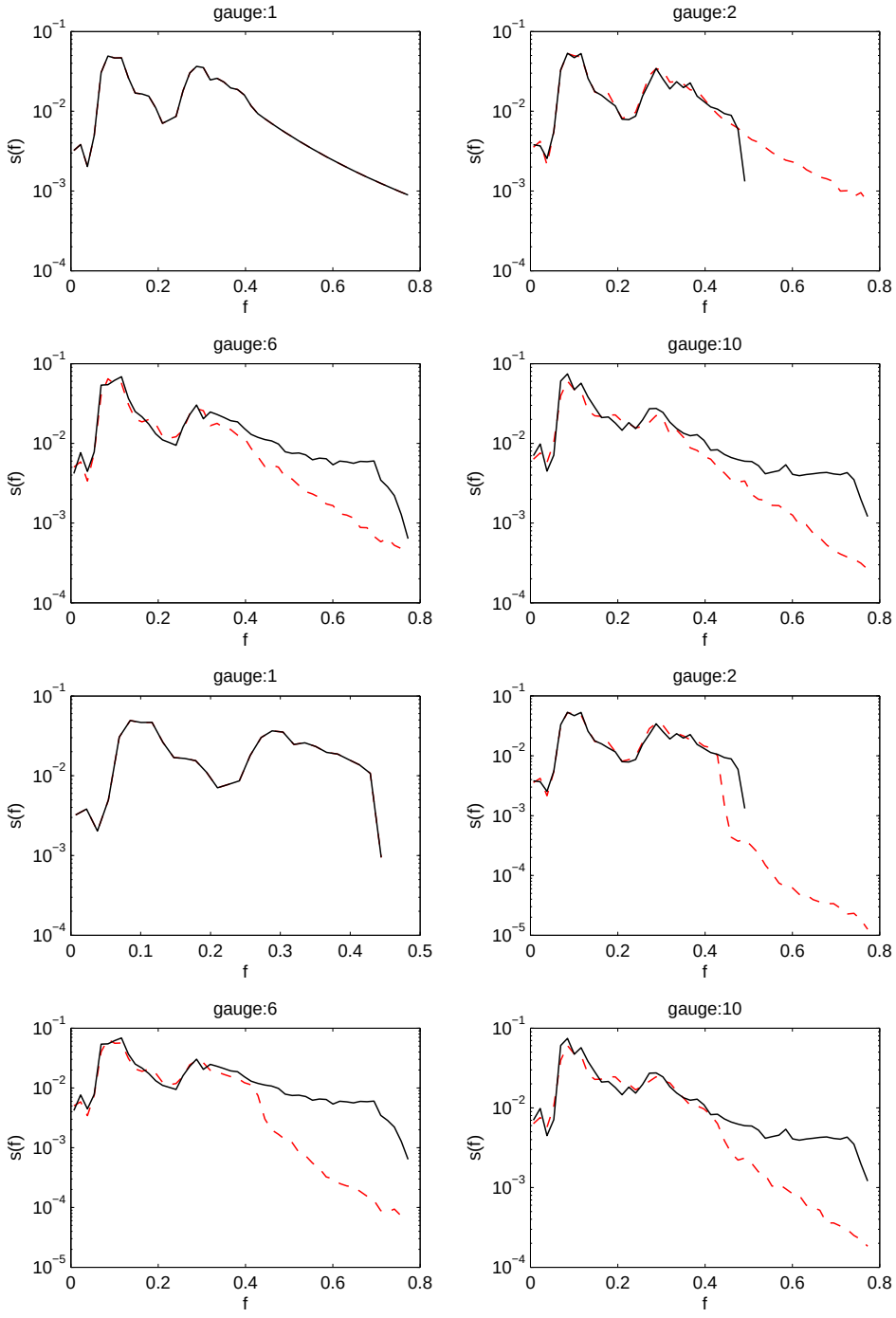

Figure 2.4: Comparison of spectra for model of Kaihatu and Kirby (1995) and Duck 94 field data set with (top four) and without using tail (bottom four) for offshore spectra (line: measured field data and dash-line: model result.)

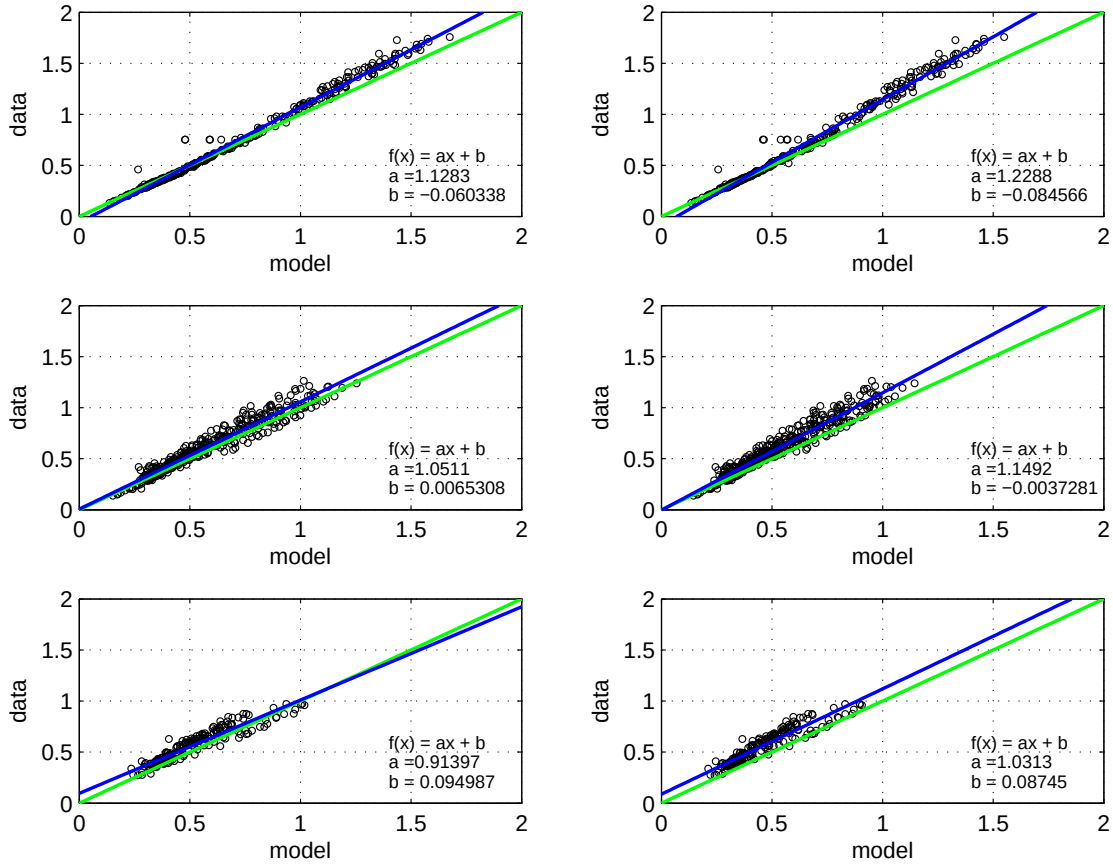

Figure 2.5: Comparison of Kaihatu and Kirby (1995) and Freilich and Guza (1984) with measured data for Hrms. (from top to bottom, gauge no.2, 6 and 10 sorted from offshore to nearshore. Left: model of Freilich and Guza (1984) ; Right: model of Kaihatu and Kirby (1995). The green and the blue lines are the 45 degree line and the best fit line respectively.)

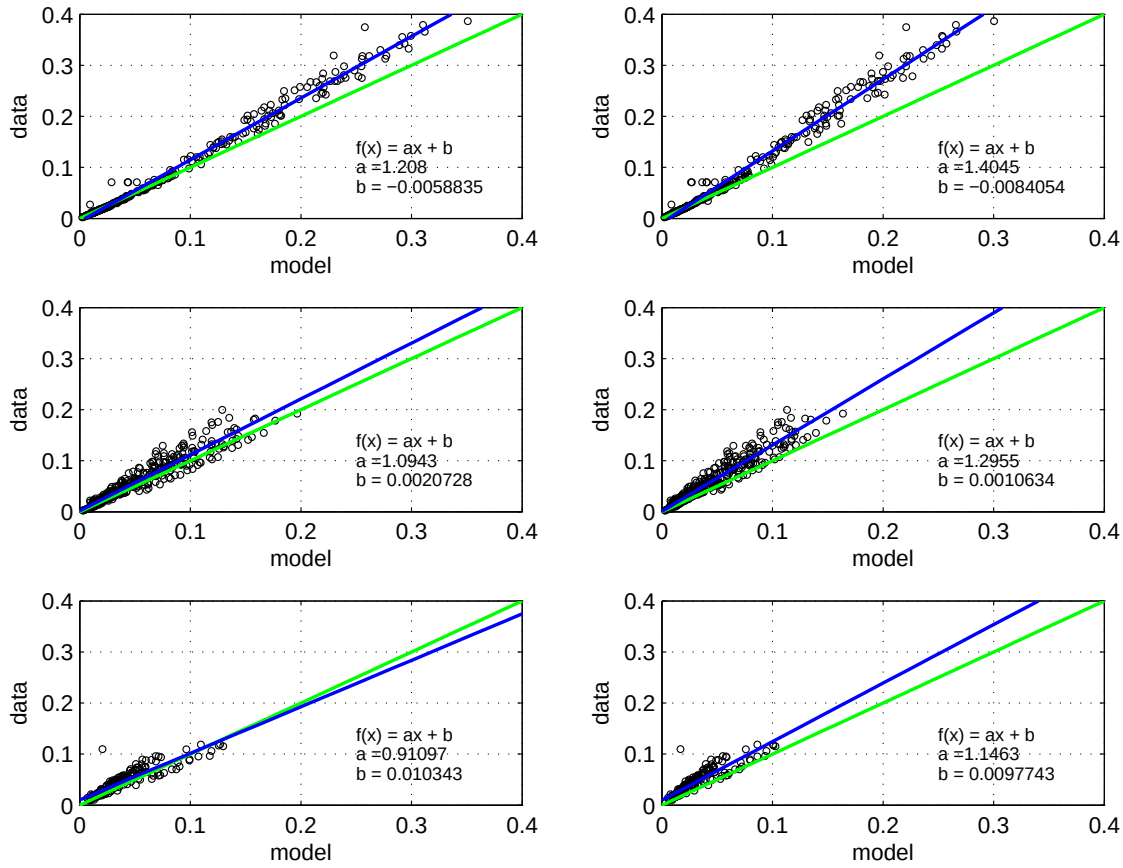

Figure 2.6: Comparison of Kaihatu and Kirby (1995) and Freilich and Guza (1984) with measured data for variance. (from top to bottom, gauge no.2, 6 and 10 sorted from offshore to nearshore. Left: model of Freilich and Guza (1984) ; Right: model of Kaihatu and Kirby (1995). The green and the blue lines are the 45 degree line and the best fit line respectively.)

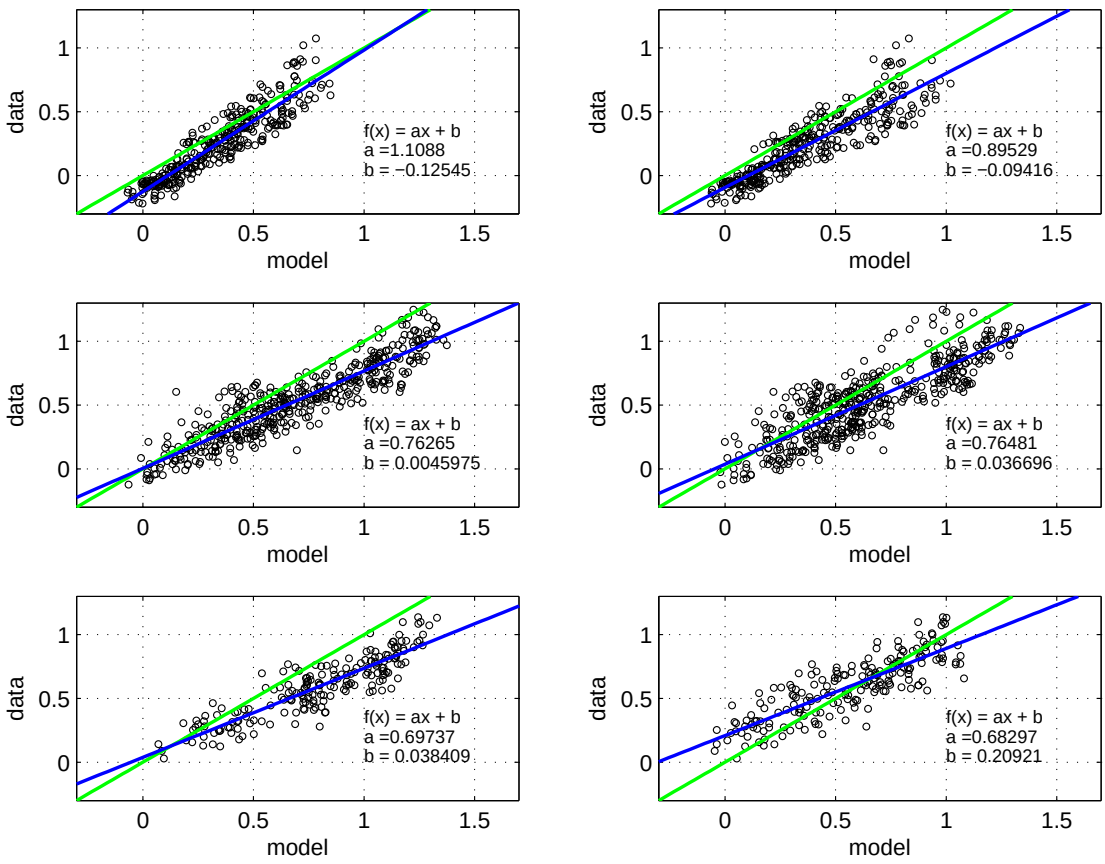

Figure 2.7: Comparison of Kaihatu and Kirby (1995) and Freilich and Guza (1984) with measured data for skewness. (from top to bottom, gauge no.2, 6 and 10 sorted from offshore to nearshore. Left: model of Freilich and Guza (1984) ; Right: model of Kaihatu and Kirby (1995). The green and the blue lines are the 45 degree line and the best fit line respectively.)

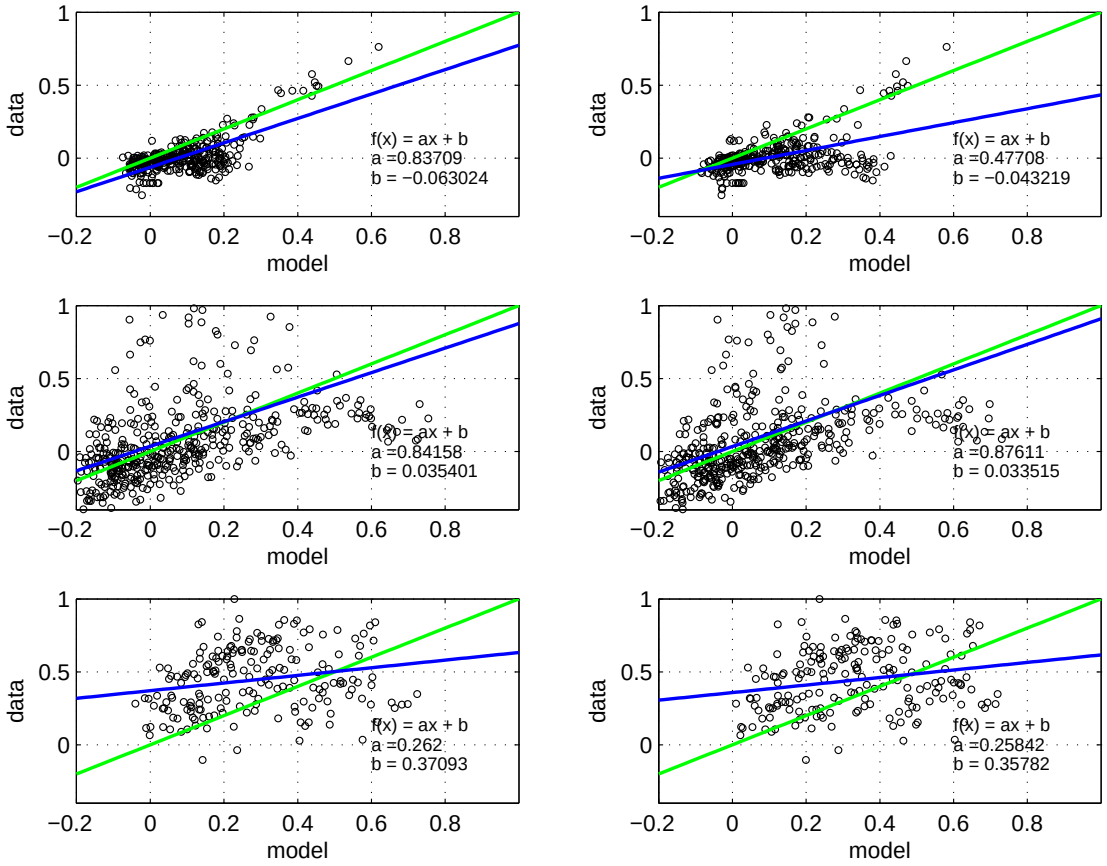

Figure 2.8: Comparison of Kaihatu and Kirby (1995) and Freilich and Guza (1984) with measured data for asymmetry. (from top to bottom, gauge no.2, 6 and 10 sorted from offshore to nearshore. Left: model of Freilich and Guza (1984) ; Right: model of Kaihatu and Kirby (1995). The green and the blue lines are the 45 degree line and the best fit line respectively.)

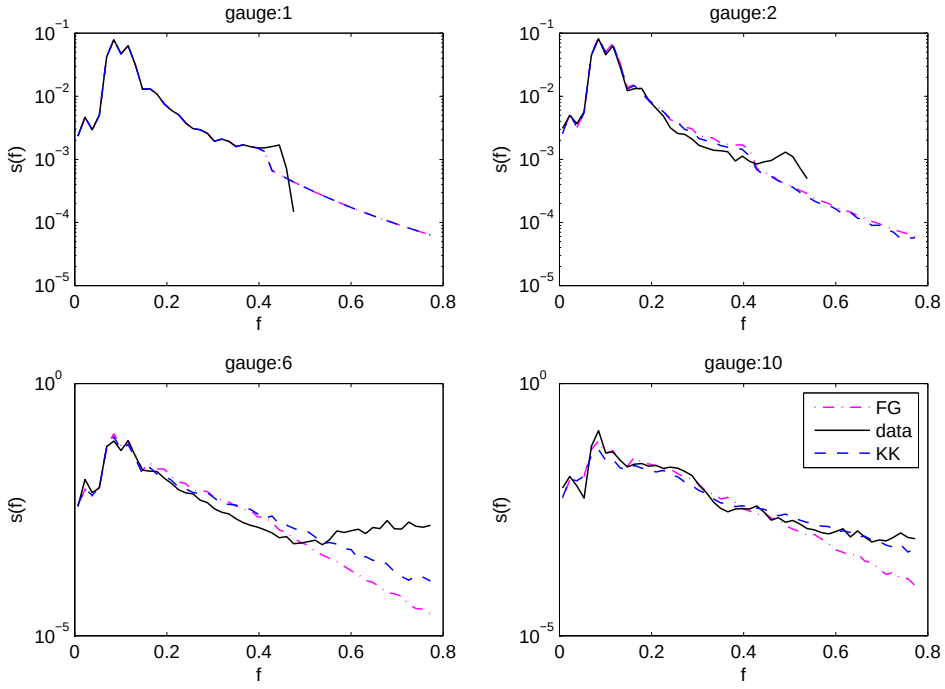

Figure 2.9: Comparison of model of Kaihatu and Kirby (1995) and Freilich and Guza (1984) with Duck94 field data set. (gauge no.2, 6 and 10 sorted from offshore to nearshore)

3. FULLY DISPERSIVE NONLINEAR WAVE MODEL

While the Boussinesq-based nearshore model in this study (i.e. the consistent model of Freilich and Guza 1984) shows good agreement with data, it has restrictions for application in deep water where the dispersiveness of the waves is a dominant feature. The fully dispersive nonlinear wave models (e.g. Kaihatu and Kirby 1995) have the ability to extend to intermediate and deep water. Kaihatu (2001) showed that these models can under certain conditions, replicate the features of Stokes-type waves in deep water. The nonlinear interaction coefficients in these models dictate the amount of energy exchanged among the frequencies (Kaihatu 1995).

The aim of this chapter is to reformulate the fully dispersive nonlinear wave model of Kaihatu and Kirby (1995) to improve the behavior of the model at high frequencies. Begining with the boundary value problem and the mild slope approximation, the new version of this model is derived mathematically and numerically. We hypothesize that the developed model will provide better estimation for higher frequencies energy evolution.

3.1 Model assumptions

It is assumed that the fluid is incompressible, inviscid and the flow is irrotational. The coordinate system is Cartesian, (x, z) with its origin placed at still water level. The $x-$axis and $z-$axis are positive shoreward and upward respectively. The model is derived in one horizontal dimension. The initial condition for the model consists of time series of free surface elevation, $\eta(t)$, where t denotes time. The free surface elevation is measured from $z = 0$.

3.2 Mathematical derivation of the model in freqency domain

As it is shown so far, most of the previous nearshore models have some limitations for higher frequency bands and they are not able to estimate higher order statistical parameters of waves accurately. To improve the performance of nearshore models, we derive a new model that takes into account the effects of third order bound waves. Assuming the fluid is inviscid and irrotational, the boundary value problem for velocity potential in non-dimensional form is formulated as

$$\nabla_h^2\phi + \phi_{zz} = 0 \qquad -h < z < \epsilon\eta \tag{3.1}$$

$$\phi_z = -\nabla_h h.\nabla_h\phi \qquad z = -h \tag{3.2}$$

$$\eta + \phi_t + \frac{\epsilon}{2}\left[(\nabla_h\phi)^2 + \phi_z^2\right] = 0 \qquad z = \epsilon\eta \tag{3.3}$$

$$\eta_t - \phi_z + \epsilon\nabla_h\eta.\nabla_h\phi = 0 \qquad z = \epsilon\eta \tag{3.4}$$

where $\nabla = (\partial/\partial x, \partial/\partial y)$ and subscripts denote partial derivatives. The velocity potential is denoted as ϕ, free surface elevation is η, h is the water depth and ϵ (ka, where a is the characteristic amplitude) is the wave steepness or nonlinearity parameter. We expand the last two equations above, which are the dynamic and kinematic free surface boundary conditions (equations (3.3) and (3.4) respectively), using Taylor series about $z = 0$

$$\eta + \phi_t + \epsilon\eta\phi_{zt} + \frac{\epsilon^2}{2}\eta^2\phi_{zzt} + \frac{\epsilon}{2}[(\nabla_h\phi)^2 + \phi_z^2] + \frac{\epsilon^2}{2}\eta[(\nabla_h\phi)^2 + \phi_z^2]_z + HOT \tag{3.5}$$

$$\eta_t - \phi_z + \epsilon\nabla_h\eta.\nabla_h\phi - \epsilon\eta\phi_{zz} - \frac{\epsilon^2}{2}\eta^2\phi_{zzz} + \frac{\epsilon^2}{2}\eta[\nabla_h\eta.\nabla_h\phi] + HOT \tag{3.6}$$

where HOT abbreviates the Higher Order Terms that are neglected. After combining the two free surface boundary conditions, perturbation analysis, substituting $\eta = -\phi_t$ and Laplace governing equation and dimensionalizing, the wave equation for each order is written as,

Second order:

$$\phi_z = -\frac{1}{g}[\phi_{tt} + \frac{1}{2}(\nabla_h\phi)_t^2 + \frac{1}{2}(\phi_z)_t^2 - \frac{1}{2g}(\phi_t)_{zt}^2 + \nabla_h.(\phi_t\nabla_h\phi)] \qquad z = 0 \qquad (3.7)$$

Third order:

$$\phi_z = -\frac{1}{g}\phi_{tt} + \frac{1}{2}[(\phi_t^2(\nabla_h^2\phi)_t]_t - \frac{1}{2}\left\{\phi_t\left[(\nabla_h\phi)^2 + \phi_z^2\right]_z\right\}_t + \frac{1}{2}\phi_t^2(\nabla_h^2\phi)_z - \frac{1}{2}\phi_t(\nabla_h\phi_t\nabla_h\phi)_z \qquad (3.8)$$

Following the method of Smith and Sprinks (1975), the linear mild slope equation is constructed by separation of the depth dependency term and summation of the solutions

$$\phi = \sum_{n=1}^{\infty} f_n(k_n, h, z)\widetilde{\Phi}_n(x, y, k_n, \omega_n, t) \qquad (3.9)$$

and

$$f_n = \frac{\cosh k_n(h+z)}{\cosh k_n h} \qquad (3.10)$$

where f_n is the depth dependency term, k_n is the total wave number and ω_n is the angular frequency. Moreover, Kaihatu and Kirby (1995) applied Green's second identity to f_n and $\widetilde{\Phi}_n$ as follows

$$\int_{-h}^{0} \{f_n\widetilde{\Phi}_n - \widetilde{\Phi}_n f_{nzz}\}\, dz = [f_n\widetilde{\Phi}_{nz} - \widetilde{\Phi}_n f_{nz}]_{-h}^{0} \qquad (3.11)$$

Plugging $f_n(0) = 1$ and substituting the boundary condition equation (equation

3.7 for second order and equation 3.8 for third order) into (3.11), the primary form of the equation is written as

Second order:

$$\frac{1}{g}\widetilde{\Phi}_{n_{tt}}+F_1\widetilde{\Phi}_n-\nabla.[F_2\nabla\widetilde{\Phi}_n]=-\frac{1}{g}\left[\frac{1}{2}(\nabla_h\widetilde{\Phi}_n)_t^2+\frac{1}{2}(\widetilde{\Phi}_{nz})_t^2-\frac{1}{2g}(\widetilde{\Phi}_{nt})_{zt}^2+\nabla_h.(\widetilde{\Phi}_{nt}\nabla_h\widetilde{\Phi}_n)\right] \tag{3.12}$$

Third order:

$$\begin{aligned}\frac{1}{g}\widetilde{\Phi}_{n_{tt}}+F_1\widetilde{\Phi}_n-\nabla.[F_2\nabla\widetilde{\Phi}_n]= \quad & -\frac{1}{g}\left[\frac{1}{2}[(\widetilde{\Phi}_t^2(\nabla_h^2\widetilde{\Phi})_t]_t-\frac{1}{2}\left\{\widetilde{\Phi}_t\left[(\nabla_h\widetilde{\Phi})^2+\widetilde{\Phi}_z^2\right]_z\right\}_t\right. \\ & \left.+\frac{1}{2}\widetilde{\Phi}_t^2(\nabla_h^2\widetilde{\Phi})_z-\frac{1}{2}\widetilde{\Phi}_t(\nabla_h\widetilde{\Phi}_t\nabla_h\widetilde{\Phi})_z\right]\end{aligned} \tag{3.13}$$

where

$$F_1=\frac{1}{\cosh^2\ k_nh}\left[\frac{\cosh\ 2k_nh}{4k_n}-\frac{1}{4k_n}-\frac{h}{2}\right] \tag{3.14}$$

$$F_2=\frac{1}{\cosh^2\ k_nh}\left[\frac{\cosh\ 2k_nh}{4k_n}-\frac{1}{4k_n}+\frac{h}{2}\right] \tag{3.15}$$

The nonlinear terms at right-hand side of (3.12), the second order equation, are treated as triad wave-wave interaction to exchange energy among frequencies. Herein, two arbitrary frequency modes, l and m are chosen

$$\frac{1}{g}\widetilde{\Phi}_{n_{tt}} + F_1\widetilde{\Phi}_n - \nabla.[F_2\nabla\widetilde{\Phi}_n] =$$
$$\frac{1}{2}\Bigg[\sum_l\sum_m\Bigg\{\frac{k_l\tanh k_l h + k_m\tanh k_m h}{g}(\widetilde{\Phi}_{l_t}\widetilde{\Phi}_{m_t})_t$$
$$-(k_l\tanh k_l h)(k_m\tanh k_m h)(\widetilde{\Phi}_l\widetilde{\Phi}_m)_t\Bigg\}$$
$$-\sum_l\sum_m\Bigg\{[\nabla_n\widetilde{\Phi}_l.\nabla_n\widetilde{\Phi}_m]_t + \nabla_n.[\widetilde{\Phi}_{l_t}\nabla_n\widetilde{\Phi}_m]$$
$$+\nabla n.[\widetilde{\Phi}_{m_t}\nabla_n\widetilde{\Phi}_l]\Bigg\}\Bigg] \tag{3.16}$$

In order to split up the spatial dependent quantities (quantities that are dependent on x), multiple scale analysis is used. One of the advantages of multiple scale analysis is that the quantity is physically separated at each order. It is assumed that the spatial variable is defined for different scales

$$x = x + \epsilon\, x + \epsilon^2\, x \tag{3.17}$$

$$x = x + X_1 + X_2 \tag{3.18}$$

Therefore, for each order, there are some other terms in the equations obtained by slow varying assumption of x that has not been shown here. According to Freilich and Guza (1984), the amplitude and phase function is assumed to vary slowly in x. Hence the solutions for each order is defined in the following form

$$\widetilde{\Phi}_{1n} = \frac{-ig}{2\omega_n}a_n(X_1)e^{i\Psi_n} \tag{3.19}$$

$$\widetilde{\Phi}_{2n} = \frac{-ig}{2\omega_n}a_n(X_2)e^{i\Psi_n} \tag{3.20}$$

where $\Psi_n = \psi_n(x) - \omega_n t$. This is referred to as a "phase function" and includes both spatial and temporal terms. The real-valued amplitude is a_n.

The nonlinearity in the model occurs due to the existence of velocity potential products in the boundary condition equations and consequently, yields the products of amplitudes. Assuming two arbitrary harmonics, l and m

$$a_l a_m e^{i(\Psi_l + \Psi_m)} \tag{3.21}$$

$$a_l a_m^* e^{i(\Psi_l - \Psi_m)} \tag{3.22}$$

$$a_l^* a_m e^{i(-\Psi_l + \Psi_m)} \tag{3.23}$$

$$a_l^* a_m^* e^{i(-\Psi_l - \Psi_m)} \tag{3.24}$$

the triad wave-wave interaction terms results in the phase function relationships

$$\Psi_n = \Psi_l + \Psi_m \tag{3.25}$$

$$\Psi_n = \Psi_l - \Psi_m \tag{3.26}$$

$$\Psi_n = -\Psi_l + \Psi_m \tag{3.27}$$

$$\Psi_n = -\Psi_l - \Psi_m \tag{3.28}$$

Assuming the following resonant conditions are satisfied among the frequency components

$$\omega_n = \omega_l + \omega_m \tag{3.29}$$

$$\omega_n = \omega_l - \omega_m \tag{3.30}$$

$$\omega_n = -\omega_l + \omega_m \tag{3.31}$$

$$\omega_n = -\omega_l - \omega_m \tag{3.32}$$

Provided we determine "m" (given l and n), the time periodicity will be canceled out by taking Fourier series in time

$$\widetilde{\Phi}_n = \frac{\widetilde{\phi}_n}{2} e^{-i\omega_n t} + \frac{\widetilde{\phi}_n^*}{2} e^{i\omega_n t} \tag{3.33}$$

After eliminating the time dependency, the second order triads, (equation (3.16)), is written as

$$\begin{aligned}
\frac{1}{g}\omega^2\widetilde{\phi}_n - F_1\widetilde{\phi}_n + \nabla.[F_2\nabla\widetilde{\phi}_n] = \\
&\frac{-i}{4g}\Bigg[\sum_l^{n-1}\Bigg\{2\omega_n\nabla_n\widetilde{\phi}_l.\nabla_n\widetilde{\phi}_{n-l} + \omega_l\widetilde{\phi}_l\nabla_n^2\widetilde{\phi}_{n-l} + \omega_{n-l}\widetilde{\phi}_{n-l}\nabla^2\widetilde{\phi}_l \\
&+ \Big[\frac{k_l\tanh k_l h + k_{n-l}\tanh k_{n-l}h}{g}(\omega_l^2\omega_{n-l} + \omega_l\omega_{n-l}^2) \\
&+ \omega_n.(k_l\tanh k_l h)(k_{n-l}\tanh k_{n-l})\Big]\widetilde{\phi}_l\widetilde{\phi}_{n-l}\Bigg\}\Bigg]_n \\
&- \frac{i}{2g}\Bigg[\sum_l^{N-l}\Bigg\{2\omega_n\nabla_n\widetilde{\phi}_l^*.\nabla_n\widetilde{\phi}_{n+l} + \omega_{n+l}\nabla_n^2\widetilde{\phi}_l^* - \omega_l\widetilde{\phi}_l^*\nabla^2\widetilde{\phi}_{n+l} \\
&+ \Big[\frac{k_l\tanh k_l h + k_{n+l}\tanh k_{n+l}h}{g}(\omega_l^2\omega_{n+l} - \omega_l\omega_{n+l}^2) \\
&+ \omega_n.(k_l\tanh k_l h)(k_{n+l}\tanh k_{n+l})\Big]\widetilde{\phi}_l^*\widetilde{\phi}_{n+l}\Bigg\}\Bigg]_n
\end{aligned} \tag{3.34}$$

The velocity potential for second and third orders is further defined as

$$\widetilde{\phi}_{1n} = \frac{-ig}{\omega_n} a(X_1) e^{i\psi} \tag{3.35}$$

$$\widetilde{\phi}_{2n} = \frac{-ig}{\omega_n} a(X_2) e^{i\psi} \tag{3.36}$$

where $\psi = \psi_n(x) = \int k_n \, dx$. Following the method of Freilich and Guza (1984), the first and second spatial derivatives of ψ in second order is written as,

$$\frac{d\psi_n}{dx} = \overline{k} + \epsilon \, k_1 \tag{3.37}$$

$$\frac{d^2\psi_n}{dx^2} = \epsilon \, \frac{d\overline{k}}{dX_1} \tag{3.38}$$

and in third order,

$$\frac{d\psi_n}{dx} = \overline{k} + \epsilon \, k_1 + \epsilon^2 \, k_2 \tag{3.39}$$

$$\frac{d^2\psi_n}{dx^2} = \epsilon \, \frac{d\overline{k}}{dX_1} + \epsilon^2 \, \frac{d\overline{k}}{dX_2} + \epsilon^2 \, \frac{dk_1}{dX_1} \tag{3.40}$$

where $\overline{k}$ is the linear or reference wave number and it is defined using the linear dispersion relation

$$\omega^2{}_n = g\overline{k} \tanh \overline{k}h \tag{3.41}$$

In (3.33), (3.35), k_1 is the modified wave number due to bottom slope and k_2 is the nonlinear wave number due to effects of bound waves.

3.2.1 Second order equation

By substituting (3.35), (3.37) and (3.38) into (3.34) and combining linear and nonlinear terms

$$2F_2a\overline{k}k_1 + 2iF_2\overline{k}\frac{da}{dx} + iF_2\frac{d\overline{k}}{dx}a + iF_{2x}a\overline{k} = \sum_{i=1}^{n-1} Ra_l a_{n-l} e^{i(\psi_l+\psi_{n-l}-\psi_n)} + \sum_{i=1}^{N-n} 2Sa_l a_{n+l} e^{i(\psi_{n+l}-\psi_l-\psi_n)} \quad (3.42)$$

where

$$R = \frac{\omega_n}{\omega_l.\omega_{n-1}}[2\omega_n k_l k_{n-l} + \omega_l k_{n-l}^2 + \omega_{n-l}k_l^2 - (\frac{k_l \tanh\ k_l h + k_{n-l}\tanh\ k_{n-l}h}{g}). (\omega_l^2\omega_{n-l} + \omega_l\omega_{n-l}^2) - \omega_n(k_l \tanh\ k_l h)\cdot(k_{n-l}\tanh\ k_{n-l}h)] \quad (3.43)$$

$$S = \frac{\omega_n}{\omega_l.\omega_{n+1}}[2\omega_n k_l k_{n+l} + \omega_l k_{n+l}^2 - \omega_{n+l}k_l^2 + (\frac{k_l \tanh\ k_l h + k_{n+l}\tanh\ k_{n+l}h}{g}). (\omega_l^2\omega_{n+l} - \omega_l\omega_{n+l}^2) + \omega_n(k_l \tanh\ k_l h)\cdot(k_{n+l}\tanh\ k_{n+l}h)] \quad (3.44)$$

$\frac{d\overline{k}}{dx}$ is calculated analytically by differentiating the linear dispersion relation

$$\frac{d\overline{k}}{dx} = \frac{dh}{dx}(\frac{-\overline{k}^2\sinh^{-2}\overline{k}h}{\tanh\overline{k}h + \overline{k}h}) \quad (3.45)$$

where $\frac{dh}{dx}$ is the variation of bathymetry and it is calculated for each step using the first order finite difference schemes.

Since a_n in the above equation is real valued, the equation is divided into real and imaginary part and finally, the resulting system of equations are solved numerically. The homogeneous part of this second order solution is cancelled out since it has been already considered previously in the first order solution. The real part of the

equation (3.42) is used to calculate k_1 and the imaginary part is solved for a

$$k_1 = \frac{1.}{2F_2 a\bar{k}}\Bigg[\sum_{i=1}^{n-1} Ra_l a_{n-l} \quad \cos(\psi_l + \psi_{n-l} - \psi_n) + \sum_{i=1}^{N-n} 2Sa_l a_{n+l} \quad \cos(\psi_{n+l} - \psi_l - \psi_n)\Bigg] \tag{3.46}$$

and

$$\frac{da}{dx} + (\frac{1}{2\bar{k}} \quad \frac{d\bar{k}}{dx} + \frac{F_{2x}}{2F_2})a = \quad \frac{-i}{2F_2\bar{k}}\Bigg[\sum_{i=1}^{n-1} Ra_l a_{n-l} \quad \sin(\psi_l + \psi_{n-l} - \psi_n) + \sum_{i=1}^{N-n} 2Sa_l a_{n+l} \quad \sin(\psi_{n+l} - \psi_l - \psi_n)\Bigg] \tag{3.47}$$

3.2.2 Third order equation

Third order part of the equation includes linear terms, quadratic wave-wave interaction terms that are generated by slowly varying assumption of x, and cubic terms that include the bound wave component.

Substituting (3.36), (3.39) and (3.40) into (3.8), the final form of equation is:

$$
\begin{aligned}
&2F_2 a_1 \overline{k} k_1 + 2iF_2 \overline{k} \frac{da_1}{dx} + \\
&\qquad iF_2 \frac{d\overline{k}}{dx} a_1 + iF_{2x} a_1 \overline{k} \\
&\qquad = \frac{1}{2} \sum_{l=1}^{n-1} -2g^2 i \frac{\omega_n}{\omega_l \omega_{n-l}} \Bigg[2\omega_n [\overline{k}_l a_l \frac{da_{n-l}}{dx} \\
&\qquad + a_{n-l} \overline{k}_{n-1} \frac{da_l}{dx} + a_l a_{n-l} (\overline{k}_l k^1_{n-l} + \overline{k}_{n-l} k^1_l) i] \\
&\qquad + \omega_l [2a_l \frac{da_{n-l}}{dx} \overline{k}_{n-l} + a_l a_{n-l} (\frac{d\overline{k}_{n-l}}{dx} + 2\overline{k}_{n-l} k^1_{n-l}) i] \\
&\qquad + \omega_{n-l} [2a_{n-l} \frac{da_l}{dx} \overline{k}_l + a_l a_{n-l} (\frac{d\overline{k}_l}{dx} + 2\overline{k}_l k^1_l) i] e^{i(\psi_l + \psi_{n-l} - \psi_n)} \Bigg] \\
&\qquad + \sum_{l=1}^{N-n} -2g^2 i \frac{\omega_n}{\omega_l \omega_{n+l}} \Bigg[2\omega_n [\overline{k}_l a_l \frac{da_{n+l}}{dx} \\
&\qquad + a_{n+l} \overline{k}_{n+1} \frac{da_l}{dx} + a_l a_{n+l} (\overline{k}_l k^1_{n+l} + \overline{k}_{n+l} k^1_l) i] \\
&\qquad - \omega_l [2a_l \frac{da_{n+l}}{dx} \overline{k}_{n+l} + a_l a_{n-l} (\frac{d\overline{k}_{n+l}}{dx} + 2\overline{k}_{n+l} k^1_{n+l}) i] \\
&\qquad + \omega_{n+l} [2a_{n+l} \frac{da_l}{dx} \overline{k}_l + a_l a_{n+l} (\frac{d\overline{k}_l}{dx} + 2\overline{k}_l k^1_l) i] e^{i(\psi_{n+l} - \psi_l - \psi_n)} \Bigg] \\
&\qquad + i \sum_n \frac{1}{4} a_n^3 \overline{k}^2 [3/8\omega_n^2 + 3/8(\overline{k}_n \tanh\ \overline{k}_n h)] e^{2i\psi_n} \qquad (3.48)
\end{aligned}
$$

The left hand side of the equation or the linear terms in the third order are analogous to those of the second order except the order of amplitude which is in third order.

3.2.3 Dissipation mechanism due to the wave breaking

One problem with incorporation of a energy dissipation mechanism based on wave statistics (e.g. Thornton and Guza 1983) is that some ad hoc means of specifying the frequency dependence of the mechanism is required. This is because these models usually assume that the wave field is narrow-banded, in which a single average frequency is considered sufficiently descriptive. Mase and Kirby (1992) provided arguments for using a frequency-squared dependence, while Eldeberky and Battjes (1996) assume that the dissipation is constant over frequency. Both provide evidence for the frequency-squared distribution, but Kirby and Kaihatu (1996) note that the inability to easily model wave motions up to the nyquist frequency might affect how well this particular distribution would work.

Following Kirby et al. (1992a), Mase and Kirby (1992) and Kaihatu and Kirby (1995), a dissipation term, $\alpha_n a_n$, is added to the linear part of the evolution equation (equation (3.47)) to have a better estimation of waves in the surf zone. The dissipation term α_n is

$$\alpha_n = \alpha_{n0} + (\frac{f_n}{f_{peak}})^2 \alpha_{n1} \tag{3.49}$$

$$\alpha_{n0} = F\beta(x) \tag{3.50}$$

$$\alpha_{n1} = (\beta(x) - \alpha_{n0}) \frac{f_{peak}^2 \sum_{n=1}^{N} |A_n|^2}{\sum_{n=1}^{N} f_n^2 |A_n|^2} \tag{3.51}$$

$$\beta(x) = \frac{3\sqrt{\pi}}{4\sqrt{gh}} \frac{B^3 f_{peak} H_{rms}^5}{\gamma^4 h^5} \tag{3.52}$$

$$H_{rms} = 2\sqrt{\sum_{n=1}^{N} |A_n|^2} \tag{3.53}$$

where β is the energy dissipation rate as dictated by Thornton and Guza (1983)

and B, γ and F are free parameters; F denotes the frequency dependency of the dissipation term. According to Kaihatu and Kirby (1996), $F = 1.0$ determines that there is no dependence on frequency for dissipation, while $F = 0$ leads to an f_n^2 dependency for dissipation.

In next section, we will compare different nearshore models to measured data by choosing similar free parameters for models. The frequency dependency parameter for all laboratory and field tests was chosen to be $F = 0$ to have the full dependency of dissipation to frequency.

3.2.4 Comparison of the mathematical model with Kaihatu and Kirby (1995)

In the present calculations, we take a different style of derivation compare to Kaihatu and Kirby (1995). The free surface amplitudes are treated as real quantities whereas in Kaihatu and Kirby (1995), the complex free surface amplitudes are used. Assuming the amplitudes are real, all nonlinear effects on dispersion are presented in the phase part of the solution (refer to (3.35) and (3.36)); thus k_n includes linear and nonlinear wave numbers. This is not a case for complex amplitudes since by assuming complex number for amplitude, the solution in terms of velocity potential is defined as

$$\widetilde{\phi}_n = \frac{-ig}{\omega_n} A_n e^{i\int k_n\, dx} \tag{3.54}$$

where k_n contains just the linear wave number ($\overline{k}$) and $A_n = a_n e^{i\theta}$, where θ represents all nonlinear phase effects and a_n is the real amplitude.

3.2.5 Comparison of the mathematical model with Janssen et al. (2006)

Janssen et al. (2006) generated a model for waves by including the effect of third order bound waves. Similar to the model of Kaihatu and Kirby (1995), the free surface amplitudes are defined as a complex number and the wave number is that

calculated by the linear dispersion relation. In contrast, in the real amplitude model developed here, we used the multiple scale assumption to define different scales of wave number. Janssen et al. (2006) also included the quadratic nonlinear coupling terms in their model. As it is mentioned earlier in chapter 1, in this model, the wave wave interaction terms switch from quartet terms to triad terms during the transformation of the waves from deep to shallow water.

3.3 Numerical analysis and verification of the model

Using the Fast Fourier Transform (FFT), the time series of free surface elevation is transfered into the frequency domain. The FFT algorithm decomposes the timeseries into its complex frequency components, $\overline{A_n}$ and $\overline{B_n}$.

$$F_n = \frac{\overline{A_n}}{2} - i\frac{\overline{B_n}}{2} \tag{3.55}$$

where F_n is the complex amplitude of the free surface elevation.

$$\eta(t) = \sum_{i=1}^{N/2} (\overline{A_n} \cos \frac{2\pi n}{T} t + \overline{B_n} \sin \frac{2\pi n}{T} t) \tag{3.56}$$

In order to adjust the definition of FFT algorithm for free surface elevation with that of the wave theory derived earlier

$$\frac{A_n}{2} = F_n^* \tag{3.57}$$

where F^* is the conjugate form of the (3.55). The outputs of the FFT are then used as an input to the wave model. A fourth order Runge Kutta is used for modeling purposes. The model outputs are generated in the form of the complex components for all of the realizations in each gauge location.

As we discussed earlier, in this model the real amplitudes are used instead of the

complex amplitudes calculated by (3.57). In order to initialize the model with real amplitudes, the complex amplitudes are replaced with their real and imaginary parts

$$a_n = \sqrt{R(A_n)^2 + I({A_n}^2)} \tag{3.58}$$

$$\psi_n = \arctan(I(A_n)/R(A_n)) \tag{3.59}$$

where R and I denote the real and imaginary part of the complex free surface amlitude respectively, a_n is the real amplitude of free surface elevation and ψ_n is the phase function.

3.3.1 Harmonic test of Chapalain et al. (1992)

One early experiment on nonlinear wave-wave interaction was carried out by Boczar-Karakiewicz et al. (1972) demonstrating the energy exchange between the first and second harmonics. Chapalain et al. (1992) investigated the energy exchange between first four harmonics for weakly nonlinear and dispersive long waves for a constant depth. This experimental model is simple but useful to illustrate the possible interactions between a limited number of frequencies. The wave characteristics for each test is shown in Table 3.1. The first four harmonics are chosen for comparison to data. The free surface amplitudes for each harmonics is calculated from the model at particular gauge locations and is compared with that of the Chapalain et al. (1992). Figures 3.1 through 3.4 illustrates the comparison of three models: model of Kaihatu and Kirby (1995), consistent model of Freilich and Guza (1984) and the real amplitude model with tests A,C, D and H of this experiment. It is apparent that the model of Freilich and Guza (1984) underpredicts the free surface amplitudes for all test cases and harmonics. The model of Kaihatu and Kirby

(1995) shows better agreement with the data compare to the other two models. This descrepancy between the model of Freilich and Guza (1984) and the experimental data probably is due to the violation of weakly dispersive limit that governs this model. The pursuit model shows a high degree of oscillation at the third and fourth harmonics, which might suggest that splitting of the wave number into components with different scales of variability might not be appropriate for this case and more investigation is required.

Table 3.1: Parameters of Chapalain et al. (1992) experiments

Trial	Water depth (m)	Wave period (s)	Ursel number
A	0.4	2.5	14.9
C	0.4	3.5	30.2
D	0.3	2.5	22.8
H	0.4	3.0	17.6

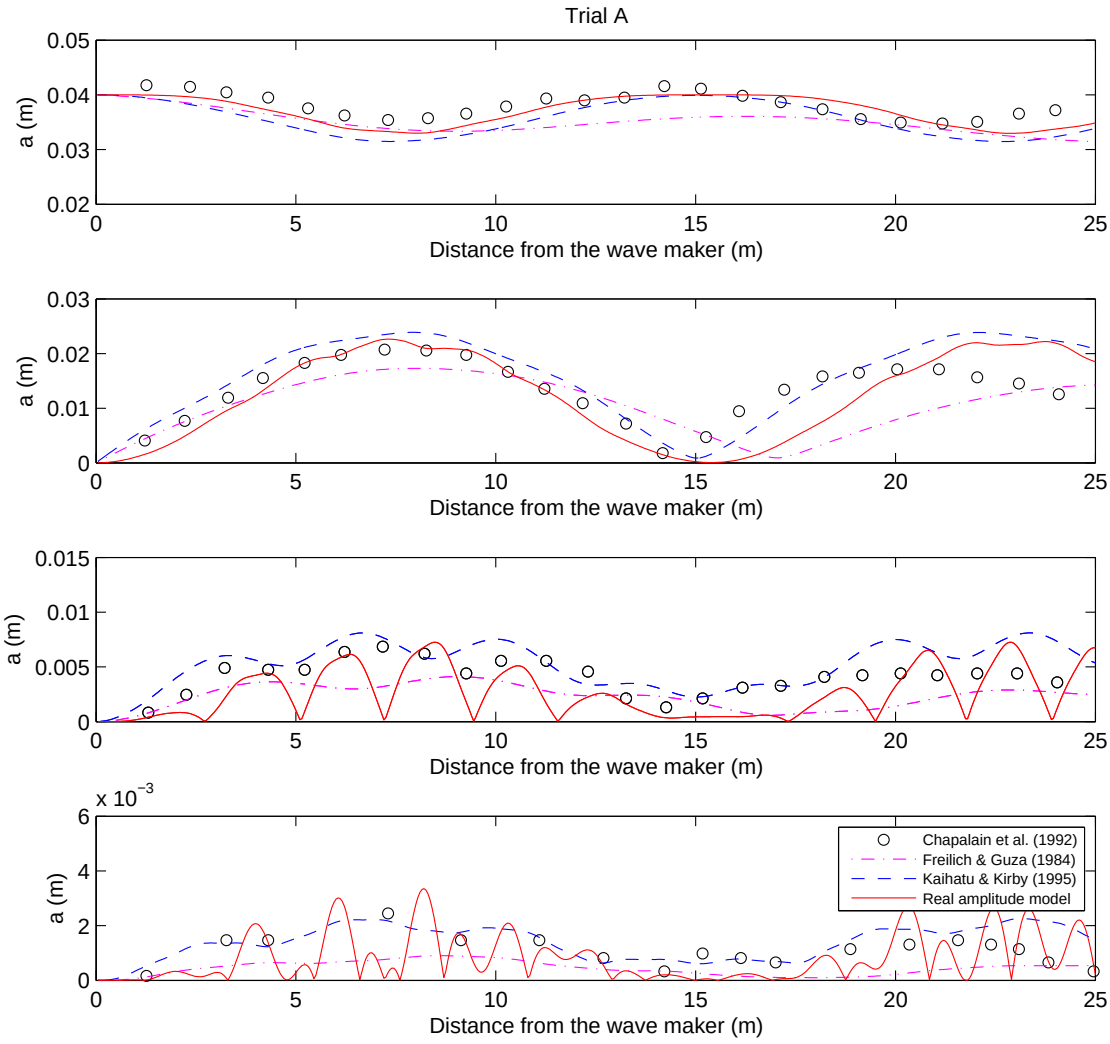

Figure 3.1: Comparison of Chapalain et al. (1992) experiment with real amplitude model, Kaihatu and Kirby (1995) mild slope model and the consistent model of Freilich and Guza (1984), $h = 0.4m$ and $T = 2.5S$

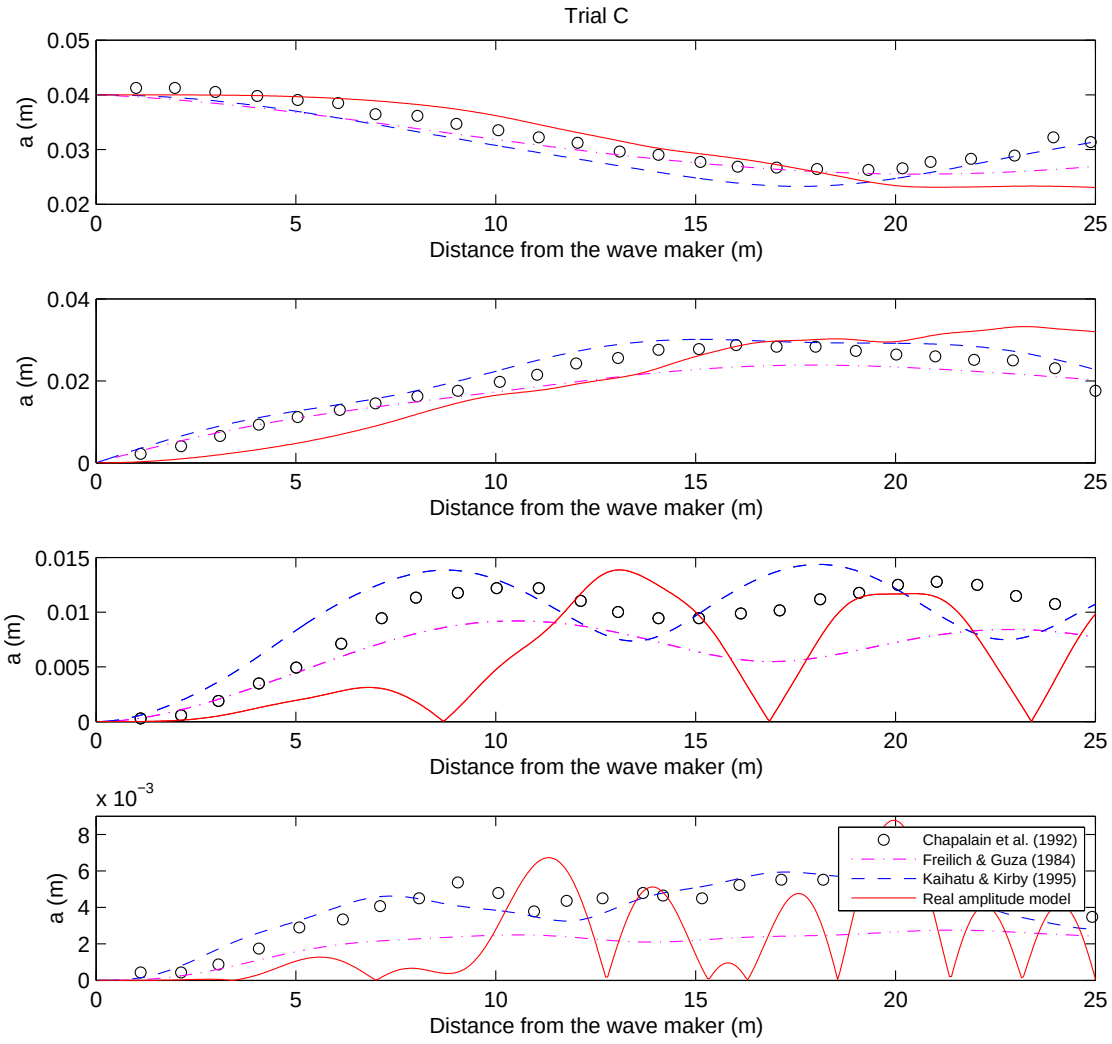

Figure 3.2: Comparison of Chapalain et al. (1992) experiment with real amplitude model, Kaihatu and Kirby (1995) mild slope model and the consistent model of Freilich and Guza (1984), $h = 0.4m$ and $T = 3.5S$

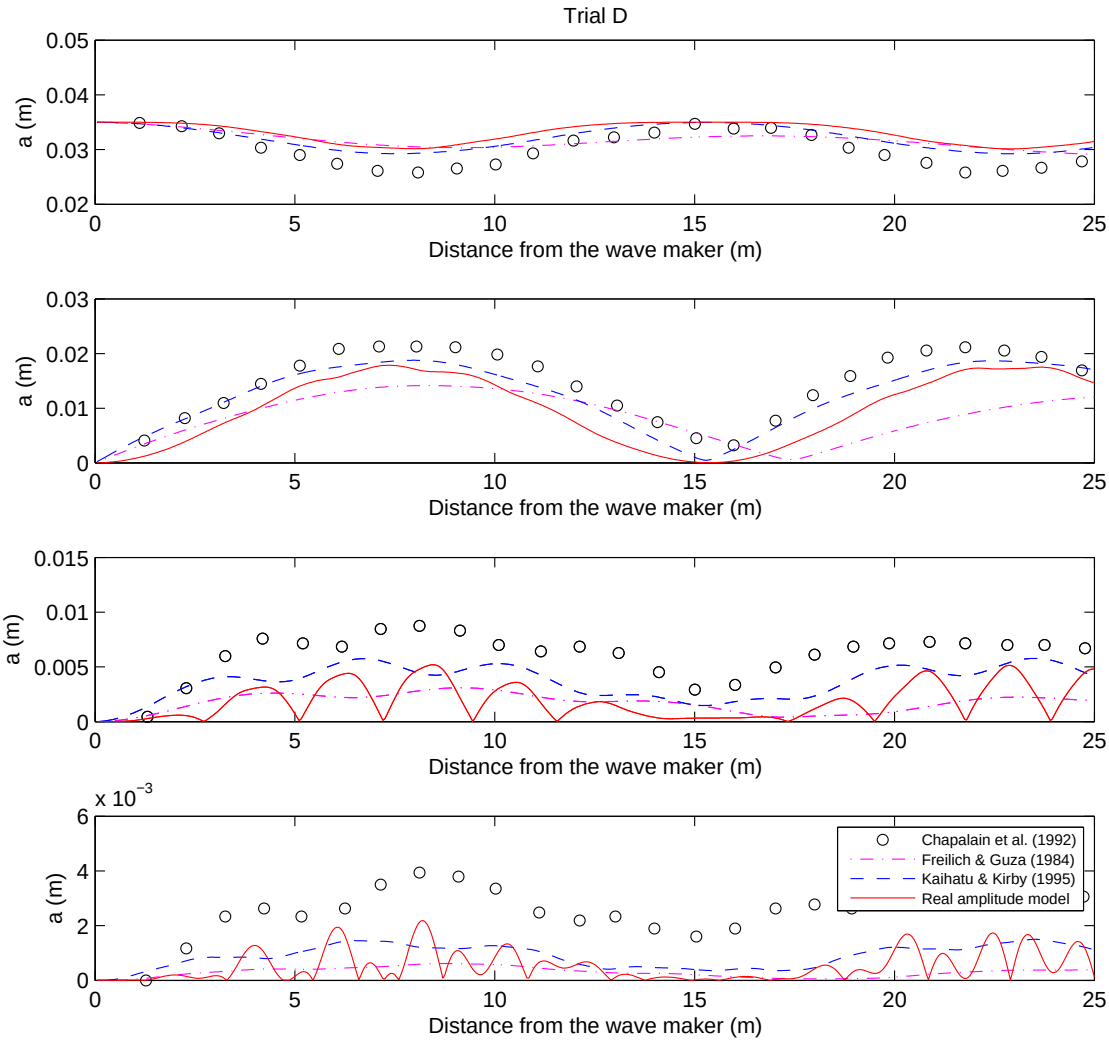

Figure 3.3: Comparison of Chapalain et al. (1992) experiment with real amplitude model, Kaihatu and Kirby (1995) mild slope model and the consistent model of Freilich and Guza (1984), $h = 0.3m$ and $T = 2.5S$

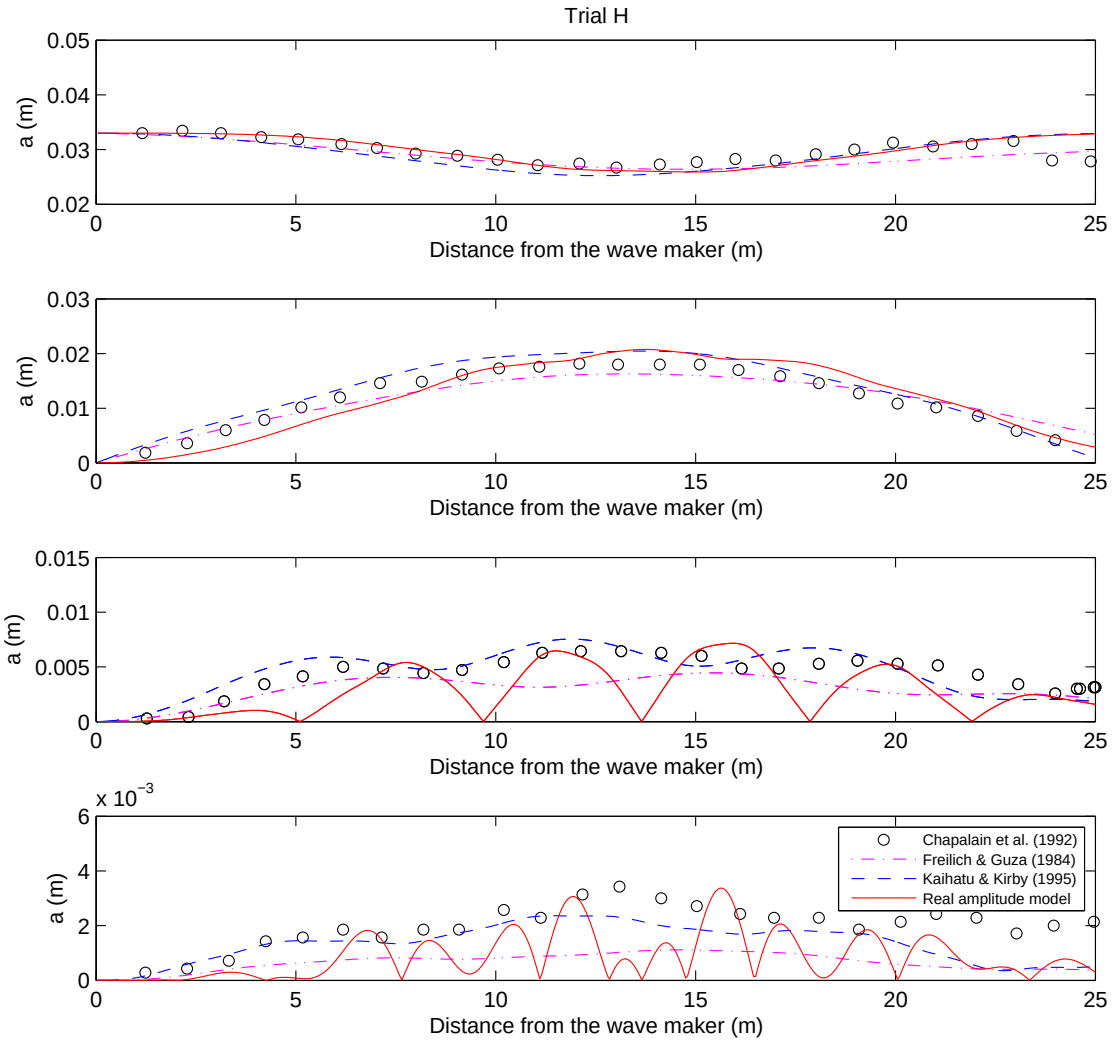

Figure 3.4: Comparison of Chapalain et al. (1992) experiment with real amplitude model, Kaihatu and Kirby (1995) mild slope model and the consistent model of Freilich and Guza (1984), $h = 0.4m$ and $T = 3S$

3.3.2 Comparison of the model with laboratory datasets for random waves

For comparison to experiment, the time series at all gauges is required. By running the model, the complex Fourier components is obtained for each gauge location and each realization. The power spectra is calculated using the real and imaginary parts of the Fourier components. Bartlett averaging is used to take the avarage of the calculated power for all realizations. Band averaging is used further to reduce the noise in the power spectrum and smooth the spectral estimate.

To test the model performance, we use two laboratory experimental data sets. The results from Mase and Kirby (1992), who conducted a set of experiments in two cases for investigation of shoaling and breaking characteristics of random waves. Case 2 of this experiment is a most suitable one for testing dispersive models because the relative depth is high enough ($kh = 1.9$) and is outside the shallow water range (Kaihatu and Kirby 1995). This is a rigorous test for dispersive wave models. Figure 3.5 shows the experimental setup of Mase and Kirby (1992). In this experiment, the free surface elevation has been measured in the sampling rate of 20 Hz. The dataset is devided into 7 realizations and each realization has 2048 data points. The peak frequency of the free surface spectra is 1 Hz and the total number of frequency components taken for this analysis is 400. Figures 3.6 and 3.7 compares the laboratory measurement with the real amplitude model and the model of Kaihatu and Kirby (1995).

The comparison of models shows that the real amplitude model agrees very well with the data. The difference between this model and the model of Kaihatu and Kirby (1995) shows that the real amplitude model has a significant improvements in resolving higher frequencies particularly at nearshore gauges compare to other model.

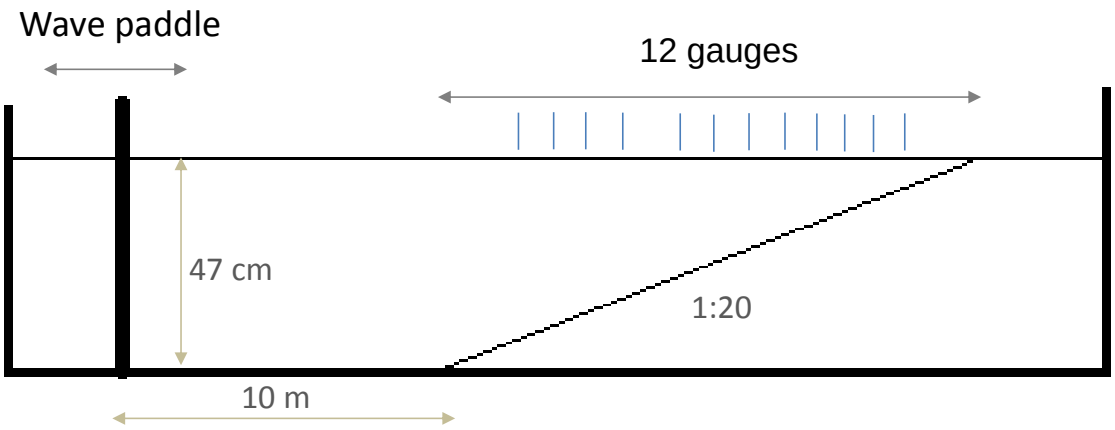

Figure 3.5: Mase and Kirby (1992) experimental setup

The second dataset is that of Bowen and Kirby (1994) which is used to analyze the behavior of the dissipation in the model. Figure 3.8 shows the experimental setup of Bowen and Kirby (1994).This dataset, hereafter denoted BK94, provides three different wave conditions. The free surface elevation was measured at 47 gauges with the sampling rate of 25 Hz for the duration of 17 min. The dataset is divided into 12 realizations with 2048 data points in each. Case B of BK 94 is used for this comparison. In this case, the H_{rms} and the peak frequency, f_p are 0.08 m and 0.225 Hz respectively. Figure 3.9 compares real amplitude models; the model of Kaihatu and Kirby (1995) and the model of Freilich and Guza (1984) with the experimental dataset.

The results of the comparisons show that the real amplitude model works reasonably well. Although the model of Freilich and Guza (1984) compares better for the lower frequency (nearshore part of the spectra), the real amplitude model has a better agreement at higher frequencies in more nearshore gauge locations compare to other two models.

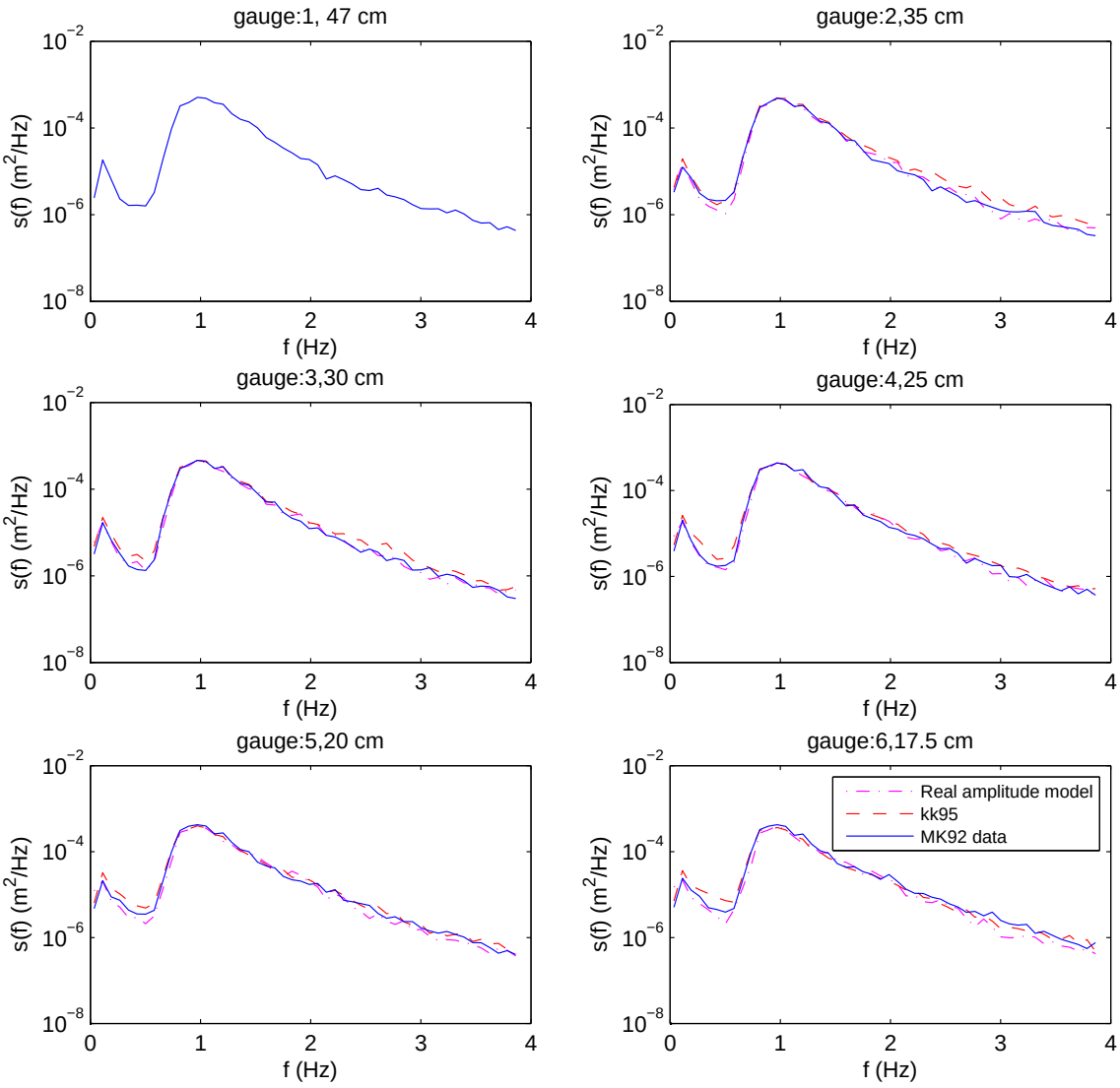

Figure 3.6: Comparison of Mase and Kirby (1992) experiments with real amplitude model and the mild slope model of Kaihatu and Kirby (1995)

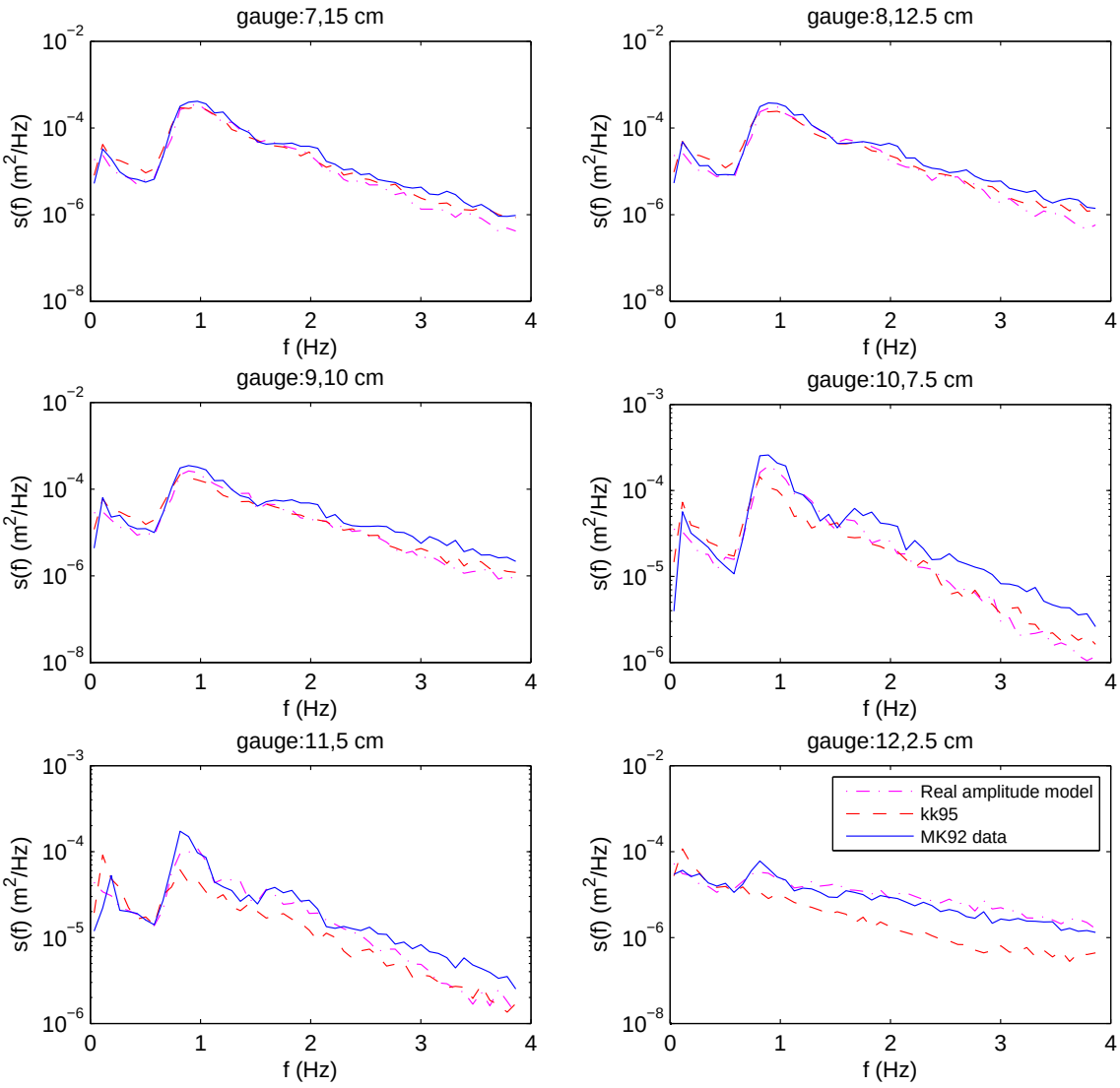

Figure 3.7: Comparison of Mase and Kirby (1992) experiments with real amplitude model and the mild slope model of Kaihatu and Kirby (1995)

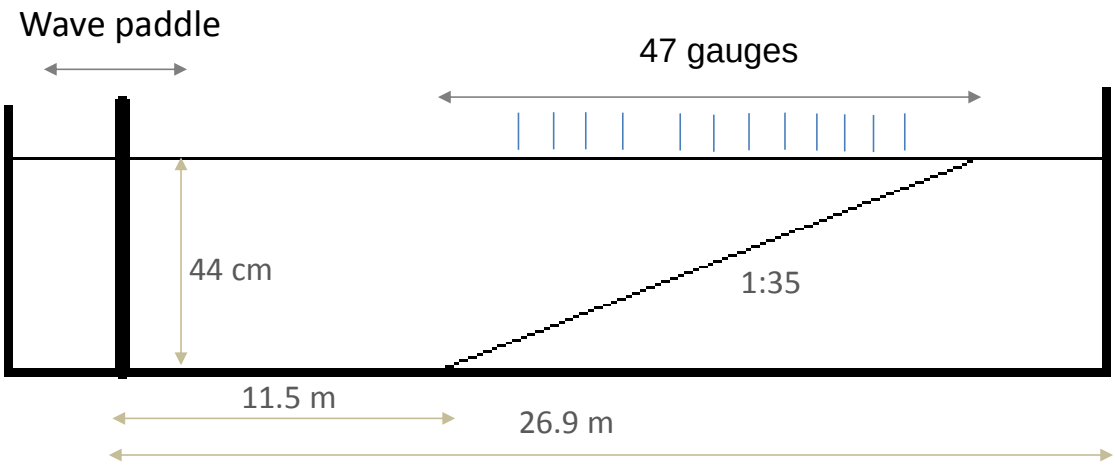

Figure 3.8: Bowen and Kirby (1994) experimental setup

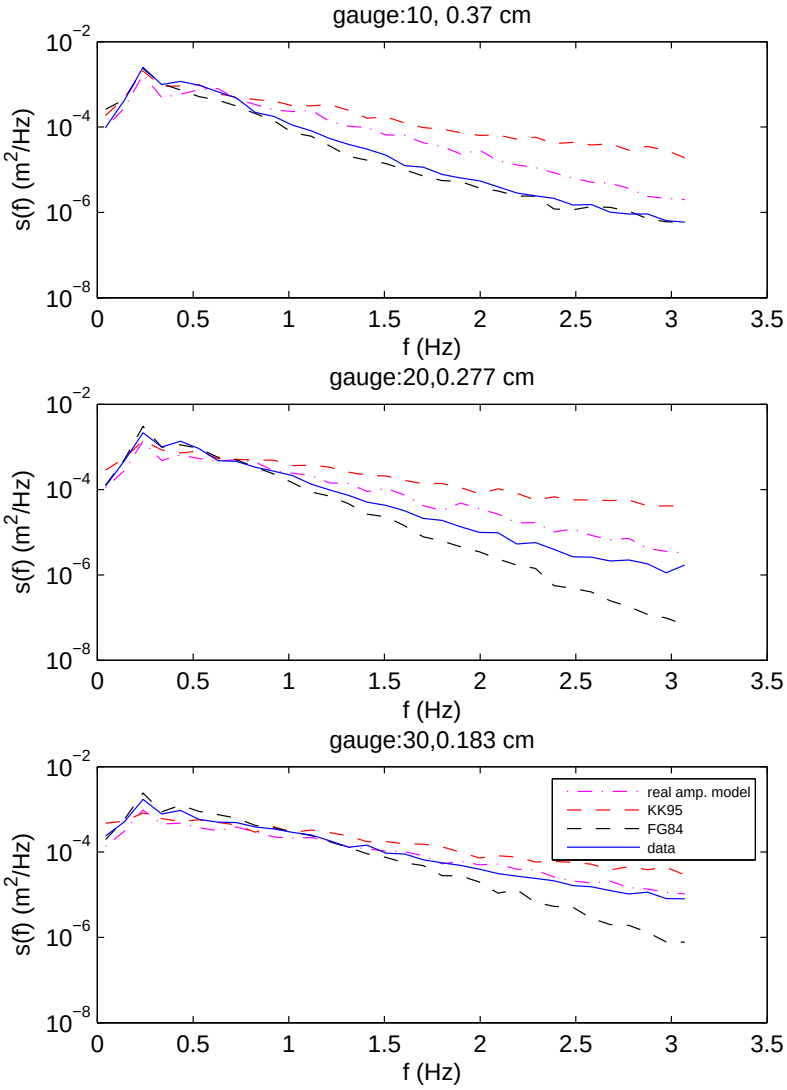

Figure 3.9: Comparison of Bowen and Kirby (1994) experiments with real amplitude model, Kaihatu and Kirby (1995) mild slope model and the consistent model of Freilich and Guza (1984)

3.3.3 Comparison of the model with field data sets in terms of spectra

In addition to compare the models with experimental dataset, the model is verified using field data from the Duck 94 experiment which was conducted at the U.S. Army

Field Research Facility at Duck, North Carolina, USA in the fall of 1994 (Birkemeier and Thornton 1994). The field experiments capture a wide range of conditions than seen in the laboratory. In this test, we examine in detail the accuracy of the model for four different cases of wave height and peak frequency: high and low wave height and high and low wave period. Table 3.2 represents the characteristics of each case in terms of wave height and wave period.

Table 3.2: Characteristics of field experiments cases

Test case	Wave height	Wave period
09030100	High	Low
09011000	Low	High
09011600	Low	Low
09051600	High	High

Figures 3.10 through 3.17 presents the comparison of nearshore wave models with Duck 94 field data for 256 and 400 retained frequency components. For test case 09030100 (figure 3.10 and figure 3.14), it is apparent that the real amplitude model has a better performance for all gauges particularly at high frequencies compare to the other models. It is expected result since this case includes a wider range of higher frequencies and the improved properties of real amplitude model are more evident at higher frequencies. It is also clearly seen that the real amplitude model for case 09051600 (figures 3.13 and 3.17) predicts the behavior of the waves better that other models, particularly for nearshore gauges. In case 09011000 (figure 3.11 and figure 3.15) the real amplitude model compares as well to data as the other nearshore models and they follow the same behavior. Figures 3.12 and 3.16 show the comparison of nearshore models for test case 09011600. In this case, the model

of Kaihatu and Kirby (1995) has the better agreement compare to the other models while the real amplitude model does not show significant improvements. Generally speaking, the real amplitude model is able to improve the estimation of the waves for higher frequency part of the spectra.

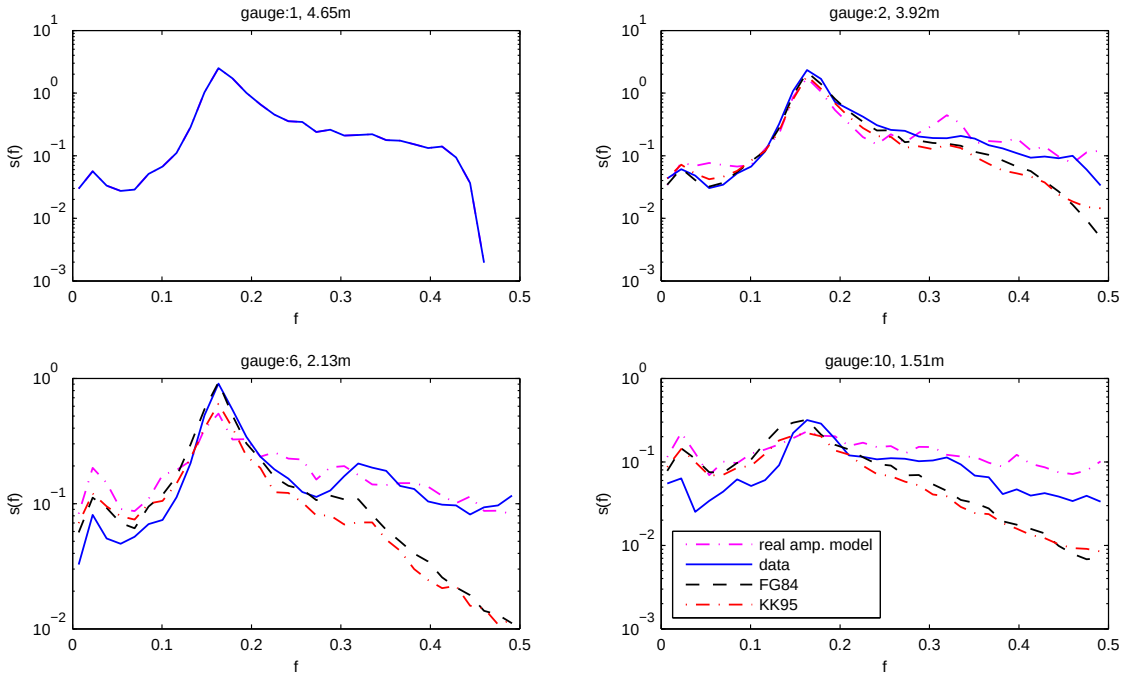

Figure 3.10: Comparison of Duck94-0903100 field dataset with real amplitude model, Kaihatu and Kirby (1995) mild slope model and the consistent model of Freilich and Guza (1984)-256 frequency components

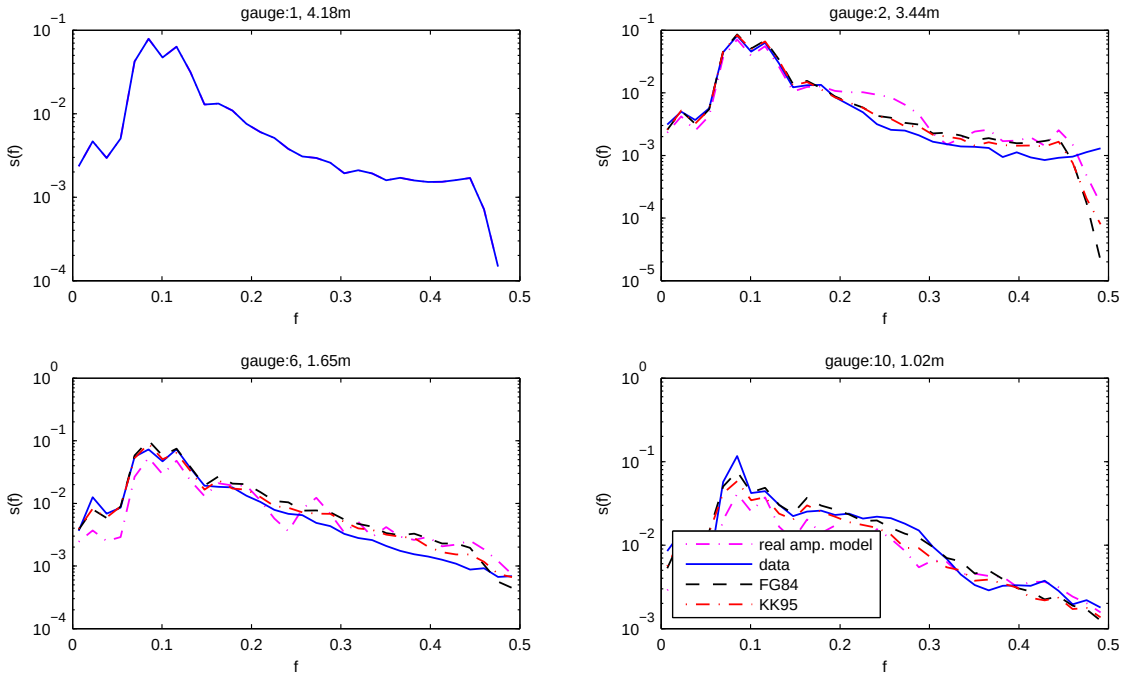

Figure 3.11: Comparison of Duck94-09011000 field dataset with real amplitude model, Kaihatu and Kirby (1995) mild slope model and the consistent model of Freilich and Guza (1984)-256 frequency components

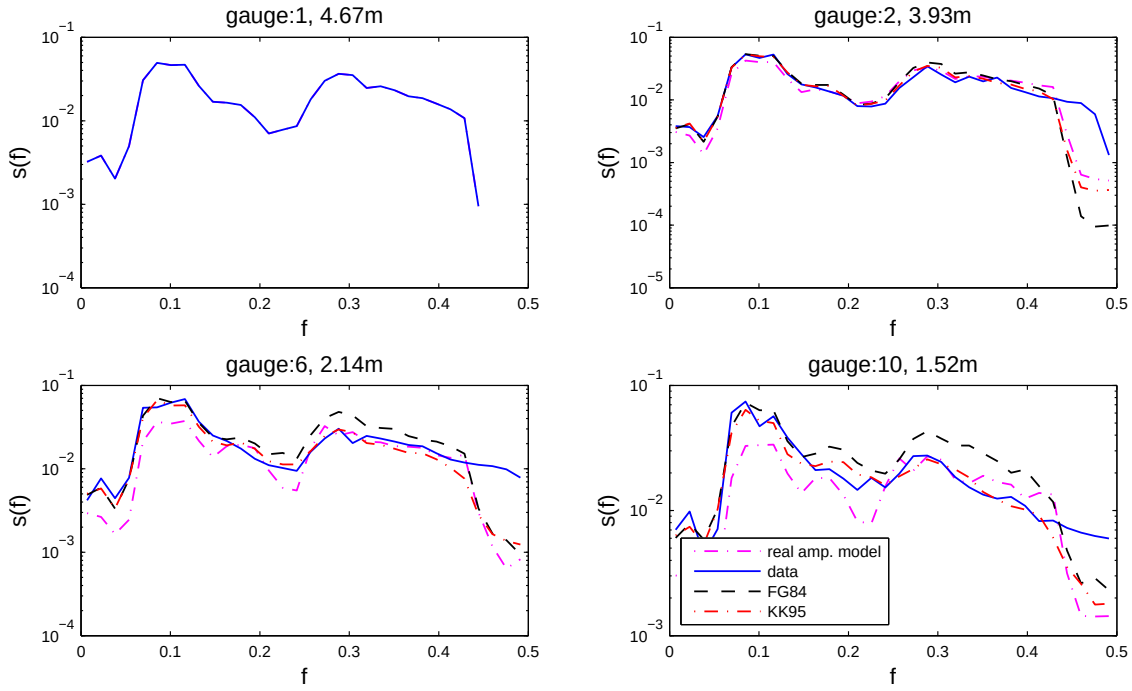

Figure 3.12: Comparison of Duck94-09011600 field dataset with real amplitude model, Kaihatu and Kirby (1995) mild slope model and the consistent model of Freilich and Guza (1984)-256 frequency components

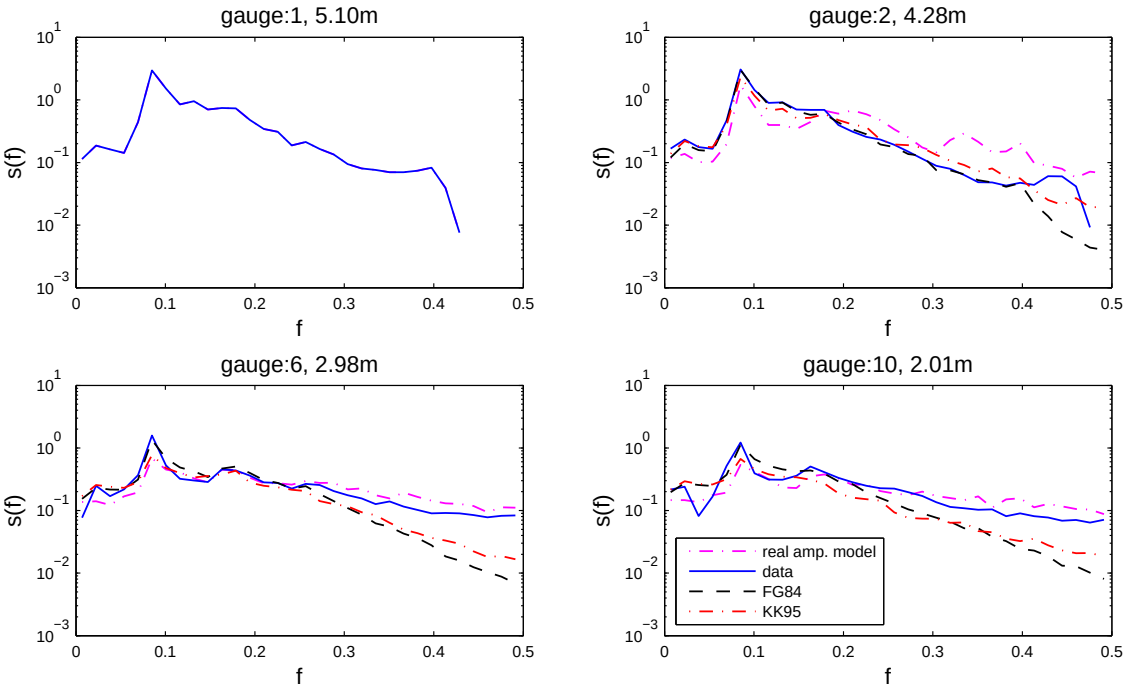

Figure 3.13: Comparison of Duck94-09051600 field dataset with real amplitude model, Kaihatu and Kirby (1995) mild slope model and the consistent model of Freilich and Guza (1984)-256 frequency components

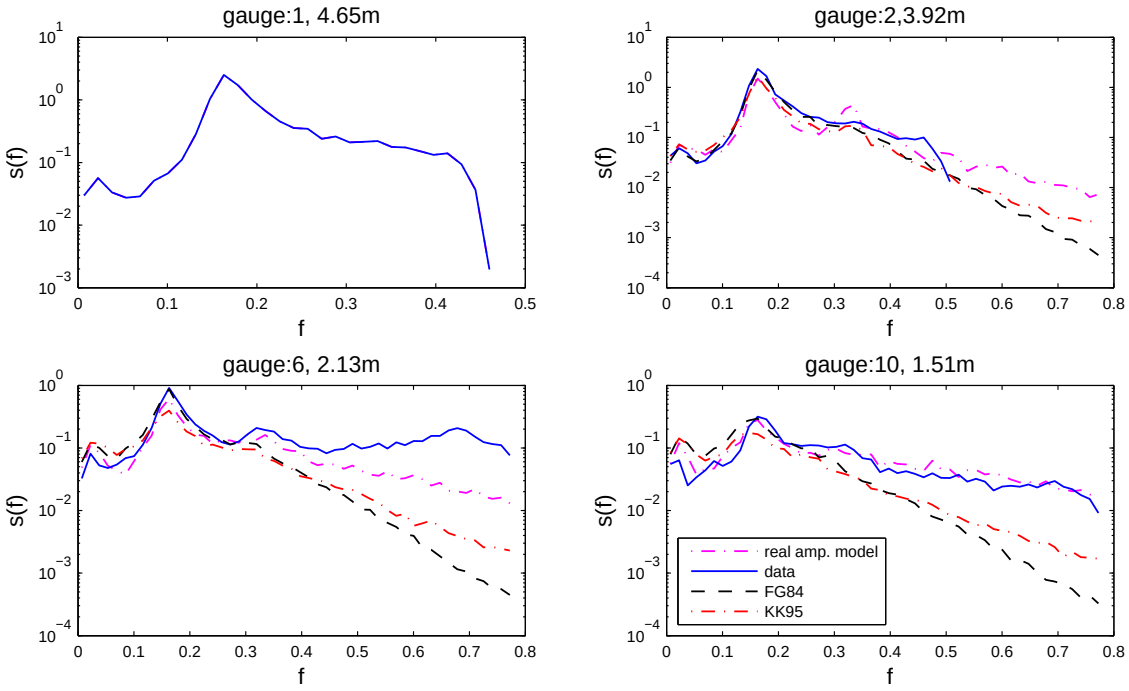

Figure 3.14: Comparison of Duck94-09030100 field dataset with real amplitude model, Kaihatu and Kirby (1995) mild slope model and the consistent model of Freilich and Guza (1984)-400 frequency components

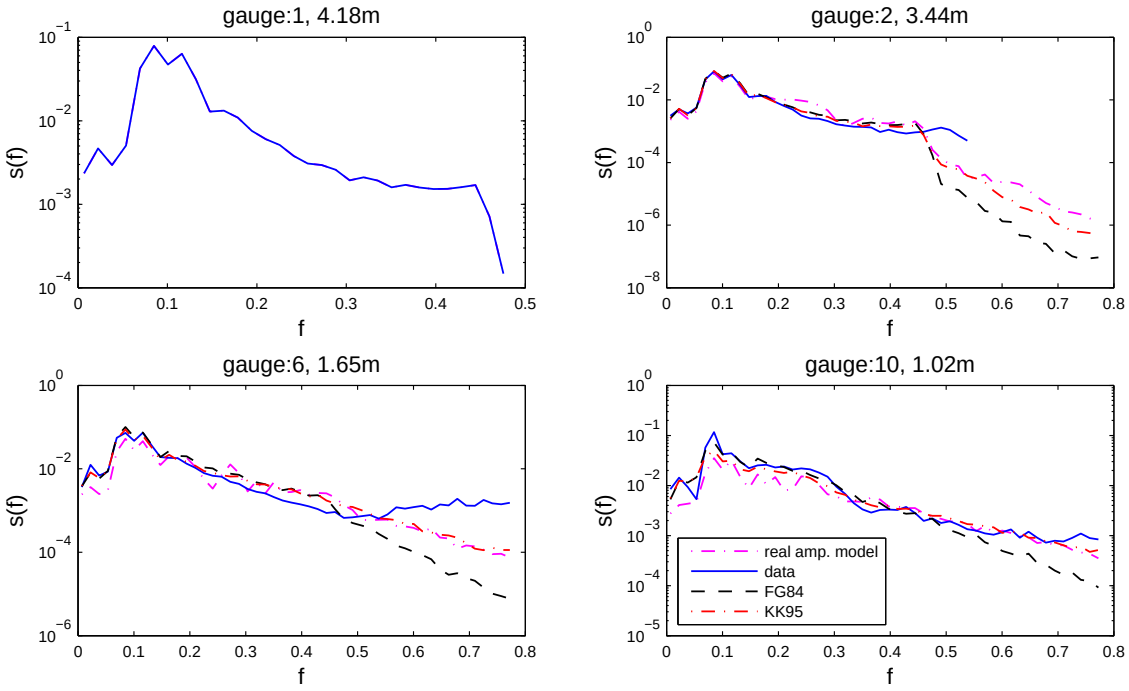

Figure 3.15: Comparison of Duck94-09011000 field dataset with real amplitude model, Kaihatu and Kirby (1995) mild slope model and the consistent model of Freilich and Guza (1984)-400 frequency components

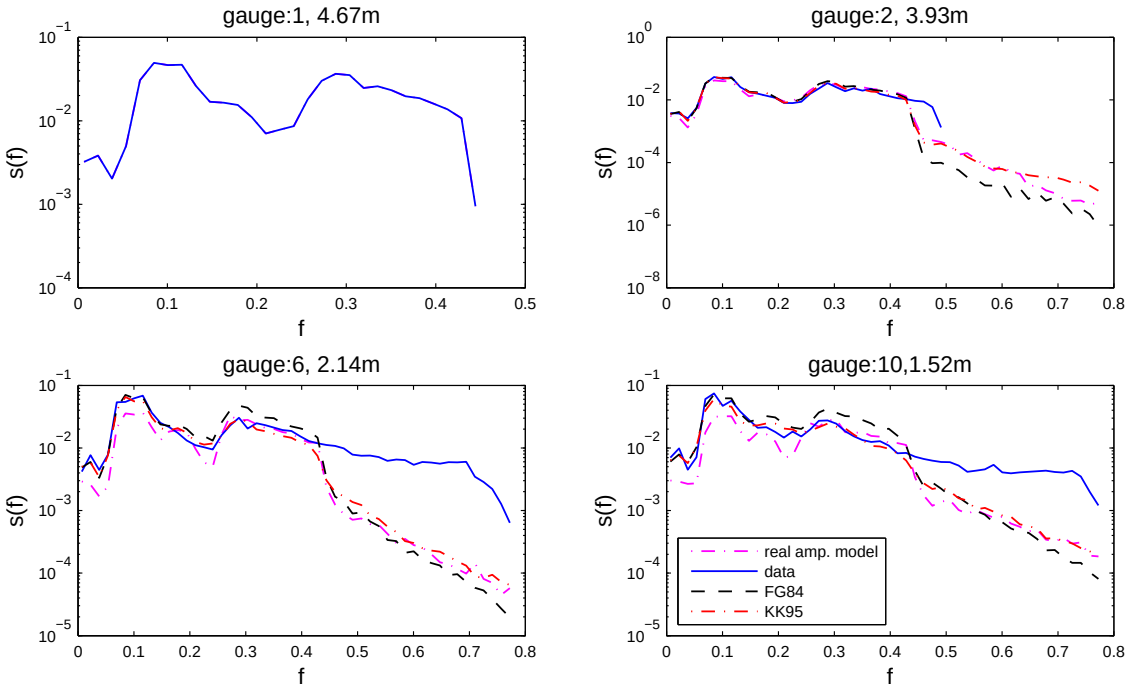

Figure 3.16: Comparison of Duck94-09011600 field dataset with real amplitude model, Kaihatu and Kirby (1995) mild slope model and the consistent model of Freilich and Guza (1984)-400 frequency components

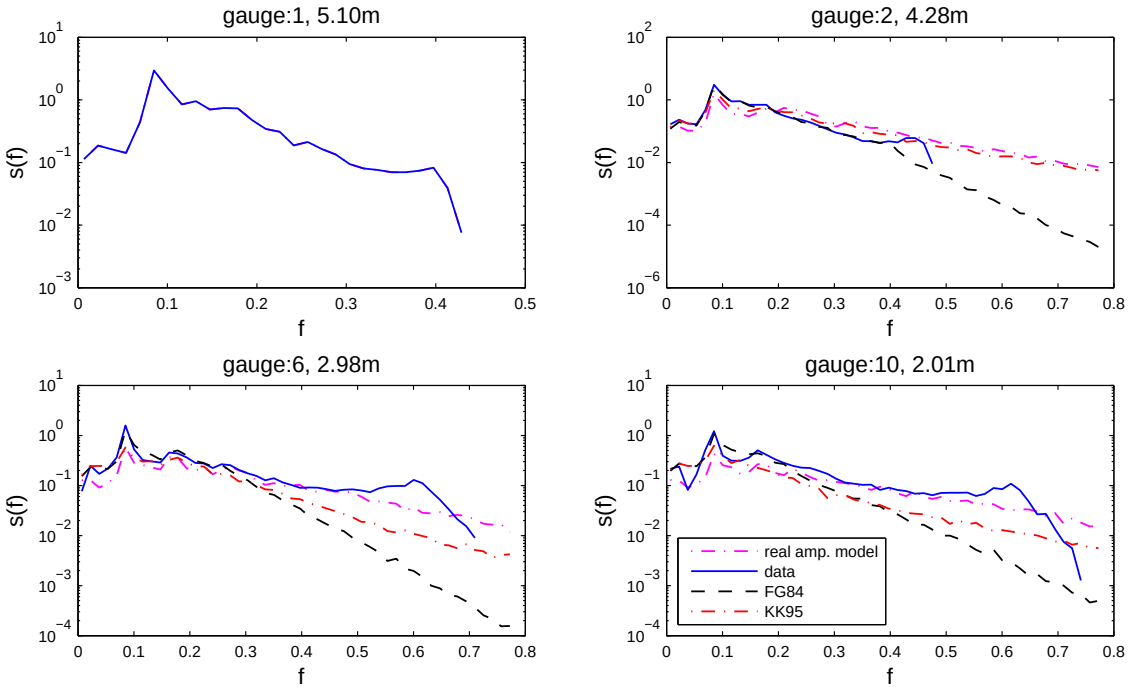

Figure 3.17: Comparison of Duck94-09051600 field dataset with real amplitude model, Kaihatu and Kirby (1995) mild slope model and the consistent model of Freilich and Guza (1984)- 400 frequency components

3.3.4 Comprehensive comparison of the model with field data

In this section, a wide range of initial wave condition from Duck 94 field dataset is used to check the validity of the model. For each data point, the real amplitude model is compared with other models for each individual part of the spectra. For each simulation the spectra is divided into its three bands: $0-0.5f_p$, $0.5f_p-1.5f_p$ and $1.5f_p$ to the last frequency where f_p is the peak frequency component. Figures 3.18 to 3.20 show the comparison of the real amplitude model with model of Kaihatu and Kirby (1995) and the consistent model of Freilich and Guza (1984) for different segments of spectra and three gauges from offshore to nearshore. At first glance,

it is seen that the real amplitude model shows a good general agreement with field data. In Figure 3.20, it is also shown that for the higher frequency band of the spectra (band 3), the real amplitude model overpredicts the amount of spectral energy compare to the other two models. That means that this model not only has improved the prediction of spectral energy at higher frequencies but also has the ability to have even better estimation for the higher frequency specra by changing the free parameters of breaking term and make the higher frequency tail more closer to that of the data. Tables 3.3 to 3.5 present the quantified statistical skills of each model for bands 1 to 3 respectively.

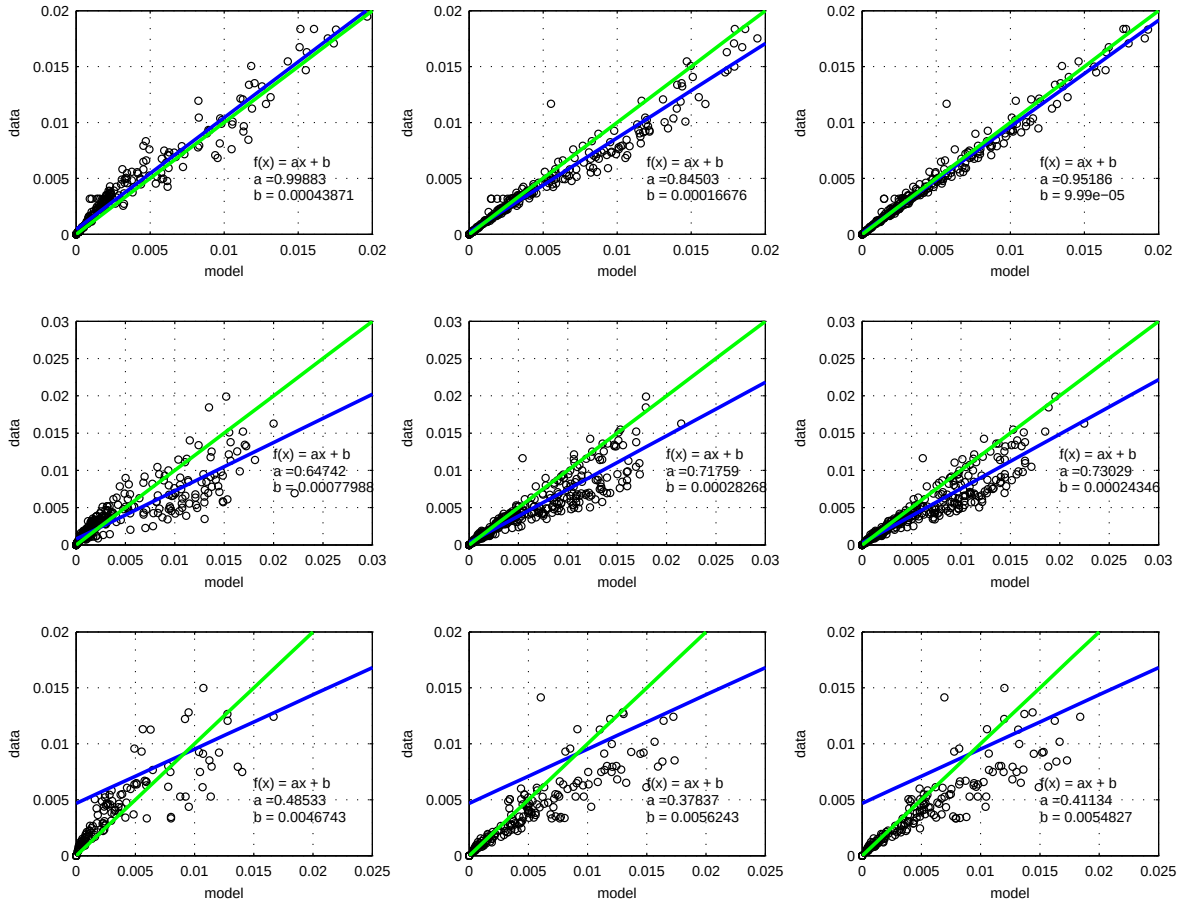

Figure 3.18: Comparison of real amplitude model with the model of Kaihatu and Kirby (1995), 256 frequency components, band:1. Left to right: real amplitude model; model of Kaihatu and Kirby (1995) and model of Freilich and Guza (1984); Top to bottom: gauges 2, 6 and 10 from offshore to nearshore.

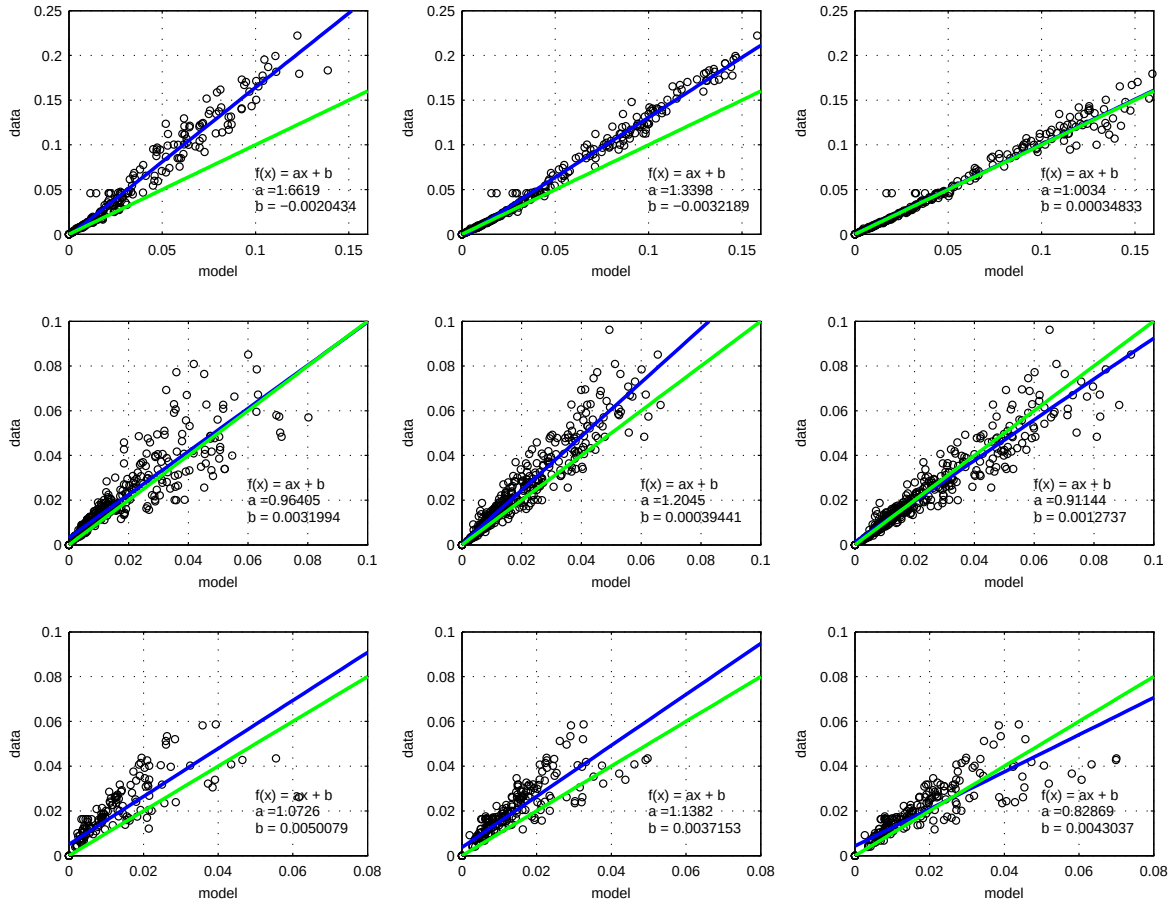

Figure 3.19: Comparison of real amplitude model with the model of Kaihatu and Kirby (1995), 256 frequency components, band:2. Left to right: real amplitude model; model of Kaihatu and Kirby (1995) and model of Freilich and Guza (1984); Top to bottom: gauges 2, 6 and 10 from offshore to nearshore.

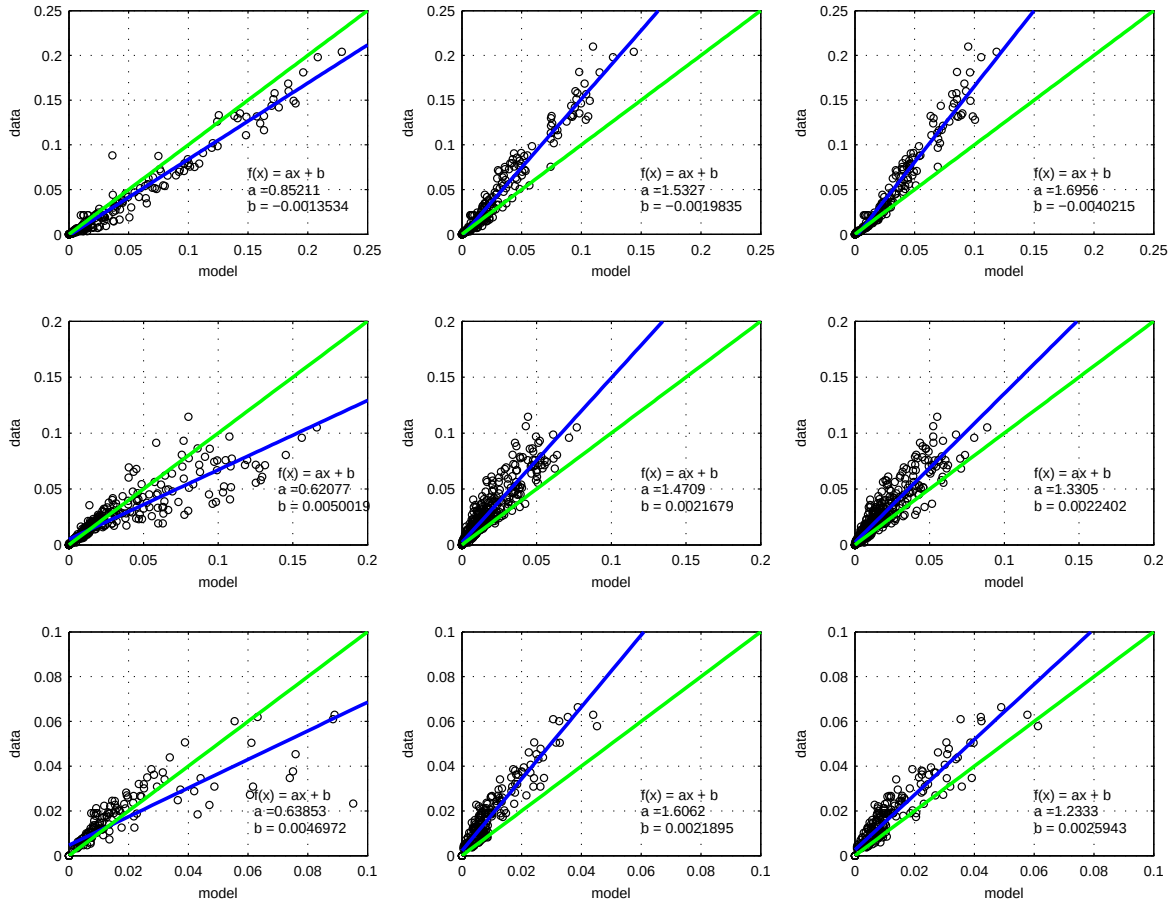

Figure 3.20: Comparison of real amplitude model with the model of Kaihatu and Kirby (1995), 256 frequency components, band:3. Left to right: real amplitude model; model of Kaihatu and Kirby (1995) and model of Freilich and Guza (1984); Top to bottom: gauges 2, 6 and 10 from offshore to nearshore.

Table 3.3: Summary of statistical skills for each model at band 1. The first row shows the standard deviation and the second row shows the correlation coefficient for each gauge.

Gauge number	real amplitude model	KK95	FG84
Gauge 2	2.3545e-04	2.0360e-04	1.1368e-04
	0.98	0.98	0.99
Gauge 6	0.0011	8.0212e-04	6.9653e-04
	0.88	0.93	0.94
Gauge 10	0.0307	0.0476	0.0475
	0.15	0.11	0.13

Table 3.4: Summary of statistical skills for each model at band 2. The first row shows the standard deviation and the second row shows the correlation coefficient for each gauge.

Gauge number	real amplitude model	KK95	FG84
Gauge 2	0.0281	0.0120	0.0230
	0.98	0.99	0.99
Gauge 6	0.0232	0.0145	0.0135
	0.90	0.96	0.96
Gauge 10	0.0112	0.0094	0.0100
	0.84	0.88	0.88

3.3.5 Evolution of the model with an arbitrary TMA spectrum

Following Kaihatu (2009), we examine the behavior of the model during propagation of an arbitrary TMA spectrum (Bouws et al. 1985) over a constant depth. The peak frequency of TMA spectrum is 0.07 and the time series of TMA spectrum is generated using random phases and an inverse Fast Fourier Transform algorithm, using the TMA spectrum shape as input. The time series of free surface elevation is then divided into 32 realizations with 2048 data point in each. The water depth is 2 m, the wavelength is 71 m and the length of the domain of interest is 5100m. This distance is relatively long (70 wavelengths) to test the evolution of waves and

Table 3.5: Summary of statistical skills for each model at band 3. The first row shows the standard deviation and the second row shows the correlation coefficient for each gauge.

Gauge number	real amplitude model	KK95	FG84
Gauge 2	0.0149	0.0247	0.0267
	0.99	0.98	0.98
Gauge 6	0.0372	0.0403	0.0392
	0.90	0.92	0.92
Gauge 10	0.0094	0.0047	0.0058
	0.86	0.95	0.94

the behavior of nonlinear terms caused by interaction of waves. Figure 3.21 show the results of evolution of spectra for 7 gauges. As it is seen, during the transition of waves, the level of spectral energy changes gradually. The spectra attains a wider shape, as energy at the spectral peak is lost to low and high frequency bands. After some distance, the spectrum ceases to evolve any further. This has also been seen in the model of Kaihatu and Kirby (1995) by Kaihatu (2009).

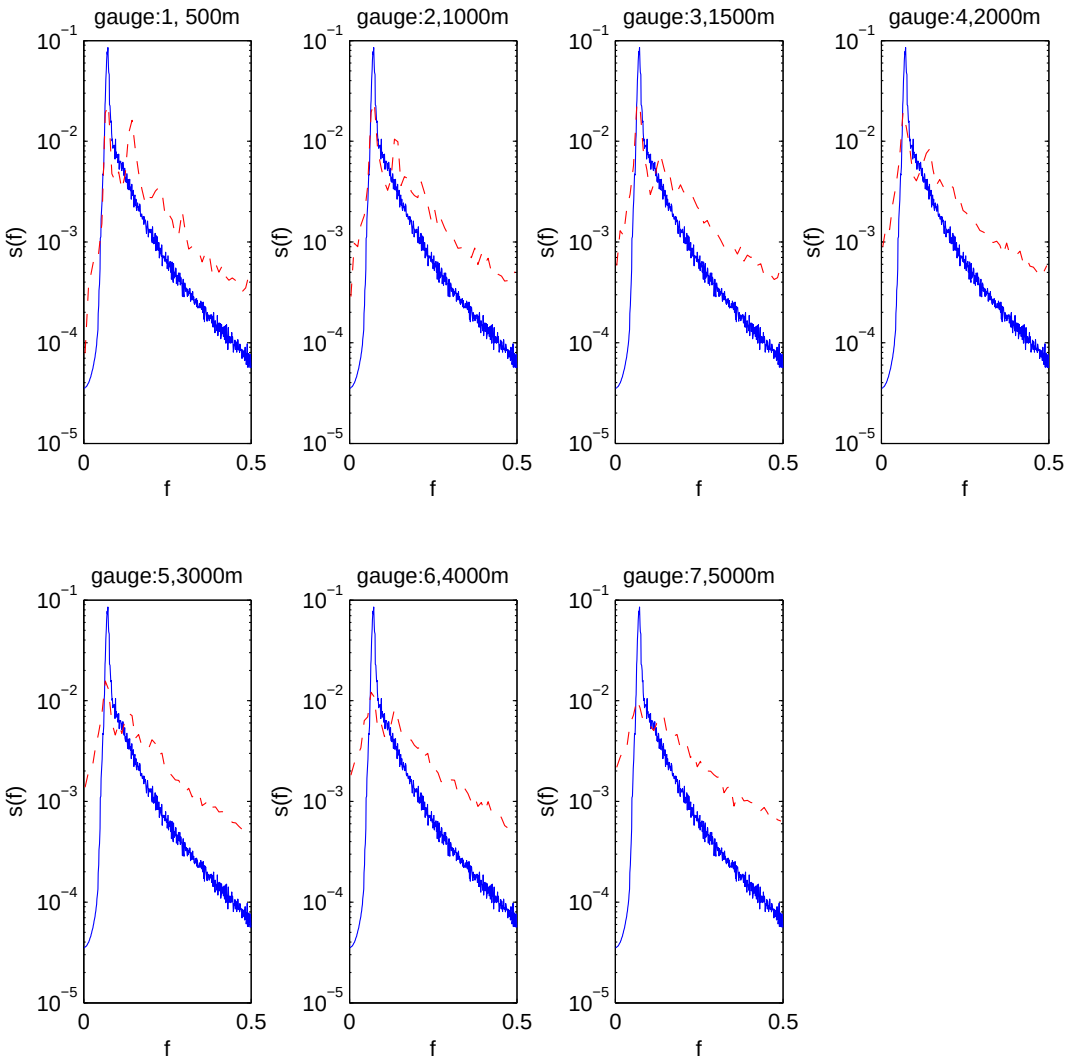

Figure 3.21: Evolution of TMA spectrum. (The blue line: the original TMA spectrum; the red dash-line: the TMA spectrum after evolution)

3.3.6 Comparison of the model with experimental datasets in terms of higher order statistical parameters

During shoaling, the wave shape changes and becomes more skewed and asymmetric. Figure 3.22 shows the concepts of wave shape parameters in graphical form. This change in waveform is described by two higher order statistical parameters, skewness and asymmetry (Elgar etal. 1992b). Skewness is defined as a deviation from sinusoidal wave shape about the horizontal plane. This generally implies a wave with wide trough and narrow crest shape. The shape of the waves becomes more asymmetric respect tovertical plane when waves propagate to surf zone; this is termed asymmetry. Surf zone waves attain a saw-tooth or forward-leaning shape. We calculate the higher order statistical parameters of waves such as skewness and asymmetry from the timeseries as follows

$$Skewness = \frac{\langle \eta^3 \rangle}{\langle (\eta^2)^{3/2} \rangle} \tag{3.63}$$

$$Asymmetry = \frac{\langle H(\eta^3) \rangle}{\langle (\eta^2)^{3/2} \rangle} \tag{3.64}$$

where η is free surface elevation and H is the Hilbert transform and the symbol $\langle\rangle$ denote the average.

The time series of free surface elevation is calculated using the inverse FFT from the amplitudes from the wave model. The timeseries is obtained for each realization separately and the parameters are calculated using (3.63) and (3.64). Then, the average is taken for all realizations to find a certain value for these quantities. This process is repeated for all gauge locations. Figure 3.23 depicts the comparison of H_{rms}, variance, skewness and asymmetry with the experimental dataset of Mase

and Kirby (1992). Despite the model compares well in terms of Hrms and variance, it cannot shows good agreements with observed data for skewness and asymmetry. Kaihatu (1995), Kirby and Kaihatu (1996); and Bowen (1994) declared that truncating the frequency components instead of using the full spectra can cause this descrepancy.

We examined the model with different values of ϵ (used as a free parameter in the phase function in equation (3.37) to (3.40)) and realized that the calculated skewness and asymmetry are sensitive to this value. However, the change in the spectrum is not significant by changing this quantity if it is chosen appropriately. This value is the nonlinearity parameter and should be much less than 1. Figure 3.24 illustrates the effects of ϵ on predicted skewness and asymmetry. It is evident that although the predicted Hrms and variance do not have significant changes, the predicted wave shape parameters show better agreement with observed data by using different value for ϵ.

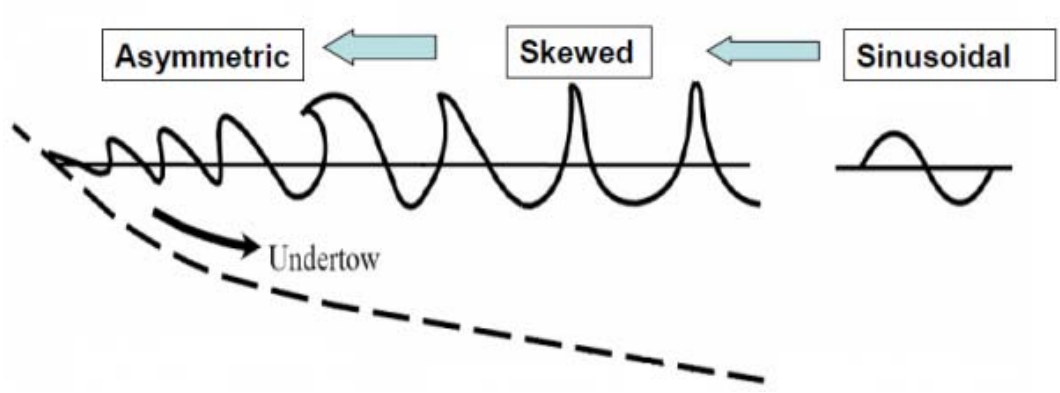

Figure 3.22: Changes in Waveform during the transformation to nearshore (Ole Secher Madsen, 2010)

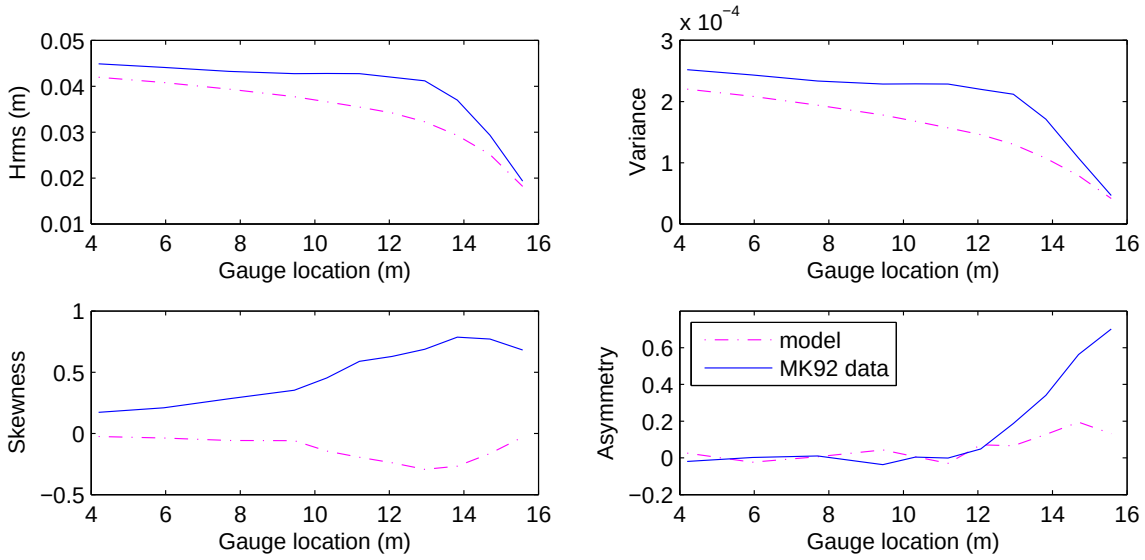

Figure 3.23: Third order comparison with Mase and Kirby (1992) dataset. The value of the ϵ is 0.01. (The blue line: the observed data; the dash-dot magenta: the model results)

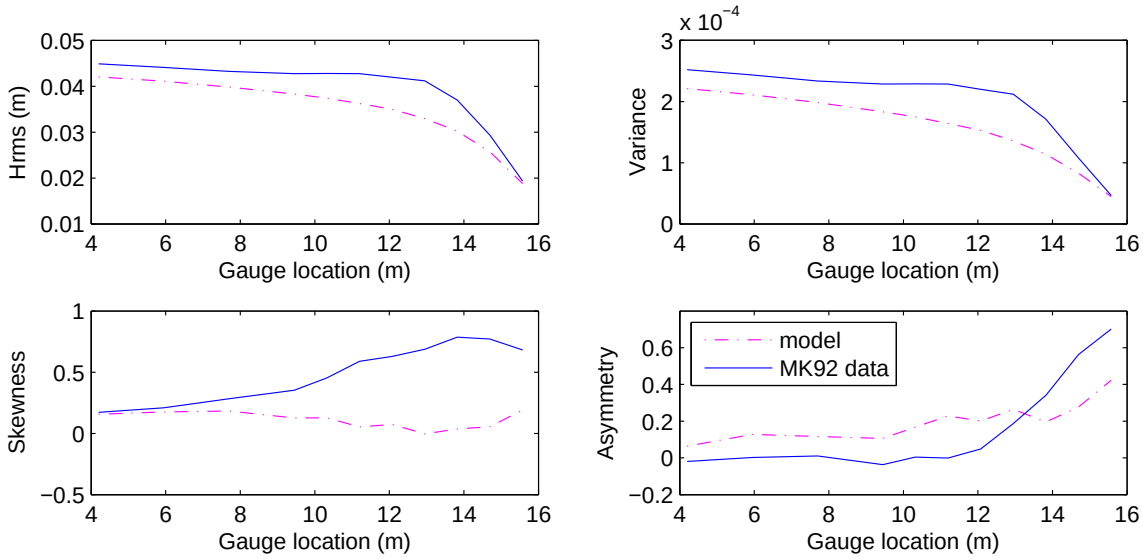

Figure 3.24: Third order comparison with Mase and Kirby (1992) dataset after changing the ϵ. The value of ϵ is 0.001. (The blue line: the observed data; the dash-dot magenta: the model results)

3.4 Summary

In this chapter, we have described the mathematical derivation of the fully dispersive nonlinear wave model in terms of the real amplitudes rather than the complex amplitudes (e.g. Kaihatu and Kirby 1995). To ameliorate the behavior at higher frequencies, the effects of third order bound waves are studied in fully dispersive nearshore wave model. The equation not only includes the second and third order triad wave-wave interaction terms but also the third order bound waves for the first harmonics. This model is based on the boundary value problem and is extended up to third order via multiple scale analysis. Since the spatial phase function varies slowly in x, the multiple scale analysis is a useful method to split up this quantity into certain parts based on the required order.

The evolution of the amplitude from the first harmonics to the fourth harmonics for the real amplitude model is compared with the dispersive model of Kaihatu and Kirby (1995) and the consistent model of Freilich and Guza (1984). For this aim, the experimental dataset of Chapalain et al. (1992) was used. The comparisons show that the model of Freilich and Guza (1984) tends to underpredict the higher harmonics amplitude at all test cases. While the model of Kaihatu and Kirby (1995) demonstrates the better agreement among the other two models. The real amplitude model agrees well for the first two harmonics. However, this model shows some oscillating features for the third and fourth harmonics.

The validity of the model was investigated using appropriate experimental and fields datasets. Testing the model using laboratory data sets with a wide range of relative water depths (kh), from a higher value for Mase and Kirby (1992) dataset to the smaller value of kh in the experimental data set of Bowen and Kirby (1994) strengthen the validity of the model for different wave conditions. Comparing with Duck 94 field data set, it is more evident that the real amplitude model is able to predict the spectral tail better than the other two models (Kaihatu and Kirby 1995; and Freilich and Guza 1984) for certain wave conditions (e.g. high wave height and low wave period; high wave height and high wave period). Since the value of the relative water depth, kh, for Bowen and Kirby (1994) dataset is greater than that of the Duck94 field data sets, the good agreement of the real amplitude model with the Bowen and Kirby (1994) (Figure 3.9) reveals that the model is able to estimate even the much higher frequencies. Briefly, compared to the previous models, the real amplitude model is able to improve the prediction of high frequencies in the spectra.

Using a wider range of initial wave condition to examine the validity of the model indicates that the real amplitude model generally agrees well with field data and tends to overpredict the spectral energy at higher frequencies (band 3 or the third

segment of spectra) However the other two models underpredict the energy. It may be possible to fix energy overprediction by recalibrating mechanism.

To make sure that the real amplitude model shows a reasonable response while propagating at a long distance with constant depth, the evolution of spectra in the model was examined using a typical TMA spectrum as an initial wave condition. It is clearly seen that the spectral shape gradually becomes wider during a long distance transition which shows the energy transfers properly from lower to higher frequencies.

The final test to verify the model was the ability of the model to predict the higher order statistical parameters such as skewness and asymmetry. Although this model compares well for Hrms and variance, it is poorly compared with data for skewness and asymmetry. Kaihatu (1995); Kirby and Kaihatu (1996) showed that the predicted skewness and asymmetry would be sensitive with the number of frequency components used to calculate these parameters.

4. CHARACTERIZING THE DISSIPATION IN BREAKING WAVES

The characterization of breaking waves in models has seen much advance in recent years. This characterization, in turn, can be applied to data in order to obtain information on instantaneous breaking characteristics. Using several high-resolution laboratory data sets of wave breaking in shallow water, the threshold parameter of the breaking formulation of Zelt (1991) is parameterized at each gauge location using the corresponding bulk dissipation calculated from each dataset. Although this parameter is defined as a constant value for solitary waves over the constant depth in the original formulation, adjustment of this value allows its application to a wider range of wave conditions. The calibrated parameter is then used to calculate the instantaneous dissipation from time series of free surface elevation. We show that the relationship between this parameter and normalized water depth is best expressed as a hyperbolic tangent curve. A similar trend between third moments of the free surface and the calibrated parameter exists. These parameters are also applied to find a relationship between the slope of the free surface elevation spectra and the slope of the associated dissipation coefficient. We determine that previous work on the trends of the frequency dependence of dissipation, while changed with this calibrated parameter, is not invalidated.

4.1 Introduction

As waves propagate from offshore to nearshore regions, due to the shoaling process, the wave height and the rate of energy increases; and the group velocity of waves decreases gradually. This phenomena leads the waves to become unstable and break. Consequently, the wave height decays and the dissipation caused by breaking becomes dominant. The complexity of the resulting flow conditions are a challenge

for models intended to simulate processes in the surf zone.

Generally, wave breaking models are classified into three types of models: The first type of models are based on the probabilistic approach of wave height distribution (Battjes and Janssen 1978; Thornton and Guza 1983; Baldock et al. (1998); and Janssen and Battjes 2007). These types of models differ from each other in definition of the probability distribution function for wave height at breaking point. The second type of breaking models consists of a phase resolving wave transformation models such as the models we discussed earlier in chapters 3 and 4; and an extra term added to these models to enhance the ability of the model to simulate the waves at breaking zone. Heitner and Housner (1970); Zelt (1991); Karambas and Koutitas (1992); and Kennedy et al. (2000a) applied the concept of eddy viscosity to characterize dissipation and added the corresponding term into their Boussinesq model. Svendsen (1984) and Schaffer et al. (1993) developed a breaking model which is associated with the modeling of a "roller" generated due to the breaking. Veeramony and Svendsen (2000) also developed a model for transformation of vorticity generated beneath the roller area during the breaking process. The third type of wave breaking models employs Direct Numerical Simulation (DNS) models, that simulates the transformation of waves from the first gauge to the last gauge using one integrated model. DNS solves the Navier-Stokes equations using computationally intensive techniques of Computational Fluid Dynamics (CFD). Using the DNS methods, the behavior of the fluids under different turbulence with different spatial and temporal scales. The COBRAS model of Lin and Liu (1998) is an example for these types of models that simulates the wave propagation in non-breaking and breaking zones in one integrated model. This study has focused on the first and second type of breaking models which are extensively explained later.

One of the first studies of breaking random waves was performed by Battjes

and Janssen (1978). They developed a probabilistic model for estimating the bulk energy dissipation. In this model and earlier models, the part of wave height probability distribution function beyond the presumed breaking point is discarded. They offered truncated Rayleigh distribution function to estimate breaking wave height. The transformation model of Thornton and Guza (1983) for irregular waves in surf zone, not only describes shoaling mechanism of waves but also includes dissipation mechanism in both form of wave breaking and bottom friction. In this model, the energy dissipation due to breaking is calculated using an empirical formulation which is based on a statistical distribution of wave height. Theoretically, it is assumed that the distribution of wave height follows the full Rayleigh probability distribution function and H_{rms} represents the wave height averaged for all range of frequencies over the spectrum. Baldock et al. (1998) reformulated the model of Battjes and Janssen (1978) for steep beaches by discarding the depth restrictions on wave height for breaking criteria. Later, Janssen and Battjes (2007) proposed a new formulation for wave height distribution and modified the formulation of Baldock et al. (1998). This new formulation would be also beneficial for steep sloped beaches where the surf zone is unsaturated.

Zelt (1991) added an extra term for eddy viscosity into a Lagrangian Boussinesq model. In this model, solitary-type waves were assumed a common way to model the runup (Synolakis 1986). In addition, Kennedy et al. (2000) proposed an eddy viscosity model that calculates the dissipation in the same manner as zelt (1991) with the exception that a linear relationship for free parameter, η_t^*, is defined instead of assigning a constant value as was done in Zelt (1991).

Kirby and Kaihatu (1996) expressed a new formulation to calculate the time dependent eddy viscosity for estimation of instantaneous energy dissipation. Moreover, they assumed that dissipation coefficient, α_n, is proportional to the square of fre-

quency, f^2 justifying the choice by using the frequency dependence needed for the dissipation to result in the sawtooth-type waves seen in the surf zone. Later, Kaihatu et al. (2007) parameterized the power of dissipation coefficient for the frequency dependent dissipation model. Goertz et al. (2012) investigated the energy dissipation on top of the fringing reefs using the combination of two probabilistic breaking models: Thornton and Guza (1983) and Janssen and Battjes (2007). Moreover, they applied the obtained energy dissipation to compare it with the instantaneous dissipation calculated from zelt (1991) and find the best Zelt parameter that leads the instantaneous dissipation to be close to that of the Thornton and Guza (1983).

Breaking models, either in frequency domain or time domain, include free parameters that depend on different environmental conditions. To enhance the ability of the wave transformation models for better resolving of the breaking process, particulary in inner surf zone, free parameters need to be chosen carefully. For instance, in the time domain approach of Zelt (1991), dissipation term is expressed in terms of instantaneous dissipation. Instantaneous dissipation involves the Zelt parameter (0.3 in (4.9)) which is not defined properly for irregular waves. In frequency domain models such as Kaihatu et al. (2007), the free parameters of γ & β in the Thornton and Guza (1983) formulation and the power of frequency dependent term need to be modified as well.

Briefly, the aim of this chapter is to revisit the free parameters in the formulation of Thornton and Guza (1983) and frequency dependency term of breaking discussed in Kaihatu et al. (2007). At first, the breaking models are explained in detail and we describe our tuning method for free parameters such as γ in the formulation of Thornton and Guza (1983) and the threshold parameter in Zelt (1991). The breaking free parameter of Zelt (1991) is parameterized for each gauge location separately using the corresponding bulk dissipation calculated from dataset and

tuned Zelt parameter then is used to calculate the instantaneous dissipation and the corresponding dissipation coefficient. As a result, the corresponding power of the frequency in frequency dependent dissipation formulation is estimated. Furthermore, the relationship between the power of frequency and the damping coefficient calculated using the tuned Zelt (1991) threshold parameter is investigated. The relationship between third-moment quantities such as skewness and asymmetry with the calibrated Zelt parameter is also explained.

4.2 Classification of wave breaking models

4.2.1 Thornton and Guza (1983)

Using a statistical approach, Thornton and Guza (1983) assumed that the statistical distribution of wave heights in the surf zone can be described by a truncated Rayleigh distribution. They also found that the truncation of the distribution is used to eliminate wave heights in the distribution due to breaking, and is dependent on the free parameters fitted to data. Thornton and Guza (1983) formulated a transformation model based on the energy flux due to the breaking and friction mechanism

$$-\frac{\partial E c_g}{\partial x} = \epsilon_b + \epsilon_f \tag{4.1}$$

$$E = \frac{1}{8}\rho g H_{rms}^2 \tag{4.2}$$

$$c_g = \frac{c}{2}\left(1 + \frac{2kh}{sinh2kh}\right) \tag{4.3}$$

where c_g is the group velocity, c is the phase speed and E is the energy density. ϵ_b and ϵ_f are the dissipation due to the breaking and friction respectively. Substituting (4.2) and (4.3) into (4.1) and using the definition of Rayleigh distribution function

for wave height, the bulk dissipation is written

$$\epsilon_b = \frac{3\sqrt{\pi}}{16}\rho g B^3 \overline{f} \frac{H_{rms}^5}{\gamma^2 h^3}\left[1 - \frac{1}{(1+(H_{rms}/\gamma h)^2)^{5/2}}\right] \tag{4.4}$$

where ϵ_b is the bulk dissipation, ρ is the density of the fluid, H_{rms} is the root mean square wave height, $\overline{f}$ is the peak frequency; and γ and B are free parameters.

4.2.2 Zelt (1991)

Zelt (1991) formulated the wave breaking model by adding an artificial viscosity term in the momentum equation of Zelt and Raichlen (1990) lagrangian Boussinesq wave model. The eddy viscosity is expressed based on the mixing length and is written

$$\nu_b = -B^* l^2 \nabla u \tag{4.5}$$

where the factor B^* is the breaking criteria, and l is the mixing length

$$l = \delta(h + \eta) \tag{4.6}$$

Eliminating η using the continuity equation, substituting (4.6) into (4.5) and replacing ∇u with $-\frac{1}{h}\eta_t$, the eddy viscosity is modified

$$\nu_b = -B^* \delta^2 h \eta_t \tag{4.7}$$

where

$$B^* = \begin{cases} 1 & \eta_t > 2\eta_t^* \\ \eta_t/\eta_t^* - 1 & \eta_t^* < \eta_t < 2\eta_t^* \\ 0 & \eta_t < \eta_t^* \end{cases} \tag{4.8}$$

η_t^* is the critical criteria of free surface elevation change in time and is given by

$$\eta_t^* = 0.3\sqrt{gh} \tag{4.9}$$

Zelt (1991) assumed that waves are solitary. Hence, in general, the coefficent 0.3 in the equation above is not necessarily appropriate where the irregular swell waves exist. In the present work, rather than using the constant value, this coefficient (hereinafter Zelt parameter) is parameterized for different gauge locations.

4.2.3 Frequency dependency formulation of wave breaking

While the statistical approach of Thornton and Guza (1983) is useful, it is of limited utility for frequency domain models as no information on the frequency distribution of the dissipation is provided. Mase and Kirby (1992) hypothesized that the dissipation term should follow an f_n^2 dependence, where f_n is the frequency for each component. They developed a frequency domain model for random wave transformation with an extra term that takes into account the energy dacay in surf zone.

Using Zelt (1991) formulation for eddy viscosity (4.5), Kirby and Kaihatu (1996) described the instantaneous energy dissipation in terms of the eddy viscosity

$$\epsilon_b = -\rho(\frac{\eta}{h})(\nu_b \eta_t)_t \tag{4.10}$$

Using (4.10) and the definition of the energy flux, they formulated the damping coefficient in terms of the free surface and the eddy viscosity spectra

$$\alpha_n = \frac{1}{\rho g c_g} \frac{1}{\sqrt{2\Delta f}} \frac{\sqrt{S_{\epsilon_b}(n)}}{S_\eta(n)} \tag{4.11}$$

where α_n is the damping coefficient; and $S_\eta(n)$ and $S_{\epsilon_b}(n)$ are the free surface and

the instantaneous dissipation spectra respectively and are defined as

$$S_\eta(n) = \frac{|A_n|^2}{2\Delta f} \tag{4.12}$$

$$S_{\epsilon_b}(n) = \frac{|\epsilon_{bn}|^2}{2\Delta f} \tag{4.13}$$

Since the instantaneous dissipation shows up as pikes in the time series, its transformation into the spectral domain appears as a "white" spectrum (spectrum constant with frequency). The damping coefficient, therefore, will correspond to the inverse of free surface spectra via (4.11). By analysing high-resolution laboratory data sets, Kaihatu et al. (2007) proved this argument that the tendency of the damping coefficient toward the power of 2 in the very nearshore is robust.

As it is shown in Mase and Kirby (1992) and Kaihatu and Kirby (1995), the damping term, $\alpha_n A_n$, is represented in the evolution equation as

$$A_{nx} + \frac{c_{gx}}{2c_g} A_n = -\alpha_n A_n \tag{4.14}$$

where

$$\alpha_n = \alpha_{n0} + (\frac{f_n}{f_{peak}})^2 \alpha_{n1} \tag{4.15}$$

$$\alpha_{n0} = F\beta(x) \tag{4.16}$$

$$\alpha_{n1} = (\beta(x) - \alpha_{n0}) \frac{f_{peak}^2 \sum_{n=1}^{N} |A_n|^2}{\sum_{n=1}^{N} f_n^2 |A_n|^2} \tag{4.17}$$

$$\beta(x) = \frac{3\sqrt{\pi}}{4\sqrt{gh}} \frac{B^3 f_{peak} H_{rms}^5}{\gamma^4 h^5} \tag{4.18}$$

$$H_{rms} = 2\sqrt{\sum_{n=1}^{N} |A_n|^2} \tag{4.19}$$

where α_n is the damping coefficient, β is the energy dissipation rate as dictated by

Thornton and Guza (1983) and B, γ and F are free parameters. F denotes the frequency dependency of the dissipation term. According to Kaihatu and Kirby (1996), $F = 1.0$ determines that there is no dependency to frequency for dissipation, while $F = 0$ leads to an f_n^2 dependency for dissipation. They also investigated the effects of dissipation weighting factor on higher order wave statistics parameters. Moreover, Apotsos et al. (2008) enhanced the functionality of the dissipation models by parameterizing the free parameters of γ and B in the formulation.

Kaihatu et al. (2007) introduced their approach for calculation of dissipation. In this method, the dissipation is related to the damping coefficient and the damping coefficient is calculated using the instantaneous energy dissipation of Zelt (1991). The dissipation is defined by

$$D = -\rho g \sum_{n=1}^{N} C_{gn} |A_n|^2 \alpha_n \tag{4.20}$$

where D is dissipation and α_n is the damping coefficient calculated using (4.11).

4.3 Parameterization

4.3.1 Parameterization of γ and Zelt parameter

A high resolution experimental dataset, (Bowen and Kirby 1994) is used for parameterizing the threshold parameter of Zelt (1991). This dataset, hereinafter BK94, includes three different wave conditions. The free surface elevation was measured at 47 gauges with the sampling rate of 25 Hz for the duration of 17 min. The dataset is divided into 12 realizations with 2048 data points in each. Table 4.1 shows the wave condition for each case of Bowen and Kirby (1994). The experimental setup of this experiment (1994) has been also shown in chapter 3.

Calculating the bulk dissipation at each gauge location using (4.1) by ignoring

the dissipation due to friction and equating it with the calculated value of dissipation from Thornton and Guza (1983) formulation, γ is calibrated for each gauge by minimizing the calculated square error (the difference between calculated dissipation from bulk dissipation and Thornton and Guza (1984) formulation). At each step, the dissipation with a particular γ; and its associated error is calculated and the best γ with minimum error is chosen. Figure 4.1 shows the calibrated γ against the normalized water depth.

Table 4.1: Wave conditions for Bowen and Kirby (1994) experiments

Case name	Hrms (m)	Peak frequency (Hz)
A	0.07	0.5
B	0.08	0.255
C	0.09	0.255

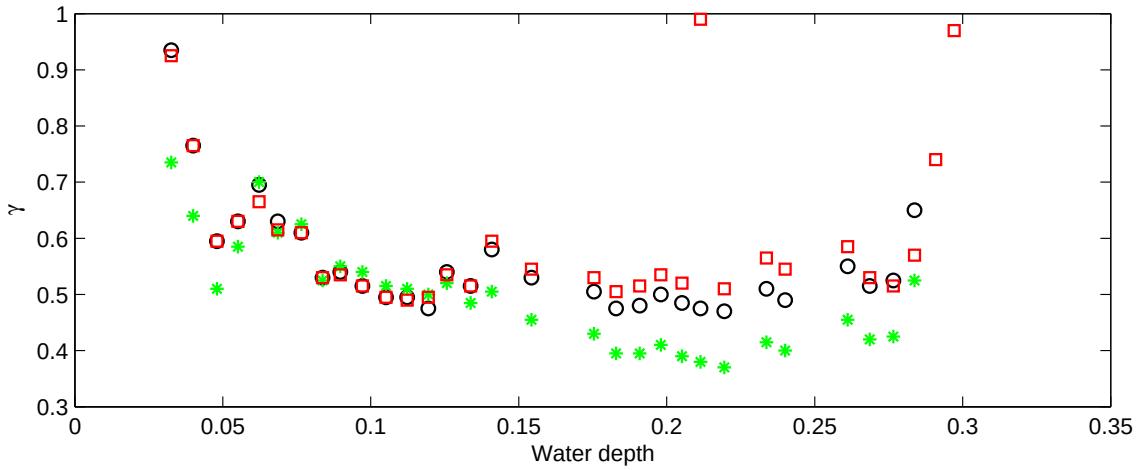

Figure 4.1: Parameterization of γ for BK94 dataset. Black circle: Case A, Green asterisk: Case B; Red square: Case C

For calibrating the Zelt parameter, the bulk dissipation at each individual gauge is calculated directly from the data set using (4.1). The Zelt parameter is chosen in the range of 0.05 to 2.5 with the step size of 0.01. The model is run for each value in this range and the damping coefficient and the dissipation for a particular value of Zelt parameter is calculated using (4.11) and (4.20) respectively. The calculated dissipation is compared with the bulk dissipation calculated from the data set and the best value for Zelt parameter assiciated with minimum square error is chosen. The calibration process is repeated for all gauge locations. Figure 4.2 and 4.3 show the calibrated Zelt parameter against water depth and the calibrated instantaneous dissipation respectively.

As it is seen in figure 4.2, the calibrated parameter is clearly correlated with water depth. For this aim, the water depth is normalized by $(H_{rms}/h)/(k_p h)^2$ where the H_{rms} is the root mean square wave height, h is the water depth and k_p is the wave number at peak frequency. The relationship between Zelt parameter and the

normalized water depth is properly explained by the hyperbolic tangent curve

$$ZP = a + b * tanh(cx) \tag{4.21}$$

where x is the normalized water depth, $(H_{rms}/h)/(k_p h)^2$; and a, b and c are the curve-fitting parameters. It is apparent from Figure 4.2 that the calibrated Zelt threshold parameter tends to a constant value as waves propagate to neashore.

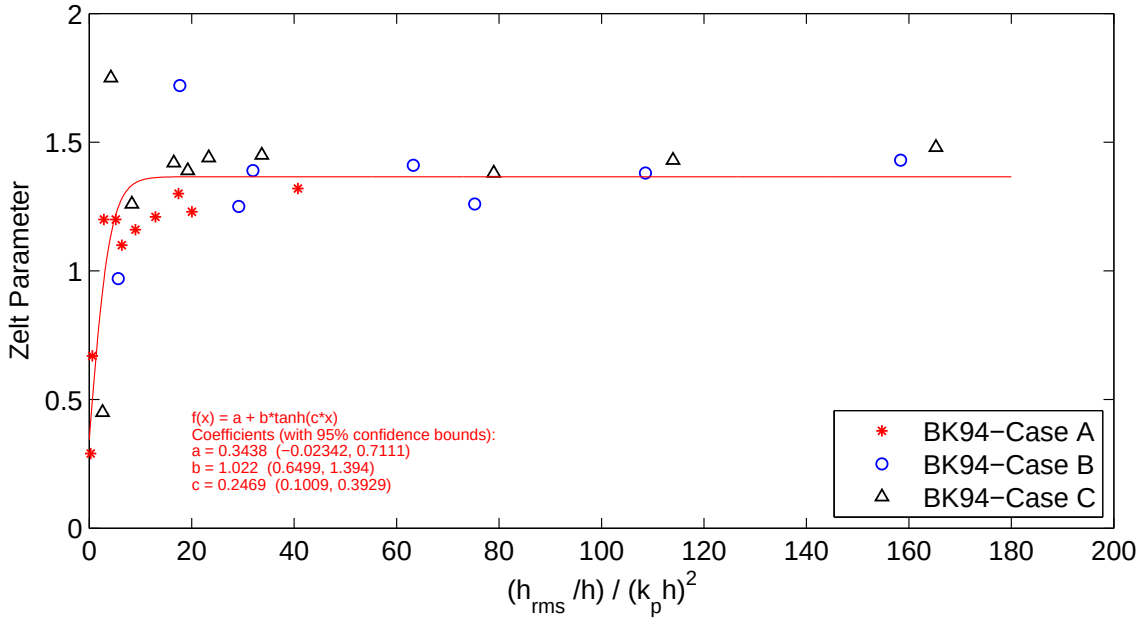

Figure 4.2: Calibrated Zelt parameter at each gauge for three cases of Bowen and Kirby (1994)

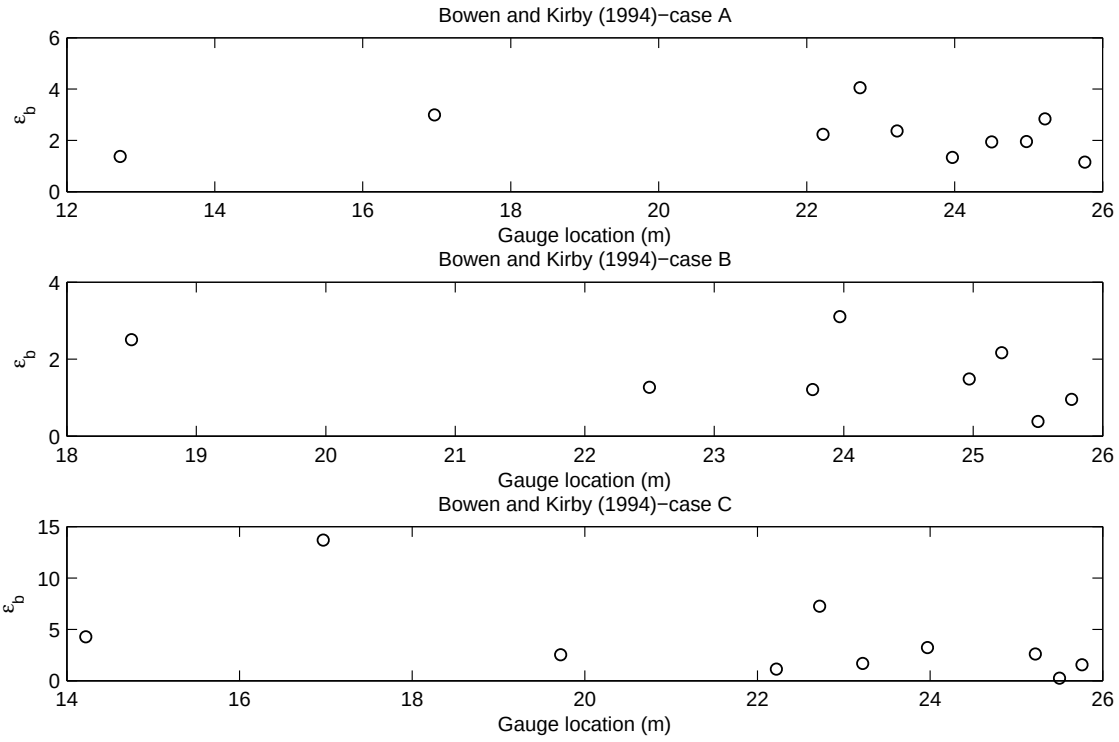

Figure 4.3: instantaneous dissipation after calibrating the threshold Zelt parameter

4.4 Analysis and comparisons

4.4.1 The frequency dependency of breaking waves

In this section, we investigate the relationship between the shape of the free surface elevation power spectrum and that of the damping coefficient, α_n. Using the parameterization of Smith and Vincent (1992), Zakharov (1999) and Toba (1973) for the slope of spectra tail, Kaihatu et al. (2007) showed that in the surf zone the slope of spectra follows the power of f^{-2}. They also strengthen this idea that the frequency dependency term in the formulation of $\alpha(n)$, follows the "power of 2" trend in the surf zone that corresponds to the negative slope of spectra tail. Following Zelt (1991), they assumed the value of 0.3 for the Zelt threshold coefficient.

Herein, we revisit this relationship between power of spectra and the damping coefficient using the calibrated Zelt threshold parameter at each gauge instead of the constant value of 0.3. The calibrated values for instantaneous dissipation value the dissipation spectra, S_{ϵ_b} and its corresponding damping coefficient, α_n are calculated using (4.13) and (4.11) respectively. Figure 4.4 shows the relationship between the negative slope of $\log(S(f))$ and the slope of $\log(\alpha(f))$ for all datasets. Comparing this results with the findings of Kaihatu et al. (2007), it is appeared that using the new values for Zelt threshold parameter causes the calculated dissipation to be evident at fewer locations. Moreover, the instantaneous dissipation has extremely changed compare to Kaihatu et al. (2007). However, the associated values for the slope of α_n are similar. Also, the tendency toward the value of 2 still occurs gradually.

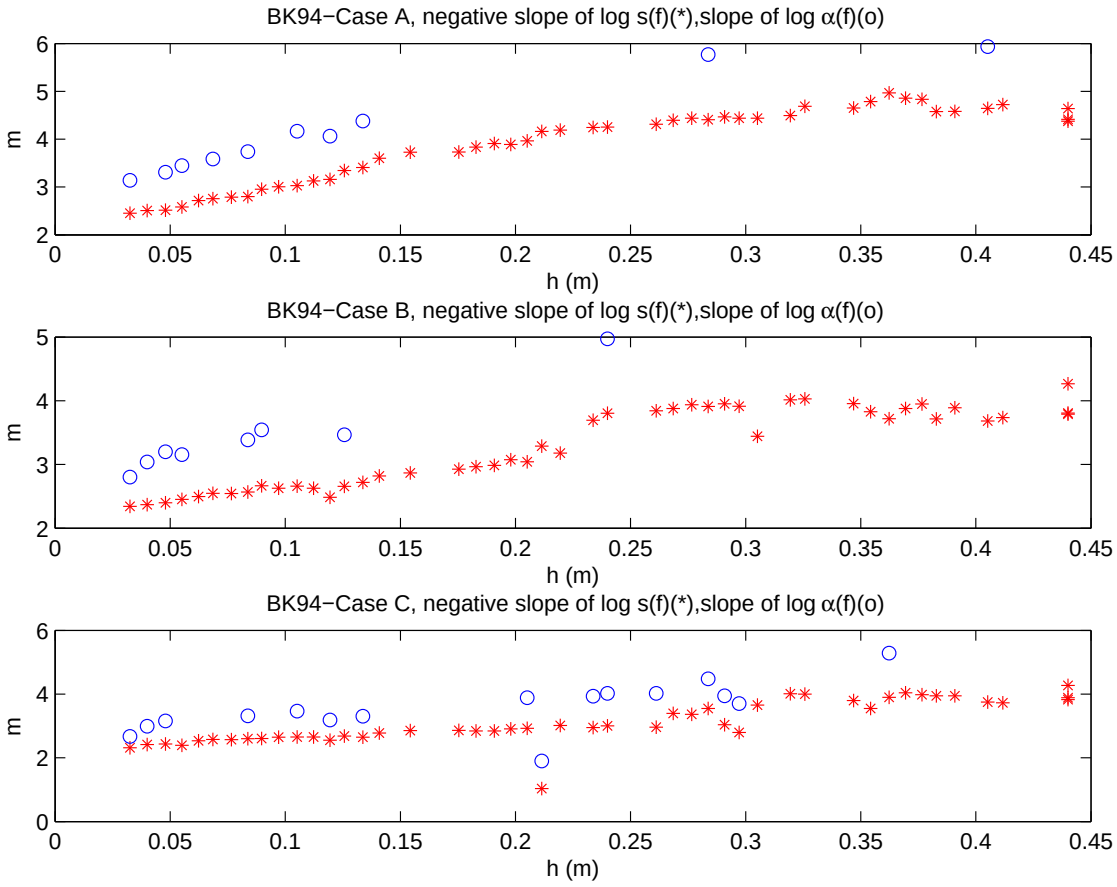

Figure 4.4: Comparing the slope of the spectra and $\alpha(n)$

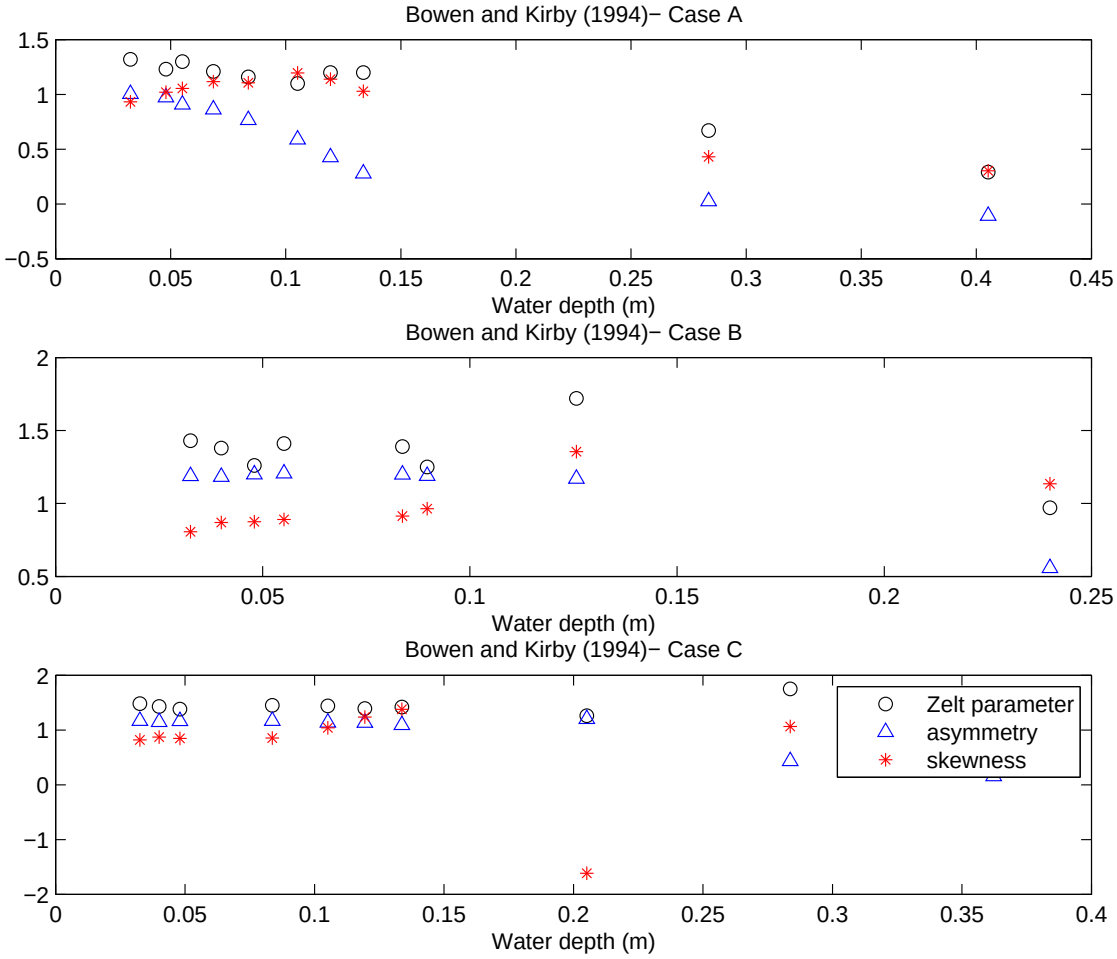

Figure 4.5: Relationship between wave shape parameters and Zelt parameter

4.4.2 Skewness and asymmetry

We calculate the higher order statistical parameters of waves such as skewness and asymmetry (discussed earlier in chapter 3) from the time series by recalling equations 4.63 and 4.64 from the previous chapter. Figure 4.5 shows the variation of skewness, asymmetry and the Zelt parameter against the water depth. It is apparent that by decreasing the water depth, where the most breaking events occurs, the value of Zelt parameter tend to be closer to the asymmetry value. This is sensible, as both

quantity (to some degree) the front face slope of wave in the surf zone.

4.5 Summary

In this chapter, γ, the free parameter in Thornton and Guza (1983) and Zelt threshold parameter of Zelt (1991) were parameterized at each gauge location based on the bulk dissipation calculated from the measured data. Moreover, we applied the calibrated values of Zelt parameter to calculate the instantaneous dissipation and its corresponding damping coefficient. The relationship between the free surface elevation spectra and the calculated damping coefficient with parameterized Zelt threshold parameter was discussed in detail.

As indicated in figure 4.4, although the threshold Zelt parameter and consequently the dissipation intensity has changed compare to Kaihatu et al. (2007) who used the constant value of 0.3 for this parameter, it does not invalidate the tendency of power of frequency dependency term toward 2. Therefore, this tendency is the nearshore asymptote for random waves and this is not affected by the rate of dissipation intensity.

It is evident that the hyperbolic tangent is the best fitted curve to explain the behavior of threshold Zelt parameter vs. normalized water depth. In addition, the tendency toward the constant value for this parameter is clearly seen from figure 4.2.

As it is shown in figure 4.5, asymmetry seems to track better with Zelt parameter than skewness which seems sensible since the Zelt parameter is concerned with the front face slope. Additionally, skewness decreases in the very inner surf zone, whereas asymmetry seems pretty monotonic for the most part. The asymmetry and skewness get quite variable as the Zelt parameter increases. It seems that the Zelt parameter is simply a lower limit on breaking, which makes the variability sensible in the inner surf zone when breaking is widespread.

5. CONCLUSION AND FUTURE WORKS

The aim of the present work was developing a fully dispersive wave model that improves the prediction of high frequency tail of the wave spectra. To do this, we have derived a deterministic model based on the reformulation of the dispersive model of Kaihatu and Kirby (1995). This frequency domain model includes the triad wave-wave interaction terms in the second order in addition to the triads and the bound waves in third order. To take into account the dissipation mechanism due to the breaking waves, the dissipation term based on the formulation of Thornton and Guza (1983) was added to the model.

The developed model (also called real amplitude model) has been verified numerically using the comparisons with either experimental or field data. The comparisons of free surface elevation amplitude for the first four harmonics with the experimental data of Chapalain et al. (1992) demonstrate that the real amplitude model has relatively good agreement with observed data. However more investigations are required for harmonics 3 and 4.

The comparisons of the model-predicted spectra with laboratory experiments shows that the model accurately predicts the high frequency tail of spectra compare to the model of Kaihatu and Kirby (1995) and the consistent model of Freilich and Guza (1984). The variety of test cases for different wave conditions confirms that the model is verified to predict wave conditions with a wide range of ursell numbers.

Furthermore, the model was compared with the Duck 94 field data. The comprehensive comarison of model-predicted spectra with observed data at three spectral band separately, illustrates that the model generally compares well with observed data. While the other two models underpredicts the amount of spectral energy at

band three, the real amplitude model overpredicts the energy and this is encouraging since the overprediction can potentially fixed by changing the dissipation parameters.

Despite the good agreements in prediction of statistical wave parameters such as Hrms and variance, the model does not compare well with data in terms of higher order wave shape parameters such as skewness and asymmetry. However, our investigation shows that these two quantities are quite sensitive to the free parameter in the model.

Characteristics of breaking free parameters is the last part of this dissertation. The free parameters of Thornton and Guza (1983) and the threshold parameter of Zelt (1991) was parameterized appropriately. Using the parameterized Zelt parameter, the relation of the spectra tail slope and the slope of damping coefficient was investigated. Comparing the results with Kaihatu et al (2007) shows that the power of two for the frequency dependency term in dissipation formulation is not affected much with new Zelt parameters.

To extend the first part of this work, three suggestions are followed. First of all, the model should be extended into two dimensions. Hence the variation of waves in y-direction can be taken into account. Using either parabolic approximation or the angular spectum method, the model can be numerically solved in two-dimension. Second, assuming an unknown depth dependency term and extending the boundary value problem up to second order, a new nearshore model is derived mathematically. As another suggestion, the difference between third and second order bound waves and their effects on the modeling results can be determined separately.

As a suggestion for extension of the second part of the work, the dissipation term can be formulated for each frequency component. The wave-wave interactions is taken into account and the integrated evolution equeation is developed for transformation of waves from offshore to the very nearshore waves including the surf zone

with breaking waves. The second idea would be examining the tuned Zelt parameter with a time domain model and see the improvements imposed by inserting new parameter into model.

REFERENCES

Agnon, Y. and Sheremet, A. (1997). Stochastic nonlinear shoaling of directional spectra. *Journal of Fluid Mechanics*, 345:79–99.

Agnon, Y., Sheremet, A., Gonsalves, J., and Stiassnie, M. (1993). Nonlinear evolution of a unidirectional shoaling wave field. *Coastal Engineering*, 20(1):29–58.

Apotsos, A., Raubenheimer, B., Elgar, S., and Guza, R. T. (2008). Testing and calibrating parametric wave transformation models on natural beaches. *Coastal Engineering*, 55(3):224–235.

Baldock, T., Holmes, P., Bunker, S., and Weert, P. V. (1998). Cross-shore hydrodynamics within an unsaturated surf zone. *Coastal Engineering*, 34(3):173–196.

Battjes, J. (1994). Shallow water wave modelling. *Proc.Int.Symp.: waves - Pysical and numerical modeling, Vancouver, University of British Columbia*, pages 1–23.

Battjes, J. and Janssen, J. (1978). Energy loss and set-up due to breaking of random waves. *Coastal Engineering Proceedings*, 1(16).

Beji, S. and Nadaoka, K. (1999). A spectral model for unidirectional nonlinear wave propagation over arbitrary depths. *Coastal Engineering*, 36(1):1–16.

Benney, D. (1962). Non-linear gravity wave interactions. *Journal of Fluid Mechanics*, 14(04):577–584.

Birkemeier, W. A. and Thornton, E. B. (1994). The duck94 nearshore field experiment. In *Coastal Dynamics 94*, pages 815–821. ASCE.

Bocza-Karakiewicz, B., Bona, J., and Cohen, D. (1986). Interaction of shallow-water waves and bottom topography.

Boussinesq, J. (1872). Thorie des ondes et des remous qui se propagent le long d'un canal rectangulaire horizontal, en communiquant au liquide contenu dans ce canal

des vitesses sensiblement pareilles de la surface au fond. *Journal de Mathmatiques Pures et Appliques*, pages 55–108.

Bouws, E., Gnther, H., Rosenthal, W., and Vincent, C. (1985). Similarity of the wind wave spectrum in finite depth water: 1. spectral form. *Journal of Geophysical Research: Oceans (19782012)*, 90(C1):975–986.

Bowen, G. D. and Kirby, J. T. (1994). Shoaling and breaking random waves on a 1:35 laboratory beach. Technical report.

Bredmose, H., Schffer, H., and Madsen, P. A. (2004). Boussinesq evolution equations: Numerical efficiency, breaking and amplitude dispersion. *Coastal Engineering*, 51(11):1117–1142.

Bryant, P. (1974). Stability of periodic waves in shallow water. *Journal of Fluid Mechanics*, 66(01):81–96.

Bryant, P. J. (1973). Periodic waves in shallow water. *Journal of Fluid Mechanics*, 59:625–644.

Chapalain, G., Cointe, R., and Temperville, A. (1992). Observed and modeled resonantly interacting progressive water-waves. *Coastal Engineering*, 16(3):267–300.

Chen, Y., Guza, R., and Elgar, S. (1997). Modeling spectra of breaking surface waves in shallow water. *Journal of Geophysical Research: Oceans (19782012)*, 102(C11):25035–25046.

Chen, Y. and Liu, P. L.-F. (1995). Modified boussinesq equations and associated parabolic models for water wave propagation. *Journal of Fluid Mechanics*, 288:351–381.

Chu, V. H. and Mei, C. C. (1970). On slowly-varying stokes waves. *Journal of Fluid Mechanics*, 41(04):873–887.

Doering, J. C. and Bowen, A. J. (1995). Parametrization of orbital velocity asymmetries of shoaling and breaking waves using bispectral analysis. *Coastal Engineering*,

26(1):15–33.

Eldeberky, Y. (2012). Nonlinear effects in gravity waves propagating in shallow water. *Coastal Engineering Journal*, 54(04).

Eldeberky, Y. and Battjes, J. A. (1996). Spectral modeling of wave breaking: application to boussinesq equations. *J.Geophys.Res*, 101(C1):1253–1264.

Eldeberky, Y. and Madsen, P. A. (1999). Deterministic and stochastic evolution equations for fully dispersive and weakly nonlinear waves. *Coastal Engineering*, 38(1):1–24.

Elgar, S. and Guza, R. (1985a). Observations of bispectra of shoaling surface gravity waves. *Journal of Fluid Mechanics*, 161:425–448.

Elgar, S. and Guza, R. (1985b). Shoaling gravity waves: Comparisons between field observations, linear theory, and a nonlinear model. *Journal of Fluid Mechanics*, 158:47–70.

Elgar, S., Guza, R., Raubenheimer, B., Herbers, T., and Gallagher, E. L. (1997). Spectral evolution of shoaling and breaking waves on a barred beach. *Journal of Geophysical Research: Oceans (19782012)*, 102(C7):15797–15805.

Freilich, M. H. and Guza, R. T. (1984). Nonlinear effects on shoaling surface gravity waves. *Philosophical Transactions of the Royal Society of London (Series) A: Mathematical and Physical Sc*, 311(1515):1–41.

Goertz, J. T., Kaihatu, J. M., Sheremet, A., Smith, E. R., and Smith, J. M. (2012). Long wave effects on breaking waves over fringing reefs. *Coastal Engineering Proceedings*, 1(33):10.

Hammack, J. and Henderson, D. (1993). Resonant interactions among surface water waves. *Annual Review of Fluid Mechanics*, 25(1):55–97.

Heitner, K. L. and Housner, G. W. (1970). Numerical model for tsunami run-up. *Journal of the Waterways, Harbors and Coastal Engineering Division*, 96(3):701–

719.

Hoefel, F. and Elgar, S. (2003). Wave-induced sediment transport and sandbar migration. *Science*, 299(5614):1885–1887.

Janssen, T. and Battjes, J. (2007). A note on wave energy dissipation over steep beaches. *Coastal Engineering*, 54(9):711–716.

Janssen, T., Herbers, T., and Battjes, J. (2006). Generalized evolution equations for nonlinear surface gravity waves over two-dimensional topography. *Journal of Fluid Mechanics*, 552:393–418.

Kadomtsev, B. and Petviashvili, V. (1970). On the stability of solitary waves in weakly dispersing media. In *Sov. Phys. Dokl*, volume 15, pages 539–541.

Kaihatu, J. M. (2001). Improvement of parabolic nonlinear dispersive wave model. *Journal of waterway, port, coastal, and ocean engineering*, 127(2):113–121.

Kaihatu, J. M. (2003). *Frequency domain wave models in the nearshore and surf zones*. Amsterdam: Elsevier.

Kaihatu, J. M. (2009). Application of a nonlinear frequency domain wavecurrent interaction model to shallow water recurrence effects in random waves. *Ocean Modelling*, 26(3):190–205.

Kaihatu, J. M. (2013). Combined random swell and transient long waves: Dissipation characteristics. In *ASME 2013 32nd International Conference on Ocean, Offshore and Arctic Engineering*, pages V005T06A042–V005T06A042. American Society of Mechanical Engineers.

Kaihatu, J. M. and Kirby, J. T. (1995). Nonlinear transformation of waves in finite water depth. *Physics of Fluids*, 7(8):1903–1914.

Kaihatu, J. M. and Kirby, J. T. (1996). Effects of mode truncation and dissipation on predictions of higher order statistics. *Coastal Engineering Proceedings*, 1(25).

Kaihatu, J. M. and Kirby, J. T. (1998). Two-dimensional parabolic modeling of

extended boussinesq equations. *Journal of waterway, port, coastal, and ocean engineering*, 124(2):57–67.

Kaihatu, J. M., Veeramony, J., Edwards, K. L., and Kirby, J. T. (2007). Asymptotic behavior of frequency and wave number spectra of nearshore shoaling and breaking waves. *Journal of Geophysical Research: Oceans (19782012)*, 112(C6).

Karambas, T. V. and Koutitas, C. (1992). A breaking wave propagation model based on the boussinesq equations. *Coastal Engineering*, 18(1):1–19.

Keller, J. B. (1988). Resonantly interacting water waves. *Journal of Fluid Mechanics*, 191:529–534.

Kennedy, A., Chen, Q., Kirby, J., and Dalrymple, R. (2000). Boussinesq modeling of wave transformation, breaking and runup. i: One dimension. In *Journal of Waterway, Port, Coastal, and Ocean Engineering*. Citeseer.

Kirby, J. T. and Kaihatu, J. M. (1996). *Structure of frequency domain models for random wave breaking*.

Korteweg, D. J. and Vries, G. D. (1895). Xli. on the change of form of long waves advancing in a rectangular canal, and on a new type of long stationary waves. *The London, Edinburgh, and Dublin Philosophical Magazine and Journal of Science*, 39(240):422–443.

Lin, P. and Liu, P. L.-F. (1998). A numerical study of breaking waves in the surf zone. *Journal of Fluid Mechanics*, 359:239–264.

Liu, P. L. F. and Dingemans, M. W. (1989). Derivation of the third order evolution equations for weakly nonlinear water waves propagating over uneven bottoms. *Wave Motion*, 11:41–64.

Liu, P. L.-F. and Tsay, T.-K. (1984). Refraction-diffraction model for weakly nonlinear water waves. *Journal of Fluid Mechanics*, 141:265–274.

Liu, P. L.-F., Yoon, S. B., and Kirby, J. T. (1985). Nonlinear refractiondiffraction of

waves in shallow water. *Journal of Fluid Mechanics*, 153:185–201.

Madsen, P. A., Bingham, H., and Schffer, H. (2003). Boussinesq-type formulations for fully nonlinear and extremely dispersive water waves: derivation and analysis. In *Proceedings of the Royal Society of London A: Mathematical, Physical and Engineering Sciences*, volume 459, pages 1075–1104. The Royal Society.

Madsen, P. A. and Eldeberky, Y. (1998). A new formulation of deterministic and stochastic evolution equations for three-wave interactions involving fully dispersive waves. *Coastal Engineering Proceedings*, 1(26).

Madsen, P. A., Murray, R., and Sorensen, O. R. (1991). A new form of the boussinesq equations with improved linear dispersion characteristics. *Coastal Engineering*, 15(4):371–388.

Madsen, P. A. and Sorensen, O. R. (1992). A new form of the boussinesq equations with improved linear dispersion characteristics. part 2. a slowly-varying bathymetry. *Coastal Engineering*, 18(3):183–204.

Madsen, P. A. and Sorensen, O. R. (1993). Bound waves and triad interactions in shallow water. *Ocean Engineering*, 20:359–388.

Mase, H. and Kirby, J. T. (1992). Hybrid frequency-domain kdv equation for random wave transformation. *Coastal Engineering Proceedings*, 1(23).

Mase, H. and Kirby, J. T. (1993). Hybrid frequency-domain kdv equation for random wave transformation. *Proceedings of the international conference - Coastal Engineering Conference*, 1:474–487.

Mei, C. and Mehaute, B. L. (1966). Note on the equations of long waves over an uneven bottom. *Journal of Geophysical Research*, 71(2):393–400.

Mei, C. C. and Unluata, U. (1972). Harmonic generation in shallow water waves. *Waves on Beaches and Resulting Sediment Transport*, pages 181–202.

Nwogu, O. (1993). Alternative form of boussinesq equations for nearshore wave prop-

agation. *Journal of waterway, port, coastal, and ocean engineering*, 119(6):618–638.

Peregrine, D. (1967). Long waves on a beach. *Journal of Fluid Mechanics*, 27(04):815–827.

Radder, A. (1979). On the parabolic equation method for water-wave propagation. *Journal of Fluid Mechanics*, 95(1):159–176.

Roelvink, J. and Stive, M. (1989). Bargenerating crossshore flow mechanisms on a beach. *Journal of Geophysical Research: Oceans (19782012)*, 94(C4):4785–4800.

Schffer, H. A., Madsen, P. A., and Deigaard, R. (1993). A boussinesq model for waves breaking in shallow water. *Coastal Engineering*, 20(3):185–202.

Smith, J. M. and Vincent, C. L. (2003). Equilibrium ranges in surf zone wave spectra. *Journal of Geophysical Research: Oceans (19782012)*, 108(C11).

Smith, R. and Sprinks, T. (1975). Scattering of surface waves by a conical island. *Journal of Fluid Mechanics*, 72(02):373–384.

Suh, K. D., Dalrymple, R. A., and Kirby, J. T. (1990). An angular spectrum model for propagation of stokes waves. *Journal of Fluid Mechanics*, 221:205–232.

Svendsen, I. A. (1984). Wave heights and set-up in a surf zone. *Coastal Engineering*, 8(4):303–329.

Synolakis, C. E. (1986). *The runup of long waves*.

Tang, Y. and Ouellet, Y. (1997). A new kind of nonlinear mild-slope equation for combined refraction-diffraction of multifrequency waves. *Coastal Engineering*, 31(14):3–36.

Thornton, E. B. and Guza, R. (1983). Transformation of wave height distribution. *Journal of Geophysical Research: Oceans (19782012)*, 88(C10):5925–5938.

Toba, Y. (1973). Local balance in the air-sea boundary processes. *Journal of the Oceanographical Society of Japan*, 29(5):209–220.

Tolman, H. L. (1991). A third-generation model for wind waves on slowly varying,

unsteady, and inhomogeneous depths and currents. *Journal of Physical Oceanography*, 21(6):782–797.

Tolman, H. L., Banner, M. L., and Kaihatu, J. M. (2013). The nopp operational wave model improvement project. *Ocean Modelling*, 70(0):2–10.

Veeramony, J. and Svendsen, I. A. (2000). The flow in surf-zone waves. *Coastal Engineering*, 39(2):93–122.

Wei, G. and Kirby, J. T. (1995). Time-dependent numerical code for extended boussinesq equations. *Journal of Waterway, Port, Coastal, and Ocean Engineering*, 121(5):251–261.

Wei, G., Kirby, J. T., Grilli, S. T., and Subramanya, R. (1995). A fully nonlinear boussinesq model for surface waves. part 1. highly nonlinear unsteady waves. *Journal of Fluid Mechanics*, 294:71–92.

Witting, J. M. (1984). A unified model for the evolution nonlinear water waves. *Journal of Computational Physics*, 56(2):203–236.

Zakharov, V. (1999). Statistical theory of gravity and capillary waves on the surface of a finite-depth fluid. *European Journal of Mechanics-B/Fluids*, 18(3):327–344.

Zelt, J. (1991). The run-up of nonbreaking and breaking solitary waves. *Coastal Engineering*, 15(3):205–246.

Zelt, J. and Raichlen, F. (1990). A lagrangian model for wave-induced harbour oscillations. *Journal of Fluid Mechanics*, 213:203–225.